WWW.OEAW.AC.AT

ÖAW ÖSTERREICHISCHE AKADEMIE DER WISSENSCHAFTEN

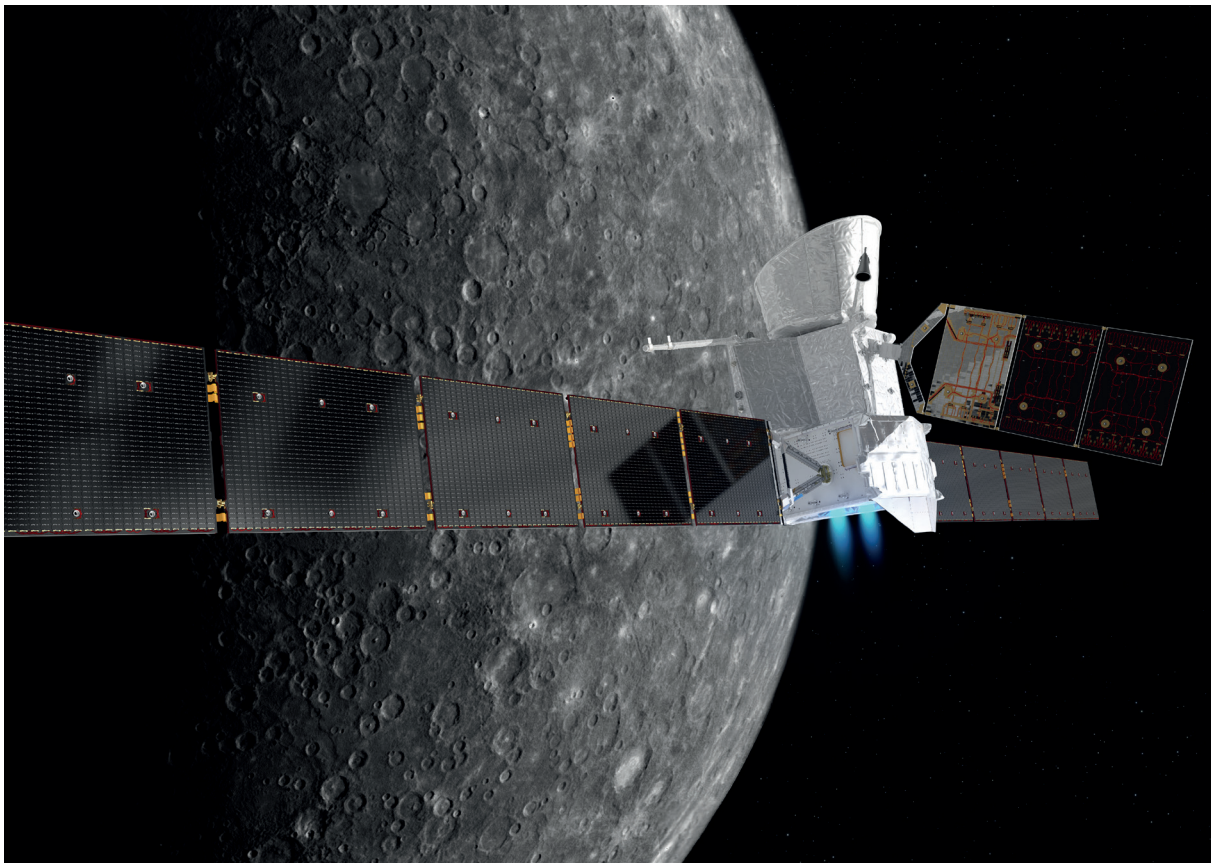

ANNUAL REPORT 2018

IWF INSTITUT FÜR WELTRAUMFORSCHUNG

WWW.IWF.OEAW.AC.AT

ÖSTERREICHISCHE AKADEMIE DER WISSENSCHAFTEN

ANNUAL REPORT 2018

INSTITUT FÜR WELTRAUMFORSCHUNG

COVER IMAGE

Artist's impression of the *BepiColombo* spacecraft in cruise configuration, with Mercury in the background (© spacecraft: ESA/ATG medialab; Mercury: NASA/JPL).

TABLE OF CONTENTS

INTRODUCTION

The Space Research Institute (Institut für Weltraumforschung, IWF) in Graz focuses on the physics of space plasmas and (exo-)planets. With about 100 staff members from 20 nations it is one of the largest institutes of the Austrian Academy of Sciences (Österreichische Akademie der Wissenschaften, ÖAW, Fig. 1).

IWF develops and builds space-qualified instruments and analyzes and interprets the data returned by them. Its core engineering expertise is in building magnetometers and on-board computers, as well as in satellite laser ranging, which is performed at a station operated by IWF at the Lustbühel Observatory. In terms of science, the institute concentrates on dynamical processes in space plasma physics and on the upper atmospheres of planets and exoplanets.

IWF cooperates closely with space agencies all over the world and with numerous other national and international research institutions. A particularly intense cooperation exists with the European Space Agency (ESA).

The institute is currently involved in twenty active and future international space missions; among these:

- ESA's *Cluster* mission, launched in 2000, still provides unique data to better understand space plasmas.
- *MMS*, launched in 2015, uses four identically equipped spacecraft to explore the acceleration processes that govern the dynamics of the Earth's magnetosphere.
- The *China Seismo-Electromagnetic Satellite (CSES)* was launched in February to study the Earth's ionosphere.
- NASA's *InSight (INterior exploration using Seismic Investigations, Geodesy and Heat Transport)* mission was launched in May to place a geophysical lander on Mars to study its deep interior.
- *BepiColombo* was launched in October to investigate planet Mercury, using two orbiters, one specialized in magnetospheric studies and one in remote sensing.
- The Korean satellite *GEO-KOMPSAT-2A (GK-2A)* was launched in December to conduct space weather investigations.
- ESA's first Small-class mission *CHEOPS (CHaracterizing ExOPlanets Satellite)* will classify exoplanets in detail. Its launch is expected in 2019.

Fig. 1: In spring, the entrance to the Victor Franz Hess Research Center, housing IWF Graz, got an impressive "facelift".

- Along an innovative trajectory, *Solar Orbiter* is to study solar and heliospheric phenomena, planned for launch in 2020.
- ESA's *JUpiter ICy moons Explorer (JUICE)* will observe Jupiter and three of its largest moons, Ganymede, Callisto, and Europa. It is planned for launch in 2022.
- ESA's third Medium-class science mission *PLATO* is a space-based observatory to search for planets orbiting alien stars. It is planned for launch by 2026.

HIGHLIGHTS IN 2018

- 2018 broke all records as far as launches are concerned. With *CSES*, *InSight*, *BepiColombo*, and *GK-2A* four missions with contributions from IWF Graz were sent into space (Fig. 2).
- Astronomers have detected an excess of massive stars in 30 Doradus, member of the Large Magellanic Cloud. The study was published in "Science".
- In a "Nature Physics" paper, it was shown that the solar atmosphere can be heated through plasma waves.
- A "Nature Astronomy" study concluded that pseudo-shocks can act as an energy source for the solar corona.
- "Science" presented the latest results of NASA's *MMS* satellites, which for the first time captured the 3D structure of electron-scale dynamics also on the nightside of the magnetosphere.

THE YEAR 2018 IN NUMBERS

Members of the institute published 179 papers in refereed international journals, of which 48 were first author publications. During the same period, articles with authors from the institute were cited 5143 times in the international literature. In addition, 85 talks and 41 posters were presented at international conferences by IWF members. Last but not least, institute members were involved in the organization of nine international meetings or workshops.

IWF STRUCTURE AND FUNDING

IWF is structured into four research fields represented by eight research groups. Wolfgang Baumjohann serves as Director, Werner Magnes as Deputy Director.

The bulk of financial support is provided by ÖAW. Significant support is also given by other national institutions, in particular the Austrian Research Promotion Agency (Österreichische Forschungsförderungsgesellschaft, FFG) and the Austrian Science Fund (Fonds zur Förderung der wissenschaftlichen Forschung, FWF). Furthermore, European institutions like ESA and the European Union contribute substantially.

Fig. 2: Clockwise, from top left, the launch of *CSES* (© IWF), *InSight* (Credits: NASA/JPL-Caltech), *GK-2A* (Credits: ESA-CNES-Arianespace), and *BepiColombo* (© ESA).

NEAR-EARTH SPACE

Recent advancements in the in-situ measurements of charged particles together with electric and magnetic fields at high cadence make near-Earth space a most suitable place to study fundamental space plasma processes. IWF has been participating in hardware activities of numerous space missions in the Earth's magnetosphere, now operating, being build, as well as in the planning phase. Data taken from operating missions have been extensively analyzed at IWF by applying different analysis methods and by theoretical modeling. The obtained knowledge contributes to the better understanding of different space plasma processes in our solar system and beyond.

CSES

The *China Seismo-Electromagnetic Satellite (CSES)* was launched in February 2018. It is the first Chinese platform for the investigation of natural electromagnetic phenomena with major emphasis on earthquake monitoring from a Sun synchronous, polar Low Earth Orbit (LEO).

The *CSES* magnetometer was developed in cooperation between China's National Space Science Center (NSSC), the Institute of Experimental Physics of TU Graz (TUG), and IWF. NSSC is responsible for the dual sensor fluxgate magnetometer, the instrument processor and the power supply unit, while IWF and TUG participate with the newly developed absolute scalar magnetometer, called *Coupled Dark State Magnetometer (CDSM)*.

In 2018, the technology readiness of *CDSM* for space application was successfully demonstrated. After its first turn-on beginning of March it has been operational for more than 200 days (Fig. 3). Consequently, the accuracy of the magnetic field measurements could be improved by more than a factor of thirty. This is also an important step towards a successful implementation of the *CDSM* technology for ESA's *JUICE* mission to Jupiter.

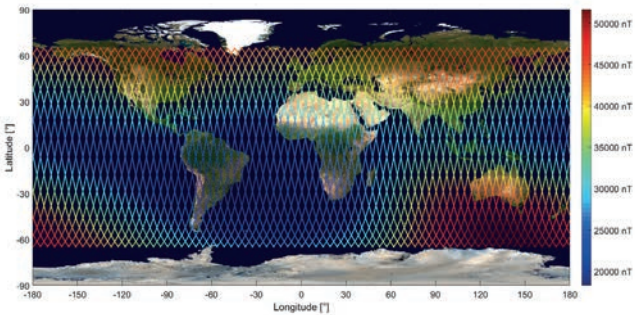

Fig. 3: Strength of the Earth's magnetic field measured by *CDSM* along the *CSES* orbits within a latitude range of ±65°.

GEO-KOMPSAT-2A

GEO-KOMPSAT-2 (Geostationary Korea Multi-Purpose Satellite-2) consists of two spacecraft, which are built and managed by the South Korean Space Agency KARI. Both satellites focus on meteorological survey measurements from a geostationary orbit above Korea. One of the spacecraft, *GEO-KOMPSAT-2A (GK-2A)*, carries additional instrumentation to investigate space weather phenomena.

In cooperation with ESA and international partners, IWF is engaged in *GK-2A* with a four-sensor magnetometer called *Service Oriented Spacecraft MAGnetometer (SOSMAG)*. It was developed with ESA technology grants and serves as a ready-to-use space weather monitoring system to be mounted on a variety of different spacecraft built without a magnetic cleanliness program. Up to two high-resolution boom-mounted fluxgate magnetometers, the Digital Processing Unit (DPU) and the boom are provided by Magson GmbH and Technische Universität Braunschweig. For detection and characterization of magnetic disturbers on the spacecraft, two magnetometers based on the anisotropic magnetoresistive (AMR) effect were developed in a joint effort by Imperial College London and IWF.

In 2018, the flight model of *SOSMAG* has undergone system level testing (vibration, thermal vacuum, ...) on the *GK-2A* spacecraft as part of the *Korean Space Environment Monitor (KSEM)* instrument suit. On 4 December 2018, *GK-2A* was successfully launched aboard an Ariane 5 from the European spaceport in Kourou, French-Guyana.

The measurements in Fig. 4 perfectly demonstrate that the spacecraft field measured by the AMR sensors can be used for the correction of the magnetic field measured by the outer boom mounted sensor. It enables a much higher quality of the magnetic field measurements and confirms the usefulness of the four-sensor *SOSMAG* design.

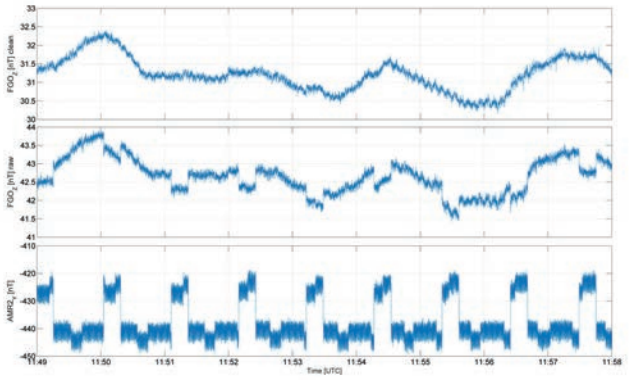

Fig. 4: Spacecraft interference in the Z component of the outboard sensor is corrected with the Y component of AMR sensor 2.

CLUSTER

The *Cluster* spacecraft have been providing data since 2001 for studying small-scale structures of the magnetosphere and its environment as the first four spacecraft mission in space. Currently the mission is planned to be extended to December 2020. IWF is PI/Co-I on five instruments and has maintained the *Austrian Cluster Data Center*. In addition to data analysis, IWF also contributes to data archiving activities at the *Cluster Science Archive (CSA)* by also producing supporting data products such as science event lists.

MMS

NASA's *MMS (Magnetospheric MultiScale)* mission explores the dynamics of the Earth's magnetosphere and its underlying energy transfer processes. Four identically equipped spacecraft carry out measurements with high temporal and spatial resolution. *MMS* investigates small-scale basic plasma processes, which transport, accelerate and energize plasma in thin boundary and current layers. The orbit of *MMS*, launched in March 2015, was dedicated to study dayside magnetopause reconnection during the first two years. The apogee was then raised to encounter near-Earth magnetotail reconnection in mid 2017. The extension phase is proposed for further five years.

IWF has taken the lead for the satellites' spacecraft potential control *(ASPOC)* and is participating in the electron beam instrument *(EDI)* and the digital fluxgate magnetometer *(DFG)*. In addition to the operation of these instruments and scientific data analysis, IWF is contributing in inflight calibration activities.

THEMIS/ARTEMIS

NASA's *THEMIS (Time History of Events and Macroscale Interactions during Substorms)* mission, launched in 2007, consisted of five identical satellites flying through different regions of the magnetosphere. In autumn 2010 the two outer spacecraft became *ARTEMIS* in orbit around the Moon, while the other three *THEMIS* spacecraft remained in their orbit. As Co-I of the magnetometer, IWF is participating in processing and analyzing data.

SMILE

The *Solar wind Magnetosphere Ionosphere Link Explorer (SMILE)* is a joint mission between ESA and the Chinese Academy of Sciences (CAS). It aims to build a more complete understanding of the Sun-Earth connection by measuring the solar wind and its dynamic interaction with the magnetosphere (Fig. 5). IWF is Co-Investigator for two instruments: the *Soft X-ray Imager (SXI)*, led by the University of Leicester, and the magnetometer *(MAG)*, led by CAS.

The institute, in close cooperation with international partners, contributes to the *SXI* instrument the instrument's control and power unit *EBOX*. IWF is coordinating the development and design of the Digital Processing Unit (DPU) and is responsible for the mechanical design and the tests at box level. In 2018, IWF established the concept for the DPU prototype and completed the preliminary design of the box mechanics.

In addition to the hardware activities, IWF is participating in the *SMILE* science preparation such as modeling and in-situ science working group activities.

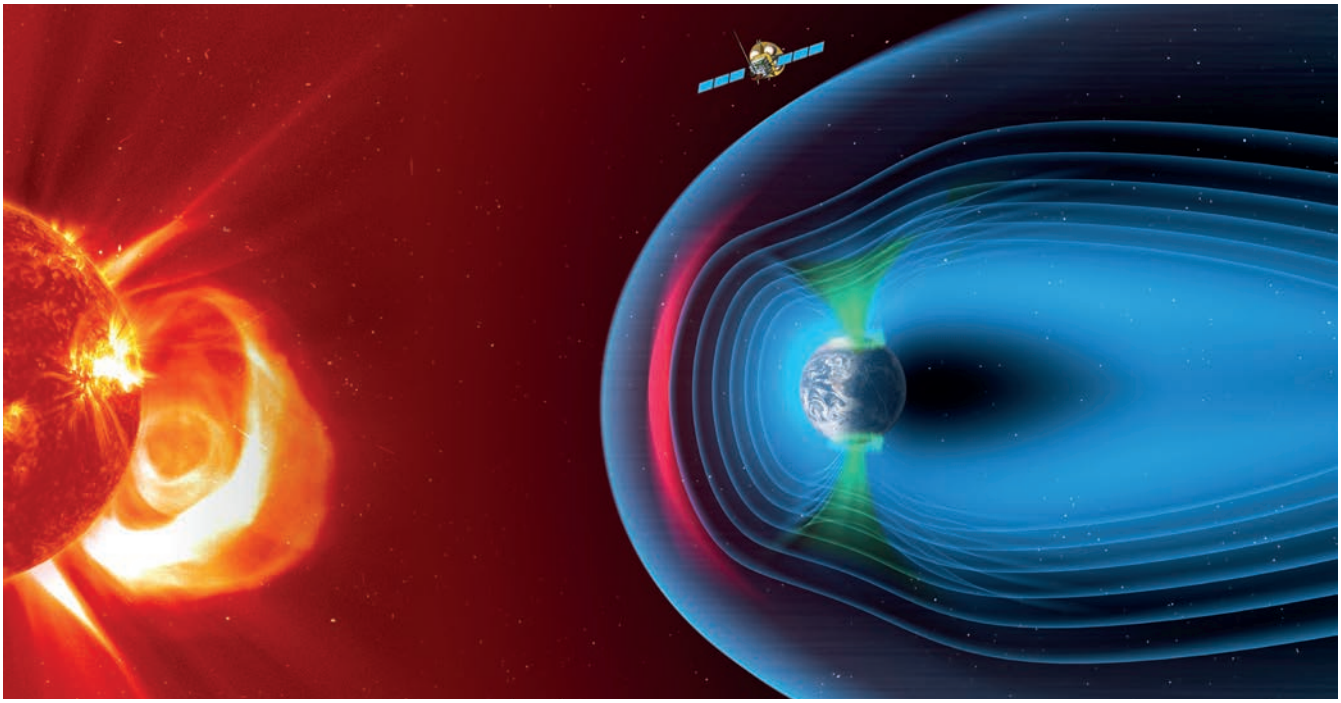

Fig. 5: *SMILE* aims to form an accurate picture of solar-terrestrial magnetospheric physics (© ESA/ATG medialab).

ANALYTICAL MODEL FOR A BENT MAGNETOTAIL

Most of the existing analytical models of two-dimensional magnetotail-like configurations are symmetrical with respect to the equatorial plane. In this study an analytical model is created for asymmetrical configurations and is used to reproduce the current sheet bending and shifting in the vertical plane (see Fig. 6). Such an asymmetry is expected to arise from the Earth dipole tilting and non-radial propagation of the solar wind, as observed by spacecraft such as *THEMIS* in the Earth's magnetotail.

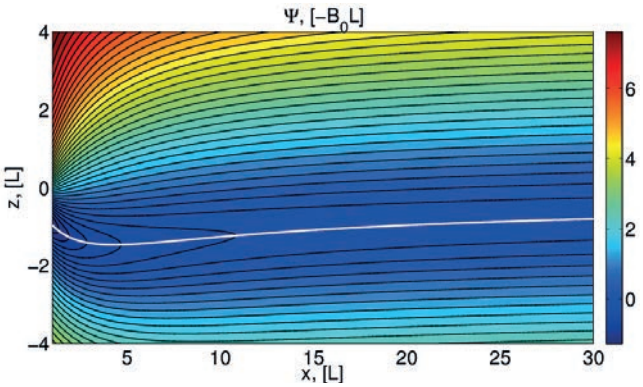

Fig. 6: Normalized magnetic potential Ψ(x,z) is shown by color in a plane, passing through the Earth and the Sun perpendicular to the ecliptic. The Earth is outside the left boundary. The solid curves plot magnetic field lines and isolines of the plasma pressure and current density. The white curve shows the current sheet center. Normalization constants are L ~1 Earth radius and B0 ~10 nT.

INTERCHANGE HEADS IN THE EARTH'S MAGNETOTAIL

On the anti-sunward side of the Earth, the terrestrial magnetic field lines are stretched out to form an elongated structure called the magnetotail. At the center of this structure the magnetic field strength normally decreases continually with increasing distance away from the Earth. However, periodically, the magnetotail is disrupted in a process called a substorm; the cause of this disruption remains controversial. A fortuitous configuration of five space probes is used to investigate a possible mechanism for this disruption. The probes observed the formation of a substantial region where the magnetic field strength possessed a minimum (rather than always decreasing). By comparing with the results of plasma computer simulations, it is shown that this region should generate an instability that produces dawnward propagating clumps of more dipolar field lines, in agreement with the probe observations.

The magnetic field minimum appeared to have radial size of about 2.5 Earth radii (R_E) and azimuthal size that could be as large as 10 R_E. This structure was present for over three hours in the plasma sheet at around -11 R_E. Ballooning/InterChange Instability (BICI) heads were observed tailward of the minimum $\partial B_Z/\partial X \approx -10 nT/R_E$. The BICI heads appeared to drift azimuthally toward dawn, in accord with Particle-In-Cell (PIC) simulations of a charged current sheet (Fig. 7). The signatures of the latter, e.g., a finite average E_Z directed toward the center of the plasma sheet, are verified by the *THEMIS* data. One dawnward-drifting BICI head is studied taking advantage of the available high-resolution *THEMIS* observations and comparing with the PIC simulation run. A prediction of the earlier PIC simulation for a neutral current sheet, that duskward-drifting BICI heads are subject to a current-driven ion-cyclotron instability, is found to be true also for dawnward-drifting BICI heads in the charged current sheet simulations. This specific prediction and the *THEMIS* data indicate the presence of electromagnetic ion-cyclotron wave activity that ripples the background BICI head shape.

Fig. 7: Structure of one BICI head as seen in the cross-product of the electric and magnetic field components that were obtained from Particle-In-Cell simulations of a charged current sheet (left) and from spin-averaged data of the *THEMIS* observations.

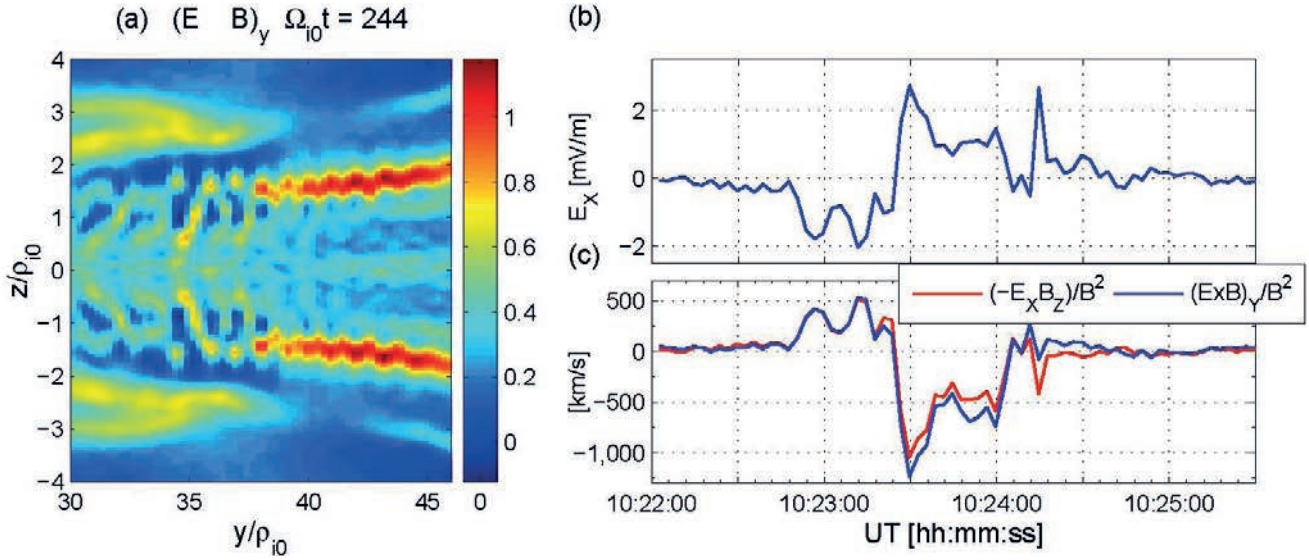

MAGNETIC RECONNECTION RATE IN THE EARTH'S MAGNETOTAIL

In the Earth's magnetotail, magnetic reconnection releases stored magnetic energy and drives magnetospheric convection. The rate at which magnetic flux is transferred from the reconnection inflow to outflow regions is determined by the reconnection electric field E_r, which is often referred to as the unnormalized reconnection rate. To better quantify the efficiency of reconnection, this electric field E_r is often normalized by the characteristic Alfvén speed and the reconnecting magnetic field. This parameter is generally called the normalized reconnection rate R. A magnetotail reconnection event with weak geomagnetic activity (AE < 200 nT) observed by *MMS* on 11 July 2017 is extensively studied and relevant simulation is performed. In this event, the *MMS* spacecraft crossed the reconnection separatrix boundary, an edge boundary of the region where the reconnected field lines are filled, and then entered the electron diffusion region (EDR), a central reconnection region where the magnetic topology change occurs and the flux is dominantly sustained by E_r. To support the observations, two-dimensional fully kinetic simulation of this *MMS* event is employed (Fig. 8) by using initial simulation parameters from the observations as input.

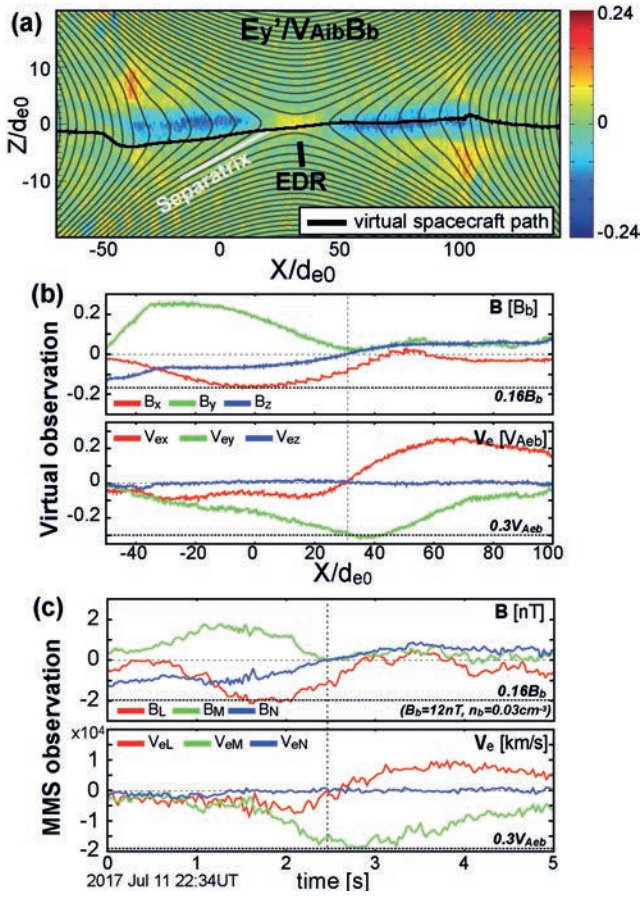

Fig. 8: (a) 2D simulation result of out-of-plane component of the electric field $E_y'=E_y+(\mathbf{V}_e \times \mathbf{B})_y$ with the orbit path of the virtual spacecraft. (b, c) Plots from virtual observations (b) and *MMS-3* observations (c) of the three components of the magnetic field and the electron bulk velocities.

In both the simulation and the *MMS* observations, R and E_r are successfully obtained from direct measurements in the EDR and indirect measurements at the separatrix using a recently proposed remote sensing technique. The measured normalized rate for this *MMS* event is R~0.15-0.2, consistent with theoretical and simulation models of fast collisionless reconnection. This corresponds to an unnormalized rate of E_r~2-3 mV/m. Based on quantitative consistencies between the simulation and the *MMS* observations, it is concluded that the estimates of the reconnection rates are reasonably accurate. Given that past studies have found E_r of the order ~10 mV/m during strong geomagnetic substorms, these results indicate that the local E_r in magnetotail reconnection may be an important parameter controlling the amplitude of geomagnetic disturbances.

MAGNETOTAIL FLOW DIRECTION AND DAWN-DUSK ASYMMETRY

Plasma sheet fast flows are the main transporter of mass, flux, and energy in the Earth's magnetotail and result directly from magnetic reconnection. With limited observations near or beyond lunar orbit during the last decades, these flows were mainly studied within $X_{GSM} > -60\ R_E$. Utilizing five years (2011–2015) of *ARTEMIS* data from around $-60\ R_E$, it is found that a significant fraction of fast flows is directed earthward, comprising 43% ($v_x > 400$ km/s) to 56% ($v_x > 100$ km/s) of all observed flows (Fig. 9). This suggests that reconnection within and beyond $-60\ R_E$ have a similar occurrence rate. For fast convective flows ($v_{px} > 400$ km/s), this fraction of earthward flows is reduced to about 29%, which is in line with reconnection as source of these flows and a downtail decreasing Alfvén velocity. More than 60% of tailward convective flows occur in the dusk sector (as opposed to the dawn sector), while earthward convective flows are nearly symmetrically distributed between the two sectors for low AL (> -400 nT) and asymmetrically distributed toward the dusk sector for high AL (< -400 nT). This indicates that the dawn-dusk asymmetry is more pronounced closer to Earth and moves farther downtail during high geomagnetic activity. It is inferred that near-Earth reconnection is preferentially located at dusk, whereas midtail reconnection ($X > -60\ R_E$) is likely symmetric across the tail during weak substorms and asymmetric toward the dusk sector for strong substorms, as the dawn-dusk asymmetric nature of reconnection onset in the near-Earth region progresses downtail.

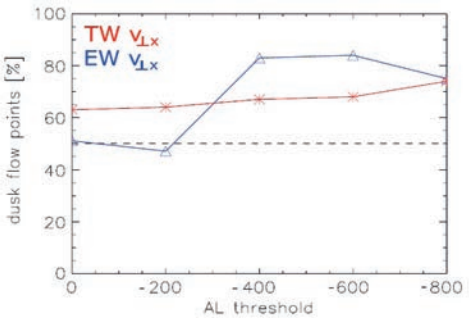

Fig. 9: Percentage of flow datapoints with $v_{px} > 200$ km/s observed in the dusk sector relative to AL thresholds.

MULTI-SCALE CURRENTS OBSERVED BY MMS IN THE FLOW BRAKING REGION

Earthward high-speed plasma jets from magnetic reconnection are braked in the near-Earth plasma sheet interacting with Earth's dipole field and creating field-aligned currents. Characteristics of current layers in the off-equatorial near-Earth plasma sheet boundary are studied with high time-resolution measurements from the *MMS* mission. The four *MMS* spacecraft observed fast flow disturbances (up to about 500 km/s), most intense in the dawn-dusk direction (green lines in Fig. 10c). Field-aligned currents (Fig. 10b) were initially within the expanding plasma sheet (event i, ii), where the flow and field disturbances showed the distinct pattern expected in the braking region of localized flows.

Subsequently, intense thin field-aligned currents layers (events iii and iv) were detected together with Earthward streaming hot ions. Average disturbances and thickness of the current layers are shown in Fig. 10e-h. Intense Hall-current layers were found adjacent to the field-aligned currents (during times indicated by black bars in Fig. 10 d). These observations show that both the near-Earth plasma jet diversion and the thin Hall-current layers formed around the reconnection jet boundary are the sites where diversion of the perpendicular currents take place that contribute to the observed field-aligned current pattern as predicted by simulations of reconnection jets. Hence, multiscale structure of flow braking is preserved in the field-aligned currents in the off-equatorial plasma sheet and is also translated to the ionosphere to become a part of the substorm field-aligned current system.

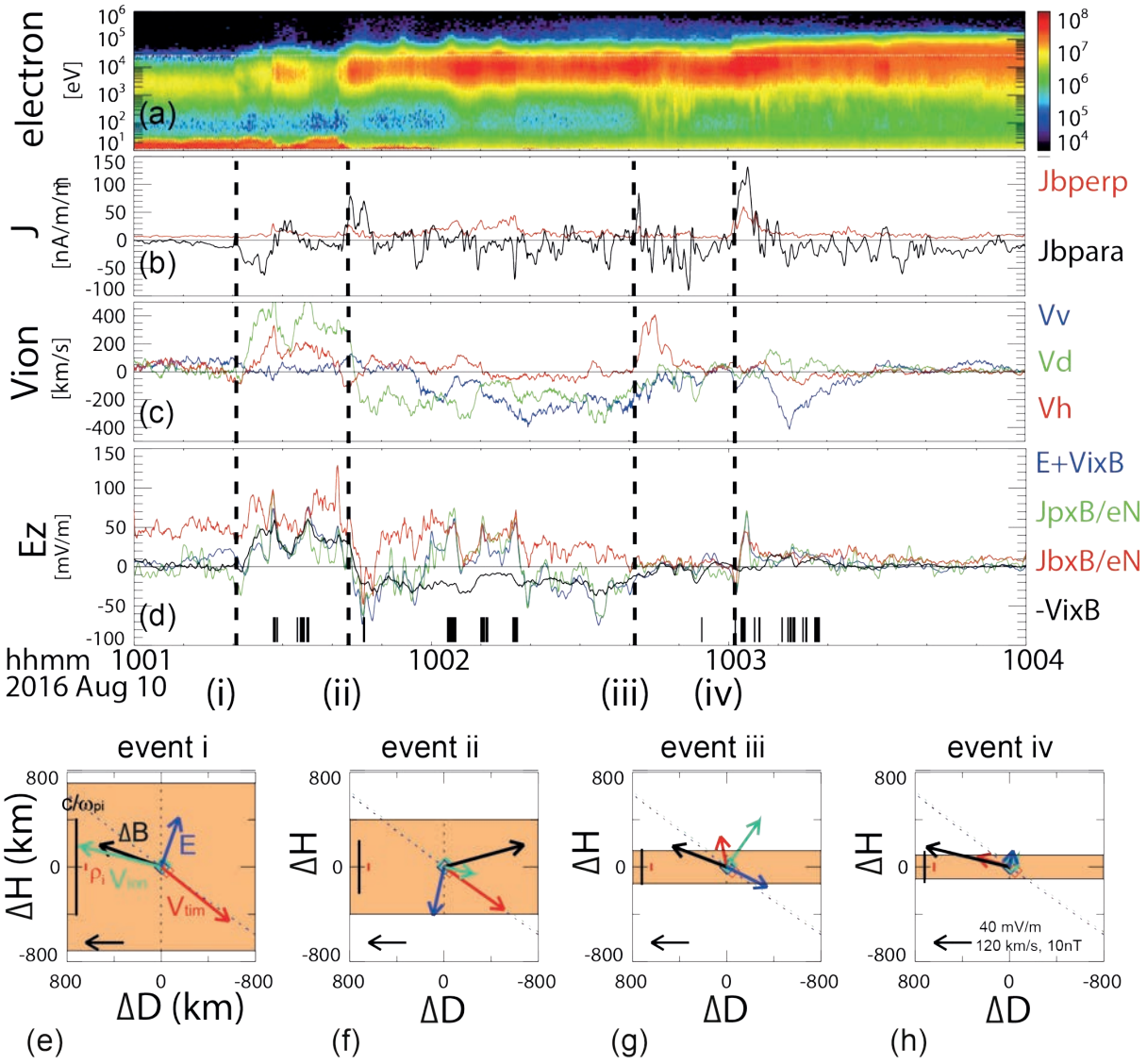

Fig. 10: *MMS* observations between 10:01-10:04 on 10 August 2016. (a) Energy spectra from electrons, (b) field-aligned (black) and perpendicular (red) components of the currents, (c) ion flow, (d) northward component of the electric field in ion frame (blue), Hall electric field (green, red), and convection electric field (black). Vertical dashed lines in (b-d) indicate the field aligned current events (i-iv). Black bars in (d) show the times of small-scale Hall-currents. (e-h) Average direction of the disturbance vectors of different parameters in northward (H) and duskward (D) direction during event (i-iv). Vertical width of orange area in (e-h) represents the thickness of the field-aligned current sheet.

PLASMA FLOW PATTERNS IN AND AROUND MAGNETOSHEATH JETS

The magnetosheath is commonly permeated by localized high-speed jets downstream of the quasi-parallel bow shock. These jets are much faster than the ambient magnetosheath plasma, thus raising the question of how the plasma reacts to incoming jets. A statistical analysis has been performed, based on 662 cases of one *THEMIS* spacecraft observing a jet and another (second) *THEMIS* spacecraft providing context observations of nearby plasma, to uncover the flow patterns in and around jets (see Fig. 11).

The following results are found: along the jet's path, slower plasma is accelerated and pushed aside ahead of the fastest core jet plasma (see yellow and orange areas in Fig. 11). Behind the jet core, plasma flows into the path to fill the wake. This evasive plasma motion affects the ambient magnetosheath, close to the jet's path. Diverging and converging plasma flows ahead and behind the jet are complemented by plasma flows opposite to the jet's propagation direction, in the vicinity of the jet. This vortical plasma motion results in a deceleration of ambient plasma when a jet passes nearby.

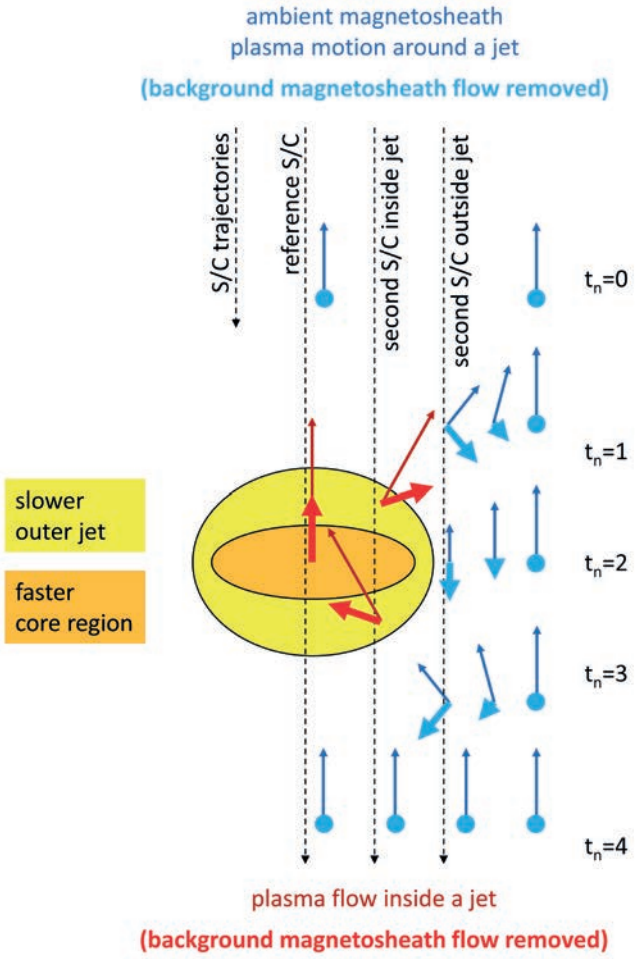

Fig. 11: Illustration showing the motion of ambient magnetosheath plasma (blue) and jet plasma (red) within and in the vicinity of a jet. Bold arrows show motion after subtracting the magnetosheath background flow.

SELF-CONSISTENT TANGENTIAL-DISCONTINUITY-TYPE CURRENT SHEET

The description of the dynamics of charged-particles in an inhomogeneous magnetic field is a fundamental problem in space plasma physics. Since this dynamics has the characteristics of a nonlinear oscillator, the traditionally used approaches involve certain limiting conditions regarding the scales of magnetic field, particle motion, and the assumptions about conservation of specific invariants (e.g., the magnetic momentum, integrals of action etc.). Such approaches naturally restrict the details considered in the particle dynamics which are described in terms of integral characteristics and averaged parameters of motion. However, in some regions, the exact account of particle trajectory details and the motion features (e.g., the phase of gyration) are of crucial importance.

A method for the description of particle dynamics, based on a new system of differential equations for the particle pitch-angle and gyro-phase derived from the analysis of the particle trajectory in a given magnetic field (Fig. 12), has been developed. It enables an easy and self-consistent description of a number of elementary problems, which form the basis for more complex natural cases in space physics. The developed method can generalize the case of particle ensembles, which enables finding a set of self-consistent solutions for tangential current sheets in the frame of a kinetic approach.

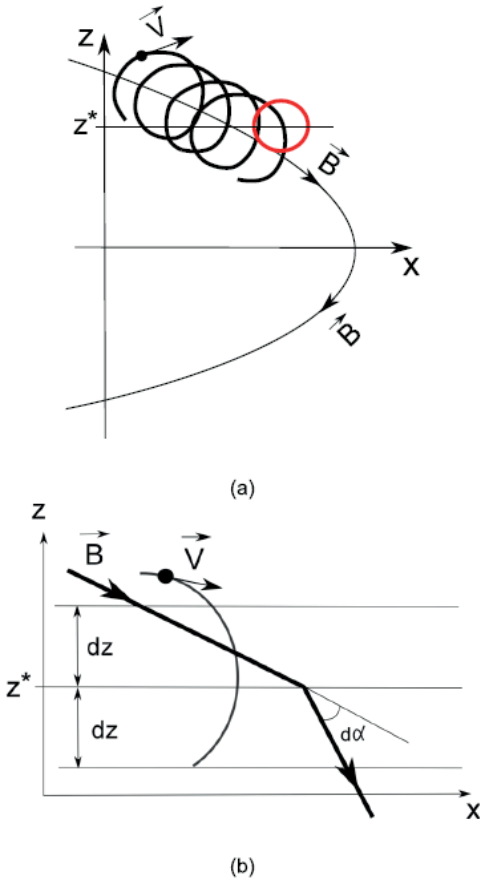

Fig. 12: Example of particle trajectory in a given magnetic field geometry.

SOLAR SYSTEM

IWF is engaged in many missions, experiments and corresponding data analysis addressing solar system phenomena. The physics of the Sun and the solar wind, its interaction with solar system bodies, and various kinds of planetary atmosphere/surface interactions are under investigation.

SUN & SOLAR WIND

The Sun's electromagnetic radiation, magnetic activity, and the solar wind are strong drivers for various processes in the solar system.

SOLAR ORBITER

Solar Orbiter is a future ESA space mission to investigate the Sun, scheduled for launch in 2020 (Fig. 13). Flying a novel trajectory, with partial Sun-spacecraft corotation, the mission plans to investigate in-situ plasma properties of the near solar heliosphere and to observe the Sun's magnetized atmosphere and polar regions.

IWF has built the Digital Processing Unit (DPU) for the *Radio and Plasma Waves (RPW)* instrument aboard *Solar Orbiter* and has calibrated the *RPW* antennas, using numerical analysis and anechoic chamber measurements. Furthermore, the institute has contributed to the magnetometer.

RPW will measure the magnetic and electric fields at high time resolution and will determine the characteristics of magnetic and electrostatic waves in the solar wind from almost DC to 20 MHz. Besides the 5 m long antennas and the AC magnetic field sensors, the instrument consists of four analyzers: the thermal noise and high frequency receiver; the time domain sampler; the low frequency receiver; and the bias unit for the antennas. The control of all analyzers and the communication will be performed by the DPU, developed by IWF.

Fig. 13: The Solar Orbiter spacecraft at the premises of prime contractor Airbus Defence and Space in Stevenage, UK (© Airbus Defence and Space).

ENSEMBLE PREDICTION OF A HALO CME USING HELIOSPHERIC IMAGERS

The "ELlipse Evolution model based on HI observations" (ELEvoHI) is a prediction utility designed to forecast arrivals of coronal mass ejections (CMEs) at Earth or at other planets in the inner heliosphere. It uses the advantage of side-view observations performed by the heliospheric imagers (HI) aboard *STEREO*, enabling continuous observations of CMEs throughout their propagation up to 1 AU and beyond. These white-light images are the main input for the ELEvoHI forecasting tool. Other input data come from solar wind in situ observations at 1 AU and from coronagraph observations. The latter provide information on the shape of the CME portion propagating within the ecliptic plane, the region of interest for the prediction.

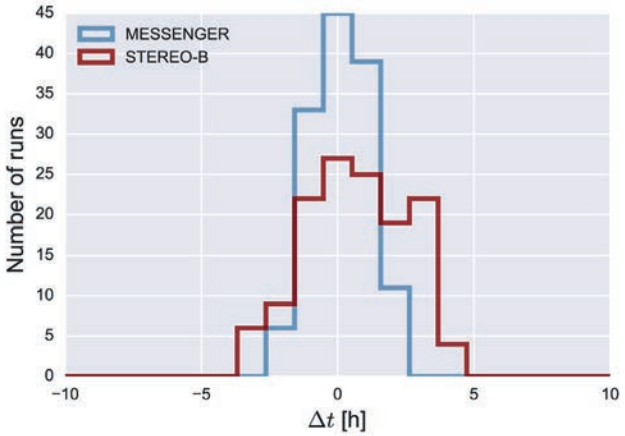

Fig. 14: Distribution of the ELEvoHI ensemble prediction for *MESSENGER* (blue) and *STEREO-B* (red).

ELEvoHI includes an interaction of the CME with the ambient solar wind leading either to a deceleration or an acceleration of the CME. In the current study, ELEvoHI was enhanced to be able to perform ensemble modeling. This is done by varying the input parameters of the CME frontal shape leading to a set of different prediction runs and therefore to an estimation of the prediction uncertainty (Fig. 14). ELEvoHI ensemble prediction was applied to a halo CME, remotely observed from *STEREO-B* and in situ detected by the *MESSENGER* spacecraft and *STEREO-B*. The almost exact arrival predictions for this event encourage the further development of ELEvoHI to prepare it for real-time predictions in the near future.

EQUATORIAL MHD SHALLOW-WATER WAVES IN THE SOLAR TACHOCLINE

The influence of a toroidal magnetic field on the dynamics of shallow-water waves in the solar tachocline is studied. A sub-adiabatic temperature gradient in the upper overshoot layer of the tachocline provides a negative buoyancy force to the deformed upper surface, which feels less gravitational field compared to the real gravity. This reduced gravity causes a significant reduction of the surface gravity speed, which leads to trapping of the shallow-water waves near the equator. It also increases the Rossby wave period up to the timescale of solar cycles (11 years). It is found that the toroidal magnetic field splits equatorial Rossby waves into fast and slow magneto-Rossby modes. For a reasonable value of normalized reduced gravity, global equatorial fast magneto-Rossby waves have a periodicity of 11 years, matching the timescale of activity cycles (Fig. 15).

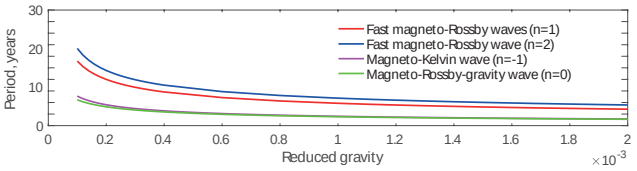

Fig. 15: Periods of global magneto-Rossby and magneto-Kelvin waves vs the normalized reduced gravity (n is the poloidal wave number).

The solutions are confined around the equator between latitudes ±20°–40°, coinciding with the sunspot activity belts. Equatorial slow magneto-Rossby waves have a periodicity of 90-100 years, resembling the Gleissberg cycle, the observed long-term modulation of the cycle strength. The equatorial magneto-Kelvin waves have a periodicity of 1-2 years and may correspond to the observed annual and quasi-biennial oscillations. It is also found that equatorial magneto-inertia-gravity waves have periods of hundreds of days and may be responsible for the observed Rieger-type periodicity. The equatorial MHD shallow-water waves in the upper overshoot tachocline capture all time-scales of observed variations in solar activity for expected physical parameters of the tachocline. The equatorial waves might play a distinct role in the temporal evolution of the solar magnetic field and hence in the solar dynamo.

MAGNETIC HELICITY IN THE CORONA OF THE SUN

A long-standing topic in Solar and Heliospheric physics research is the mechanism that heats the corona, the outer atmosphere of the Sun, to millions of °C. The corona is hence much hotter than the surface of the Sun. In particular, there are hot loops in the corona that emit EUV light. Computer simulations have now reproduced several loops in the core of the active region (CL1) at the location where they were really observed. From the model data the magnetic helicity is deduced, which can be understood as a twist within the magnetic fields. This helicity is particularly strong and changes its sense (from left- to right-handed) along the strongly heated loop CL1 in the corona. Magnetic helicity can be determined also in the heliosphere, where the same sign as on the solar surface is expected. But, so far, the heliospheric observations from the *Ulysses* mission show the opposite sign. A reversal of the helicity within the corona is now found, which can explain the *Ulysses* observations from the inner heliosphere (Fig. 16).

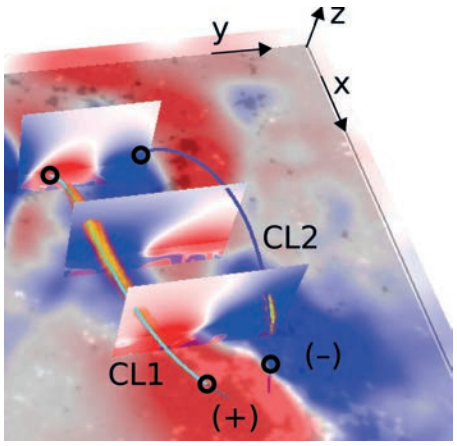

Fig. 16: 3D visualization of the magnetic helicity (red and blue for positive and negative helicity) above an active region in the solar corona. The gray background is the solar surface, where white and black are patches of strong magnetic fields with opposite polarity. Orange shows where extreme-UV light is emitted along loops (colored lines).

NONLINEAR DENSITY FLUCTUATIONS IN THE SHOCK-UPSTREAM PLASMA

Shock-upstream plasma in interplanetary space exhibits large-amplitude disturbances in the plasma density and the magnetic field, and serves as a natural laboratory of waves and nonlinear processes in space plasma. Using in-situ *Cluster* spacecraft data, the density fluctuations are found to be largely correlated to the magnetic field fluctuations which justifies the linear-mode picture of plasma dynamics (magnetosonic wave). Moreover, deviations of the density fluctuations from the linear-mode are found to be weakly and nonlinearly correlated to the magnetic energy density, which supports the theoretical prediction of quasi-static balance; that the nonlinear density response in plasma is controlled by the magnetic energy density and the thermal condition of the plasma (Fig. 17).

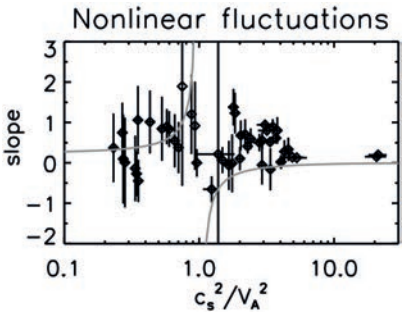

Fig. 17: Slope value of the nonlinear relation between plasma density and magnetic energy density as a function of the sound speed to the Alfvén speed squared, a measure of plasma thermal pressure. Data points represent the measurements in the shock-upstream plasma and curves in gray represent the theoretical prediction.

MERCURY

Mercury is now in the center of attention because of the ESA/JAXA *BepiColombo* mission. The planet has a weak intrinsic magnetic field and a mini-magnetosphere, which strongly interacts with the solar wind.

BEPICOLOMBO

The launch of *BepiColombo* was one of the great space flight events in 2018. The two spacecraft, JAXA's *Magnetospheric (MMO)* and ESA's *Planetary Orbiter (MPO)*, which will simultaneously explore Mercury and its environment from 2026, took off from the European spaceport in Kourou, French Guiana, aboard an Ariane-5 rocket on 20 October.

IWF played a major role in developing the magnetometers for this mission: it is leading the magnetometer investigation aboard the *MMO (MMO-MGF)* and responsible for the overall technical management of the *MPO* magnetometer *(MPO-MAG)*. For *MPO*, IWF also led the development of *PICAM*, an ion mass spectrometer with imaging capability, which is part of the *SERENA* instrument suite, to explore the composition, structure, and dynamics of the exo-ionosphere.

In the months until the launch, the spacecraft systems and their payload saw the final tests in Europe, the transportation to South America on board of two Antonov airplanes, the mating of all *BepiColombo* elements and finally the installation on the rocket only seven days before launch. The final functional test of the instruments on earth were completed on the first weekend of May and the payload was declared flight ready.

The launch, the spacecraft separation, the first acquisition of a signal, the solar array and antenna as well as magnetometer boom deployments all ran according to plan. One of three onboard monitoring cameras provided the first spectacular image from space only a few hours after launch (Fig. 18).

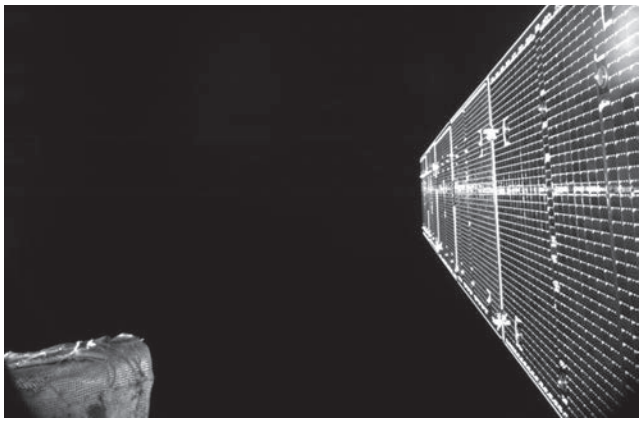

Fig. 18: First image by the onboard monitoring camera installed on the BepiColombo Mercury Transfer Module (MTM). The view looks along one of the extended solar arrays. The structure in the bottom left corner is one of the sun sensors on the MTM, with the multi-layered insulation clearly visible. (Credits: ESA/BepiColombo/MTM).

The first power-on of the two magnetometers including detailed commissioning took place end of October and beginning of November. *MPO-MAG* was even turned on before boom deployment, which allowed for a characterization of the spacecraft magnetics during the deployment (Fig. 19). All magnetic field sensors are in good health and in-flight calibration has already been started. While *MMO-MGF* was kept on only for a few hours, since the *MMO* spacecraft is sitting within the Sun shield during the cruise phase, *MPO-MAG* was already successfully operated over several weeks.

As the last sensor of all, *PICAM* was turned on in the frame of the *SERENA* commissioning on 15 December. After the acquisition of the first "Hello, world" from space, checkouts of the low and the high voltage circuits verified, that the sensor survived the launch without damages. Transition to science mode was tested successfully. The received science data contained all zeros as expected due to limitation of high voltage for safety measures. So calibration is left for the delta near-Earth commissioning phase in summer 2019.

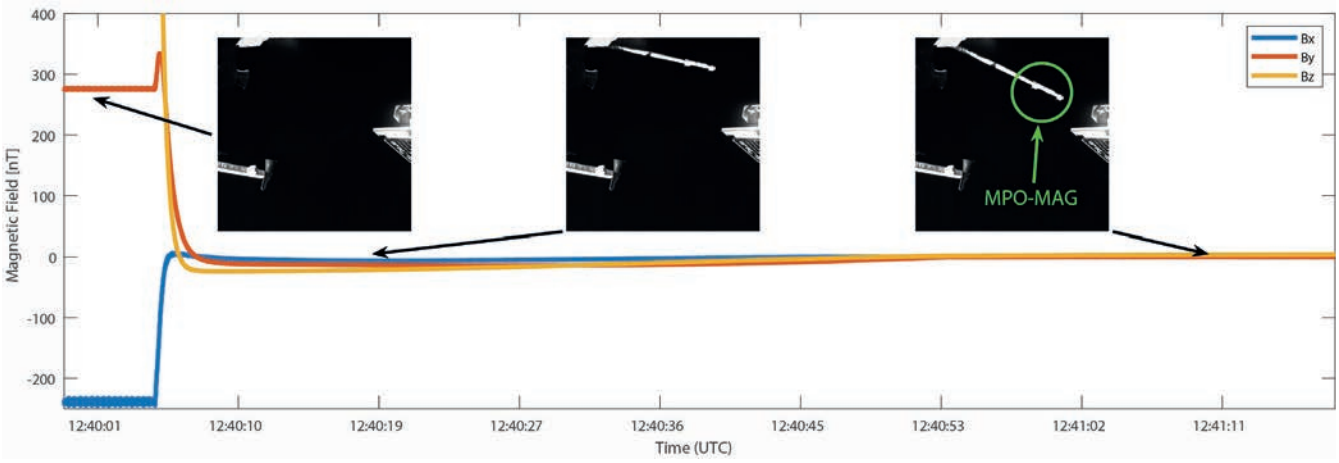

Fig. 19: *MPO* magnetometer measurements during boom deployment on 25 October with pictures taken by one of the selfie cameras of the *BepiColombo Mercury Transfer Module* (Credits: data: ESA/*BepiColombo/MPO*/MAG/TUBS-IGeP/IC London/IWF Graz; images: ESA/*BepiColombo/MTM*).

VENUS

Just inside the Earth's orbit around the Sun at 0.7 AU, the terrestrial planet Venus has a radius slightly smaller than Earth and is differentiated, but does not exhibit an internal magnetic field. Venus is characterized by a very dense atmosphere and generates a so-called induced magnetosphere by its interaction with the solar wind.

IMF PENETRATION THROUGH THE IONOSPHERE OF VENUS

Although Venus does not have an intrinsic magnetic field, interplanetary magnetic field can potentially penetrate the ionosphere of Venus by the diffusion process and permeate the planetary surface and interior. For the first time the magnetic diffusion time is quantitatively estimated. Over this time scale the magnetic field can penetrate the ionosphere of Venus and reach the planetary surface. The calculation is based on the estimate of Pedersen conductivity using the electron density data from *Pioneer Venus Orbiter*, the theoretical profile for the neutral-electron and neutral ion collision frequencies at Venus, and the magnetic field profile from *Venus Express*. The magnetic diffusion time falls in the range between 12 hours (under solar minimum conditions) and 54 hours (under solar maximum conditions, Fig. 20). Penetration of the interplanetary magnetic field through the ionosphere of Venus is possible when the solar activity and the solar wind remain undisturbed for a period of several days.

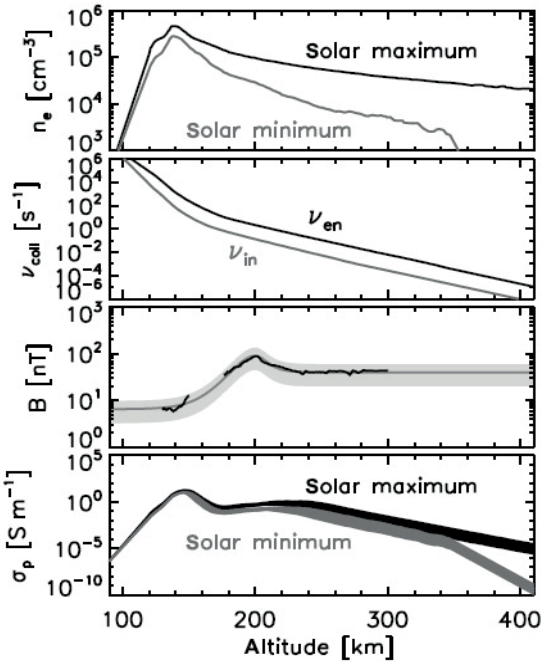

Fig. 20: Electron number density n_e from *Pioneer Venus Orbiter* radio occultation measurement, model collision frequency between electrons and neutral particles ν_{en} and that between ions and neutral particles ν_{in}, magnetic field B from *Venus Express* and model magnetic field with a fluctuation range (in gray), and Pedersen conductivity σ_p as a function of the altitude from the surface of Venus.

TURBULENCE IN THE VENUSIAN MAGNETOSHEATH

The characteristic scaling features of fluctuations in the dayside Venusian magnetosheath downstream of the bow shock were investigated using *Venus Express* data. A bow shock comes in two different types: the quasi-parallel (Q_{par}) where the bow shock normal and the interplanetary magnetic field (IMF) are quasi-parallel, and the quasi-perpendicular (Q_{perp}) bow shock where the two are perpendicular. Depending on behind which kind of bow shock the magnetic field fluctuations were measured in the magnetosheath, it was found that the characteristic scaling features of the fluctuations and turbulence were different. Although the Venusian dayside magnetosheath is much thinner than the Earth's magnetosheath, fully developed turbulence can be still observed downstream of the Q_{perp} bow shock (Fig. 21 left), while the turbulence is not dominant downstream of Q_{par} bow shock (Fig. 21 right). This means that the source of the turbulence in the Venusian magnetosheath is likely to be the Q_{perp}IMF.

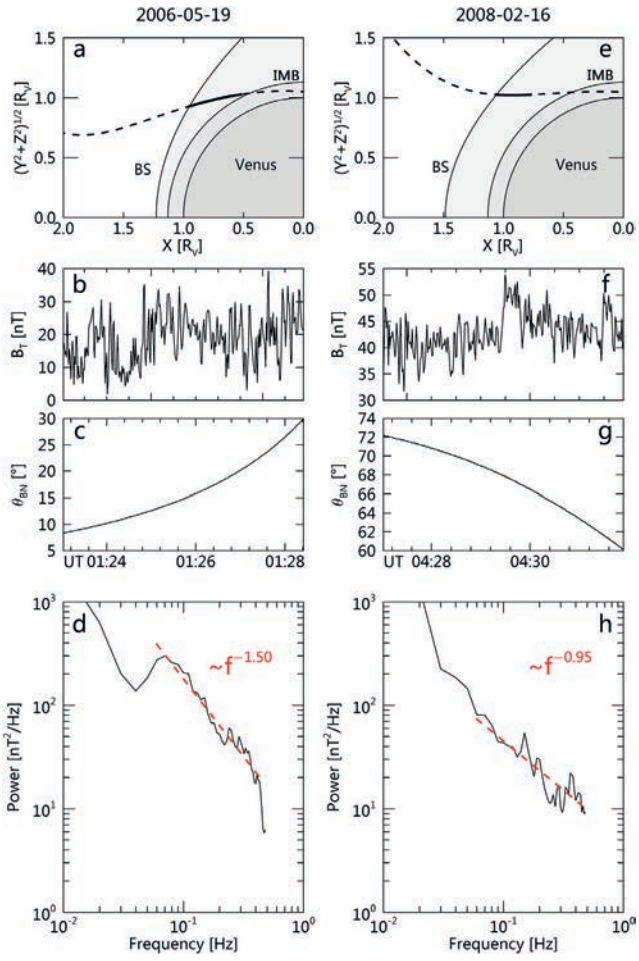

Fig. 21: *Venus Express (VEX)* trajectories, magnetic fields, the shock normal angles, and power spectrum densities for two downstream intervals of a Q_{par} bow shock on 19 May 2006 (left) and a Q_{perp} bow shock on 16 February 2008 (right). The left case with α ~1.50 in the bottom panel indicates a developed turbulence during this interval. The right case with α ~0.95 indicates that 1/f noise dominates during this interval.

MARS

Just outside the Earth's orbit around the Sun at 1.5 AU, the terrestrial planet Mars has half the radius of the Earth. It is differentiated, but only exhibits remnant surface magnetization of a now defunct internal dynamo. Mars is characterized by a very tenuous atmosphere and generates a so-called induced magnetosphere by its interaction with the solar wind.

CHINESE MARS MISSION

China plans a Mars orbiter, lander, and rover mission to be launched in 2020. The main mission will conduct a comprehensive remote sensing of the Red Planet, as well as surface investigation. IWF contributes to a magnetometer, of which the Qualification Model was delivered in summer.

INSIGHT

NASA's Mars mission was launched in May and successfully landed in Elysium Planitia on 26 November 2018. After first checkouts the seismometer instrument has already been deployed, while the *HP³ (Heat flow and Physical Properties Probe)* instrument will be put on the ground and start penetrating by the end of January or begin of February 2019. *HP³* will measure the internal heat flux of Mars as well as the thermal and mechanical properties of the Martian regolith. In order to describe the penetration progress and to derive soil mechanical parameters for the first couple of meters of the regolith two numerical models have been developed at IWF (Fig. 22).

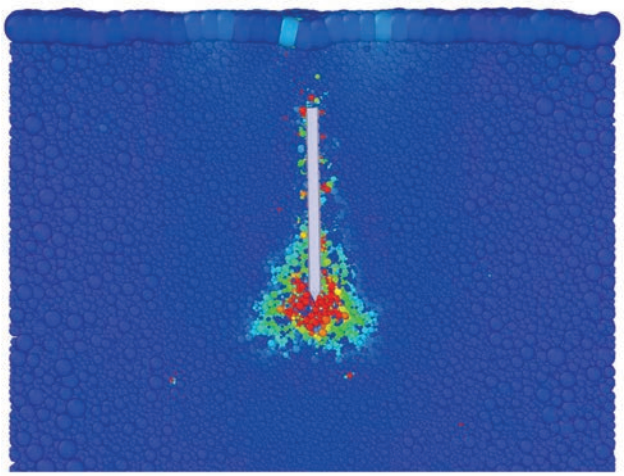

Fig. 22: Discrete element or particle code model describing the soil displacement during one hammer stroke of the *HP³* deployment mechanism.

MELTING PROBE EXPERIMENTS

A series of experiments focusing on the performance of melting probes under Mars surface environmental conditions was performed in the planetary chamber of the IWF. Hereby the influence of sand layers embedded in the Mars polar near-surface ice was studied, as well as the performance in CO_2-ice layers. The main result of the performed tests was that, even at surface pressures below the water triple point, the liquid phase exists temporarily around the heated melting tip. This allows for successful ice penetration under Mars surface conditions, with a realistic electrical power demand. Therefore a melting probe would be a useful alternative to mechanical drilling for any lander mission aiming at the exploration of the layered structures of the Martian polar regions, which are considered to contain key information about the evolution of the Martian climate in the recent past. Fig. 23 shows an ice sample at the end of a melt penetration experiment.

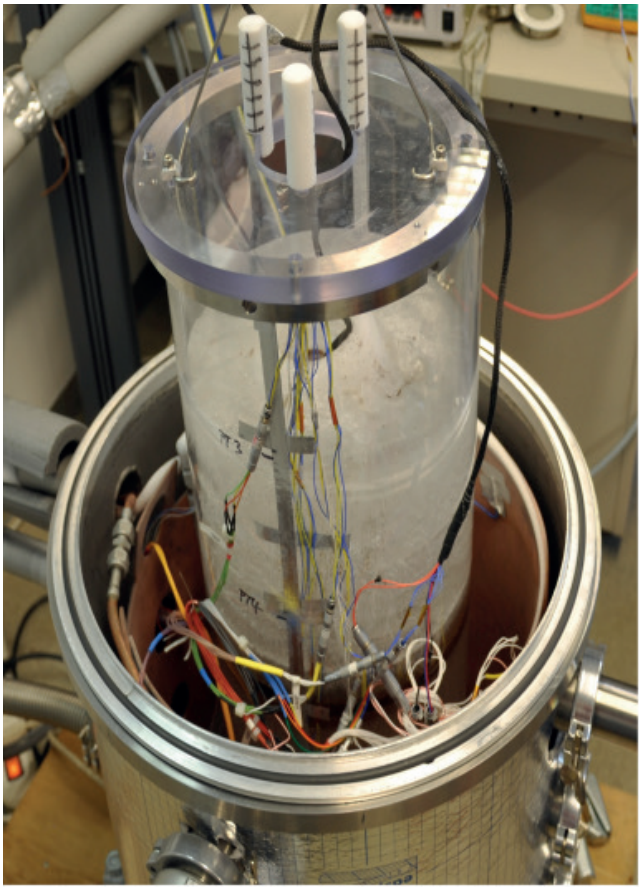

Fig. 23: Ice sample positioned inside the planetary chamber at the end of a melting probe test.

JUPITER

Jupiter, the largest planet in our solar system, mainly consists of hydrogen and helium. It is magnetized and rotates rapidly, leading to a rotationally dominated magnetosphere, where strong sources of radio emissions are located.

JUICE

ESA's first Large-class mission *JUpiter ICy moons Explorer (JUICE)* is planned for launch in 2022 and arrival at Jupiter in late 2029 or early 2030. *JUICE* will spend at least three years orbiting around Jupiter, making detailed observations of the gas giant and three of its largest moons, Ganymede, Callisto, and Europa. At the end of the mission *JUICE* will go into orbit around Ganymede. IWF is taking part as Co-I for three different selected instrument packages.

The *Jupiter MAGnetometer (J-MAG)* is led by Imperial College London and will measure the magnetic field vector and magnitude in the bandwidth DC to 64 Hz in the spacecraft vicinity. It is a conventional dual sensor fluxgate configuration combined with an absolute scalar sensor based on more recently developed technology. Science outcome from *J-MAG* will contribute to a much better understanding of the formation of the Galilean satellites, an improved characterization of their oceans and interiors, and will provide deep insight into the behavior of rapidly rotating magnetized bodies. IWF supplies the atomic scalar sensor for *J-MAG*, which is developed in collaboration with TU Graz. In 2018, the Engineering Model was tested and delivered to the prime contractor, the design of the Qualification Model was finalized and the Critical Design Review was passed.

The *Particle Environment Package (PEP)* is a plasma package with sensors to characterize the plasma environment of the Jovian system and the composition of the exospheres of Callisto, Ganymede and Europa. IWF participates in the *PEP* consortium on Co-I basis in the scientific studies related to the plasma interaction and exosphere formation of the Jovian satellites.

IWF is also responsible for the calibration of the *RWI* antennas, which are part of the *Radio and Plasma Wave Investigation (RPWI)*. In 2018, a so-called rheometry measurement with a scaled *JUICE* spacecraft model, which is shown in Fig. 24, was performed.

The model was immersed in a water-filled tank with a homogeneous electric field applied to it. By rotation the locations of the maxima and minima of the voltages induced in the *RWI* dipoles were measured. By using at least two different suspensions of the model, it was possible to derive the so-called effective length vector of each dipole, which describes the reception properties of each antenna in the quasi-static frequency range. The effective length vectors from rheometry were found to be within a few degrees of the result from numerical computer simulations with *JUICE* patch-grid models. Only with a calibrated antenna system it will be possible to derive accurate results for the polarization and the incoming wave direction in future radio wave measurements at Jupiter.

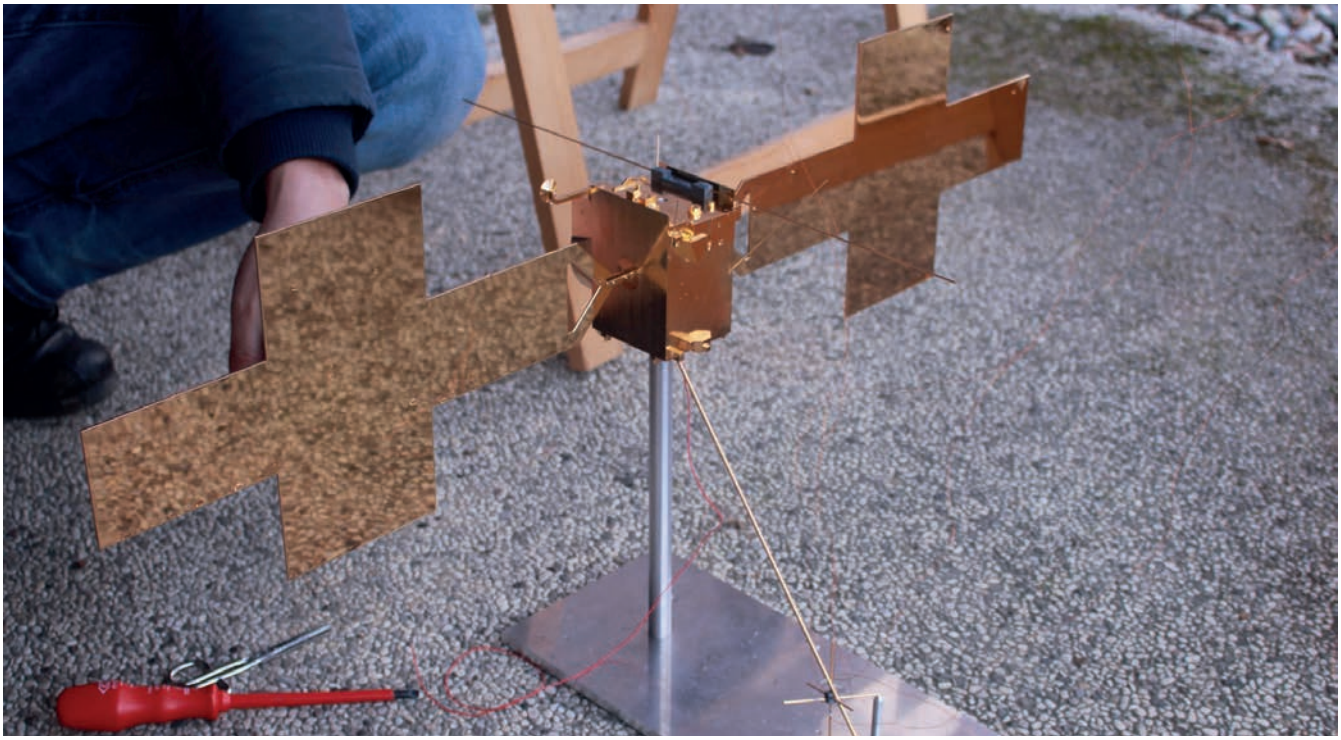

Fig. 24: The *RWI* antennas, which are located on the long magnetometer boom, are adjusted before the gold-plated 1:40 *JUICE* spacecraft model is put into the rheometry tank.

THE IO PLASMA TORUS LOCATION: VOYAGER 1 OBSERVATIONS

The Io Plasma Torus (IPT) is a doughnut-shaped gaseous cloud around Jupiter, centered on Io's orbit, consisting mainly of sulfur and oxygen. It is created by the volcanic activity of Io, which spews out 1 tonne of SO_2 per second into the Jovian magnetosphere. This gas gets dissociated and ionized and thereby creates the IPT. Through unknown processes, this torus is offset from the center of Jupiter, the distances of the approaching and receding side (related to the rotation of Jupiter) of the IPT are different and longitude dependent. *Voyager 2* and ground-based observations found average locations of 5.97 R_J (app) -5.59 R_J (rec) and 5.85 R_J (app) -5.57 R_J (rec) respectively. Recently analyzed data from *Voyager 1*, looking at the IPT from a direction almost perpendicular to *Voyager 2*, showed again a different location of 5.75 R_J (app) -5.88 R_J (rec). Knowing the average location of the IPT can help to find the reason of the offset.

However, also longitudinal variations in the IPT distance from Jupiter are found, as shown in Fig. 25. From each observatory the data are fitted by a 2nd order Fourier fit. The approaching side shows that, apart from different average distances, there is a clear similar periodicity in the signals. The receding side, however, shows that the *Voyager 1* observations do not follow the periodicity of the other observatories. The reason for this is, as yet, unknown, but it could be related to that the receding side for *Voyager 1* is located near the sub-solar point of the Jovian magnetosphere.

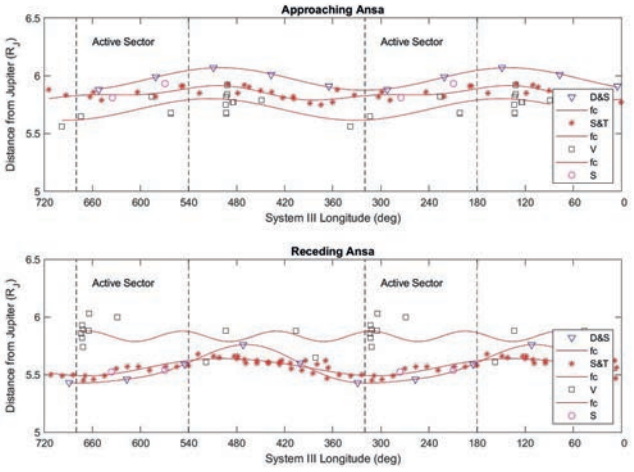

Fig. 25: Location of the IPT for the approaching (top) and receding side (bottom) with the data fitted with a 2nd order Fourier fit. For the receding side it is clear that the Voyager 1 observations do not follow the *Voyager 2* or ground based observations.

ZEBRA PATTERNS IN DAM

The first systematic analysis of zebra pattern events in the decametric radio emission (DAM) of Jupiter was performed. These rare radio fine structures were observed in a frequency range from 12-30 MHz by the large ground-based radio telescope URAN-2 in the Ukraine. Zebra patterns are quasi-harmonic bands of enhanced brightness that can last up to several minutes (see Fig. 26). They are strongly polarized radio events with intensities of 1-2 orders of magnitude lower than Io-controlled DAM. It was found that their occurrence does not depend on the position of Jupiter's moon Io, but is strongly controlled by the Jovian central meridian longitude. Zebra patterns also occur in solar radio emissions, and their generation might be linked to the double plasma resonance with electrons or ions.

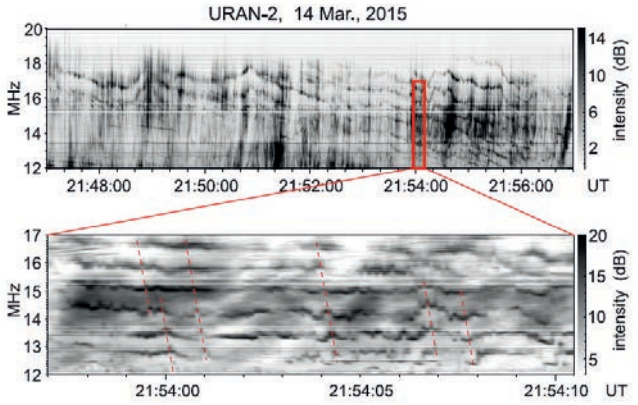

Fig. 26: Radio spectrum showing zebra patterns observed on 14 March 2015 (upper panel) and zoomed part (lower panel) with rapid oscillations in the frequency of the stripes.

COMETS & DUST

Comets and interplanetary dust are the remainders of the building blocks of the solar system, although dust can also be created by collisions of e.g. asteroids. *Rosetta*'s successful mission at comet 67P/Churyumov-Gerasimenko (67P/CG) gave new life to the study of comets and is the starting point for new future missions to asteroids and comets.

FIRST OBSERVATIONS OF MAGNETIC HOLES DEEP WITHIN A COMET'S COMA

ESA's *Rosetta* spacecraft made ground-breaking observations of comet 67P/CG and of its cometary environment. Magnetic holes were investigated in that environment. These are significant depressions in the magnetic field strength, measured by the *Rosetta* magnetometer in April and May 2015. In that time frame of two months, 23 magnetic holes could be identified. The cometary activity was intermediate and increasing because 67P/CG was on the inbound leg toward the Sun. While in April solar wind protons were still observed by *Rosetta* near the comet, in May these protons were already mostly replaced by heavy cometary ions. Magnetic holes have frequently been observed in the solar wind. It is found, for the first time, that magnetic holes exist in the cometary environment even when solar wind protons are almost absent. Some of the properties of the magnetic holes are comparable to those of solar wind holes; they are associated with density enhancements, sometimes associated with co-located current sheets and fast solar wind streams, and are of similar scales. However, particularly in May, the magnetic holes near the comet appear to be more processed, featuring shifted density enhancements and, sometimes, bipolar signatures in magnetic field strength rather than simple depressions. The magnetic holes are of global size with respect to the coma. Nevertheless, at the comet, they are compressed owing to magnetic field pile-up and draping so that they change in shape (see Fig. 27). There, the magnetic holes become of comparable size to heavy cometary ion gyroradii, potentially enabling kinetic interactions.

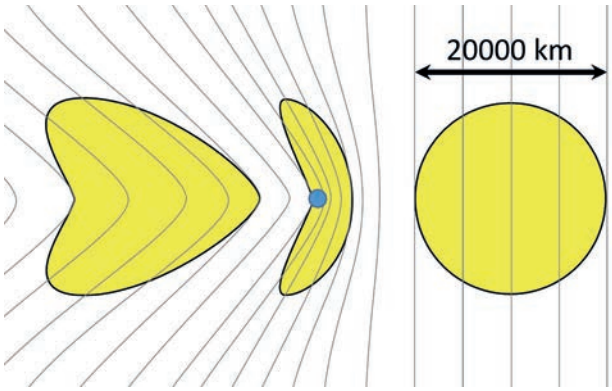

Fig. 27: Sketch of the deformation of a magnetic hole (yellow) due to interplanetary magnetic field pile up and draping at the cometary nucleus (position in blue).

ROSETTA TAIL EXCURSION

During *Rosetta*'s two-year mission around comet 67P/CG there were two "far-excursions" from the nucleus, one on the sunward-side and one on the tail-side. The latter took place towards the end of the mission, with the comet already 2.7 AU from the Sun, and therefore at low activity. Nevertheless, some interesting phenomena were found. Close to the comet, i.e. less than 500 km from the nucleus, the magnetic field did not show the classical draping pattern of a bi-lobal tail with magnetic field direction towards and away from the Sun as shown by the cone angle in Fig. 28. The magnetic field was mainly directed perpendicular to the classic tail with a clock-angle (defined as $\tan^{-1}(B_z/B_y)$) around 100°, indicating a vertical field. This can be explained by the deflection of the magnetic field caused by pick-up of freshly ionized water upstream of the comet, which is transported to the downstream region. Further away from the nucleus the field reverts to more classical draping. However, also here the field shows something new, the clock angle of the field increases steadily for *Rosetta* moving away and returning to the comet. This can only be explained by a traveling helical wave moving down the tail at a phase velocity of 136 m/s and an angular frequency around 5.7° per hour. This velocity and frequency does not correspond to any natural values in the plasma around 67P/CG, and thus the origin of this wave is, as yet, unclear.

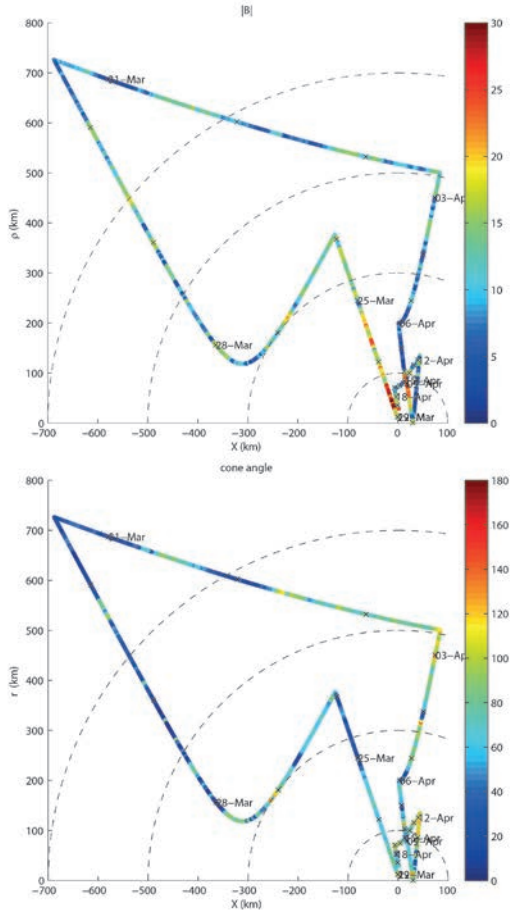

Fig. 28: The magnetic field strength and cone angle plotted along the orbit of Rosetta's tail excursion, in cylindrical coordinates.

EXOPLANETARY SYSTEMS

The field of exoplanet research (i.e. investigation of planets orbiting stars other than the Sun) has developed strongly in the past decades. Since the discovery of 51 Peg b, the first detected exoplanet orbiting a Sun-like star, about 3900 exoplanets, most in planetary systems, are now known. Improved instrumentation and analysis techniques have led to the finding of smaller and lighter planets, down to Earth-size, Earth-mass planets, some orbiting in the habitable zone of the cooler stars. However, super-Earths and ultra-hot Jupiters are now prime targets for atmospheric characterization, mostly because of their larger radii, which indicate the presence of a volatile-rich atmosphere and facilitate observations and analyses.

The main exoplanet missions in which IWF is involved are *CHEOPS*, *CUTE*, *PLATO*, and *ARIEL*. *CHEOPS* will precisely measure the radii of already known planets to greatly improve their inferred density and hence provide a first characterization. *CUTE* will obtain low-resolution near-ultraviolet transmission spectra of transiting giant planets to study upper atmospheres and mass loss processes. *PLATO* will look for planets in large portions of the sky, with the primary aim to find Earth-like planets in the habitable zone of Sun-like stars. *ARIEL* will collect low-resolution infrared transmission spectra of transiting planets to characterize planetary atmospheres, with the final goal of measuring C and O abundances, which constrain planet formation theories.

IWF concentrates on the study and characterization of planetary atmospheres using both theory and observations, focusing particularly on the analysis of exoplanet atmospheric escape and mass loss processes. Further research is conducted to study star-planet interactions and carry out atmospheric characterization through the collection and analysis of ground- and space-based observations.

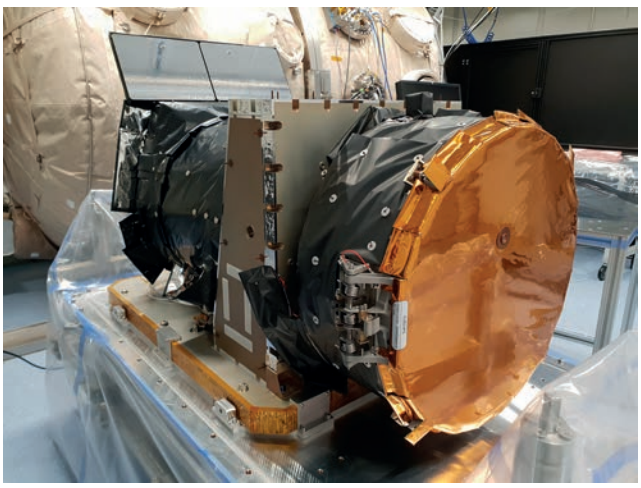

CHEOPS

CHEOPS (CHaracterising ExOPlanet Satellite), to be launched in 2019, will study extrasolar planets and observe planetary systems at an unprecedented photometric precision. The main science goals are to find transits of small planets, known to exist from radial-velocity surveys, measure precise radii for a large sample of planets to study the nature of Neptune- to Earth-sized planets, and obtain precise observations of transiting giant planets to study their atmospheric properties. IWF is responsible for the *Back-End-Electronics (BEE)*, one of the two on-board computers, which controls the data flow and the thermal stability of the telescope structure. In 2018, IWF participated in the close-out meetings declaring the flight worthiness for the *BEE* hardware and software. Finally, the *CHEOPS* spacecraft completed all environmental tests at spacecraft level successfully (Fig. 29).

CUTE

CUTE (Colorado Ultraviolet Transit Experiment) is a NASA-funded 6U-form CubeSat to be launched in the first half of 2020. It will perform low-resolution transmission spectroscopy of transiting extrasolar planets at near-ultraviolet wavelengths. *CUTE* will study the upper atmosphere of short period extrasolar planets with the aim of constraining atmospheric escape processes, which are key to understand planetary evolution, and detect heavy metals, which inform on the strengths of the atmospheric vertical velocities. Furthermore, *CUTE*'s continuous temporal coverage of planetary transits will allow to detect transit asymmetries, which are possibly connected with the presence of planetary magnetic fields, and to measure their strength.

IWF is the only technological contributor to the mission outside of the University of Colorado (Boulder), where *CUTE* is being developed. IWF has finalized the development of the *CUTE* data simulator, following a detailed analysis of the optical system and tolerances, and has started to develop the data reduction pipeline.

Fig. 29: The *CHEOPS* science instrument is ready for shipment after completion of the calibration (© University of Bern).

PLATO

PLATO (PLAnetary Transits and Oscillations of stars) is ESA's third Medium-class mission, led by DLR. Its objective is to find and study a large number of extrasolar planetary systems, with emphasis on the properties of terrestrial planets in the habitable zone around solar-like stars. *PLATO* has also been designed to investigate seismic activity in stars, enabling the precise characterization of the host star, including its age. IWF contributes to the development of the *Instrument Controller Unit (ICU)* with the development of the *Router and Data Compression Unit (RDCU)*. Launch is expected in 2026.

PLATO consists of 24 telescopes for nominal and two telescopes for fast observations. Each telescope has its dedicated front-end-electronics, reading and digitizing the CCD content. Six nominal and two fast DPUs collect the data from the front-end-electronics and extract the areas of interest. The *RDCU* is a key element in the data processing chain, providing the communication between the DPUs and the *ICU*. The second task of the *RDCU* is the lossless compression of the science data. For performance reasons, the compression algorithm is implemented in an FPGA.

Main tasks in 2018 were the finalization of the *RDCU* prototypes, the continuation with the design of the VHDL code and the development of the test environment. In total three prototypes have been built, two delivered to the project partners. The FPGA design concentrated on further tests of the SpaceWire core, and the development of the FPGA internal bus system and the memory handler. Thus the preliminary design, providing the full functionality of the compressor, has been completed.

ARIEL

ARIEL (Atmospheric Remote-sensing Exoplanet Large-survey) is ESA's fourth Medium-class mission, led by University College London, to be launched in 2028. It will investigate the atmospheres of several hundreds exoplanets to address the fundamental questions on how planetary systems form and evolve. During its four-year mission, *ARIEL* will observe 1000 exoplanets ranging from Jupiter- and Neptune-down to super-Earth-size in the visible and infrared with its meter-class telescope. The analysis of *ARIEL* spectra and photometric data will enable extracting the chemical fingerprints of gases and condensates in planetary atmospheres, including the elemental composition for the most favorable targets, with a particular focus on carbon and oxygen. Thermal and scattering properties of the atmosphere will also be studied.

ARIEL consists of a one meter telescope feeding two infrared low-resolution spectrographs and the fine guiding sensor (FGS), working in the optical. To improve the satellite's pointing stability, the FGS provides optical photometry of the target in three broad bands that are used to control instrumental systematics, measure intrinsic stellar variability, and constrain the presence of high-altitude aerosols in planetary atmospheres.

OTHER TELESCOPES

Members of the institute obtained 2.25 nights of observing time with the *FORS2* instrument at the *Very Large Telescope (VLT)* at the Paranal site of the European Southern Observatory (ESO), in Chile. These spectroscopic observations, conducted during planetary transits, will be used to study the physical properties of the atmosphere of close-in giant planets.

PHOTOMETRIC STELLAR ACTIVITY AND STARSPOT DIAGNOSTICS

Stellar X-ray emission plays an important role in the study of exoplanets as a proxy for stellar winds and as a basis for predictions of the EUV flux, unavailable for direct measurements. These are crucial factors, affecting the mass-loss of planetary atmospheres. The detection thresholds limit the number of stars with directly measured X-ray fluxes. In spite of that, the known connection between the sunspots and solar X-ray sources enables the development of an accessible proxy for the X-ray emission on the basis of the starspot variability. To realize this approach, the light curves of 1729 main-sequence stars from the *Kepler* data archive with rotation periods $0.5 < P < 30$ days and effective temperatures $3236 < T_{eff} < 7166$ K have been analyzed. The squared amplitude of the first rotational harmonic of a stellar light curve A_1^2 may be used as an activity index, related to a varying number of starspots (Fig. 30a). Being averaged, A_1^2 reveals practically the same connection with the Rossby number as the commonly used ratio Rx of the X-ray to bolometric luminosity (Fig. 30b). As a result, the regressions for stellar X-ray luminosity $L_x(P)$ (Fig. 30c) and its related EUV analogue, $L_{EUV}(P)$ Fig. 30d), were obtained for the main-sequence stars. These regressions predict the average values of $\log(L_x)$ and $\log(L_{EUV})$ with typical errors of 0.26 and 0.22, respectively.

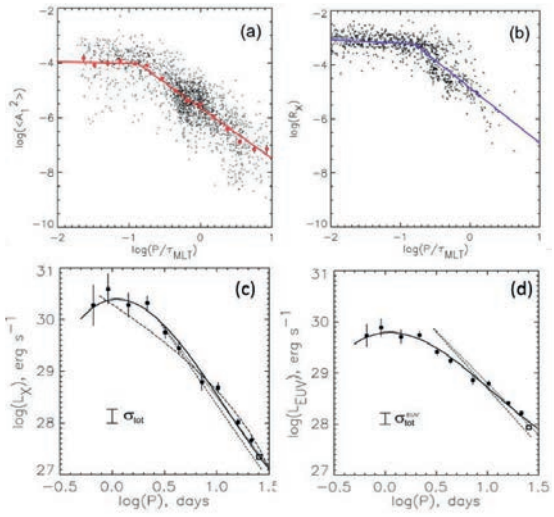

Fig. 30: Stellar activity indexes vs. the Rossby number averaged over the squared amplitude of the first rotational harmonic of the stellar light curves (a) and normalized to the X-ray luminosity (b). Solid line: predicted $L_x(P)$ (c) and $L_{EUV}(P)$ (d) for stars with $T_{eff} = 5770$ K; solid squares: averaged predictions for individual stars with $5500 < T_{eff} < 6000$ K.

SUPPRESSED FUV STELLAR ACTIVITY AND LOW PLANETARY MASS LOSS

WASP-18 hosts a massive, very close-in Jupiter-like planet. Despite its young age (< 1 Gyr), the star shows an anomalously low stellar activity level: the measured $\log R'_{HK}$ activity parameter lies slightly below the basal level, there is no significant time-variability in the $\log R'_{HK}$ value, and there is no detection of X-ray emission. Far-ultraviolet *Hubble Space Telescope (HST)* observations of WASP-18, obtained with the *Cosmic Origins Spectrograph (COS)* have been used to explain this anomaly.

The interstellar extinction, E(B-V), towards the star's line of sight has been measured, deriving a low value of 0.01 mag. This result has then been used to derive the interstellar medium (ISM) column density for a number of ions, concluding that ISM absorption is not the origin of the anomaly. The *COS* data have been used to measure the flux of the four stellar emission features detected in the spectrum, namely C II, C III, C IV, and Si IV. Comparisons of the C II/C IV flux ratio measured for WASP-18 with that derived from spectra of nearby stars with known age and similar spectral type showed that the far-UV spectrum of WASP-18 resembles that of old (>5 Gyr), inactive stars, in stark contrast with its young age (Fig. 31).

Therefore, it is most likely that WASP-18 has an intrinsically low activity level, possibly caused by star–planet tidal interaction. Re-scaling the solar irradiance reference spectrum to match the flux of the Si IV line, yielded a high-energy integrated flux at the planet orbit of 10.2 erg s^{-1} cm^{-2}. A hydrodynamic upper atmosphere code has been used to derive the planetary mass-loss rate obtaining a value of 10–20 Jupiter masses per Gyr. For such high-mass planets, thermal escape is not energy limited, but driven by Jeans escape.

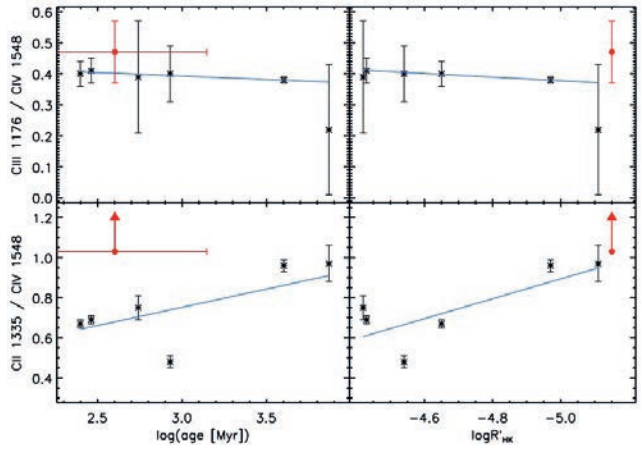

Fig. 31: Top panel: C III/C IV flux ratio as a function of stellar age (left) and $\log R'_{HK}$ value (right). WASP-18 is marked by a red circle, while the comparison stars are marked by black asterisks. The blue solid line shows the linear fit obtained by fitting the position of the comparisons stars. Bottom panel: same as the top panels, but for the C II/C IV flux ratio. Because of the possible contamination by the ISM, the C II/C IV flux ratio of WASP-18 is a lower limit.

STARSPOT VARIABILITY TIMESCALES

The stability of starspot distributions over hemispherical scales was studied by the analysis of the rotational spot variability of 1998 main-sequence stars observed by *Kepler*. It is found that in cool and fast rotators the large-scale activity patterns are much more stable than the small ones, whereas for hotter and/or slower rotating stars such difference is less pronounced. This effect is explained in terms of two mechanisms: (1) the diffusive decay of long-living spots in activity complexes of stars with a saturated magnetic dynamo, and (2) the spots emergence, modulated by turbulent gigantic convection flows in stars with weaker magnetism. This opens a way for the investigation of stellar deep convection, which is inaccessible for astroseismology. Moreover, an effect of sub-diffusion in stellar photospheres, characterized by the nonlinear dependence of the squared displacement of a magnetic element with time, was revealed from observations for the first time.

A diagnostic diagram (Fig. 32) was proposed that differentiates stars in the P-T_{eff} parameter space with respect to the dominating mechanism of their spot variability quantified in terms of the gradient function $\beta_{12} = [\log(\tau_2) - \log(\tau_1)]/\log(2)$, where τ_2 and τ_1 are the time-scales of variability of the squared amplitudes of first and second rotational harmonics of the stellar light-curve. The values of β_{12} = -2/3, -2, < -2, and -1 correspond to the domination of Kolmogorov-like turbulence, magnetic diffusion, sub-diffusion, and differential rotation, respectively.

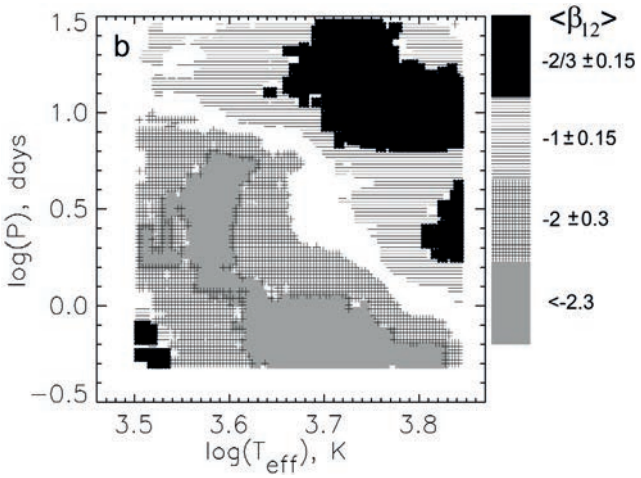

Fig. 32: Diagnostic diagram of stellar sample with respect to a dominating mechanism of spot variability.

EUV RADIATION FROM A-TYPE STARS: EFFECTS ON ULTRA-HOT JUPITERS

Extremely irradiated, close-in planets to early-type stars might be prone to strong atmospheric escape. A thorough literature review of X-ray-to-optical measurements has been performed, showing that for intermediate-mass stars (IMS) cooler than about 8250 K, the X-ray and EUV (all together XUV) fluxes are on average significantly higher than those of solar like stars, while for hotter IMS, because of the lack of surface convection, it is the opposite. Spectral energy distributions (SEDs) for prototypical IMS have been constructed and compared to solar (Fig. 33). The XUV fluxes relevant for upper planet atmospheric heating are highest for the cooler and lowest for the hotter IMS, while the UV fluxes increase with increasing stellar temperature.

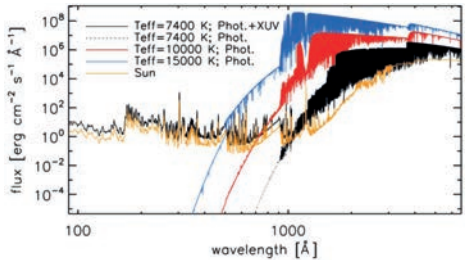

Fig. 33: Comparison between non-LTE SEDs computed for IMS with temperatures of 7400 K (black) and 10000 K (red), and for the Sun (orange) and a 15000 K star (blue).

The influence of this characteristic of the stellar fluxes on the mass loss of close-in planets has been evaluated by simulating the atmospheres of planets orbiting EUV-bright (WASP-33) and EUV-faint (KELT-9) A-type stars. For KELT-9b, the atmospheric expansion caused by heating due to absorption of the stellar UV and optical light drives mass-loss rates of the order of 10^{11} g s^{-1}, while heating caused by absorption of the stellar XUV radiation leads to mass-loss rates of the order of 10^{10} g s^{-1}, thus underestimating mass loss. For WASP-33b, the high XUV stellar fluxes lead to mass-loss rates of the order of 10^{11} g s^{-1}. Even higher mass-loss rates are possible for less massive planets orbiting EUV-bright IMS. It has been concluded that it is the weak XUV stellar emission, combined with a relatively high planetary mass, which limit planetary mass-loss rates, to allow the prolonged existence of KELT-9-like systems.

PRIMORDIAL ATMOSPHERES

Evidence that the growth time of proto-Venus and -Earth determined whether they originated after the nebular gas evaporated or whether they grew to larger masses while they were embedded in the nebula was investigated. In the later case, hydrogen could be captured around the protoplanet before the disk disappeared. Significant amounts of noble gases have been trapped from the protoplanetary disk, and were left in solar composition in the interiors of early Venus and Earth. Solar-like isotopes, which are embedded in the nebular gas, can enter the planetary interior via magma oceans that formed below the accumulated H_2-dominated envelopes. That early Venus and Earth evolved from primordial atmospheres is also in agreement with measurements of Ne isotopes in today's Earth atmosphere and the discovery of a huge number of exoplanets with masses slightly larger than the terrestrial planets but with over-sized radii. This indicates that nebular-based H_2-envelopes are a common phenomenon on small planets.

Fig. 34 illustrates the disk-captured protoatmospheres. The massive H_2/He atmospheres of large planets such as Jupiter, Saturn, Uranus and Neptune were formed because of gas capture onto rock and ice-dominated cores, while a much smaller H_2-envelope was lost via thermal escape from early Venus and Earth.

Fig. 34: Illustration of two protoatmosphere formation scenarios for terrestrial planets. The upper scenario illustrates the capture of nebula gases and the accumulation of H_2-dominated protoatmospheric layers around a protoplanetary core. In the case of protoplanet core masses that are < 1 M_{Earth}, the nebular gas can be lost to space via thermal boil off and EUV-driven hydrodynamic escape.

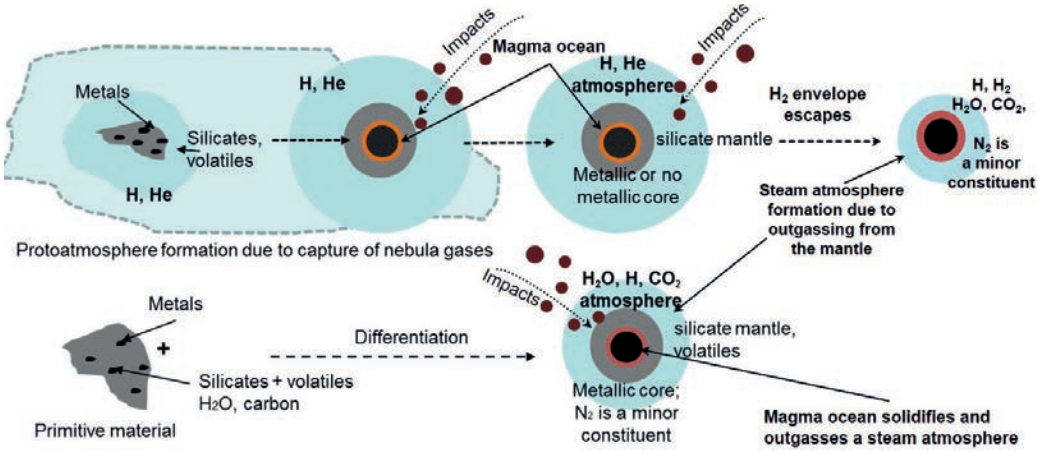

GRID OF UPPER ATMOSPHERE MODELS FOR EARTH-MASS PLANETS

There is growing observational and theoretical evidence suggesting that atmospheric escape is a key driver of planetary evolution. Commonly, planetary evolution models employ simple analytic formulae (e.g., energy limited escape) that are often inaccurate, and more detailed physical models of atmospheric loss usually only give snapshots of an atmosphere's structure and are difficult to use for evolutionary studies. To overcome this problem, an existing upper atmosphere hydrodynamic code has been employed and updated to produce a large grid of about 7000 models covering planets with masses ranging between 1 and 39 Earth masses with hydrogen-dominated atmospheres and orbiting late-type stars. The modeled planets have equilibrium temperatures ranging between 300 and 2000 K. For each considered stellar mass, three different values of the high-energy stellar flux (i.e., low, moderate, and high activity) have been accounted for.

For each computed model, the atmospheric temperature, number density, bulk velocity, X-ray and EUV (all together XUV) volume heating rates, and abundance of the considered species as a function of distance from the planetary center have been derived. From these quantities, the positions of the maximum dissociation and ionization, the mass-loss rate, and the effective radius of the XUV absorption have been derived. The obtained results are in good agreement with previously published studies employing similar codes. An interpolation routine capable to extract the modeling output parameters for any planet lying within the grid boundaries has been developed. The model grid has been used to identify the connection between the system parameters and the resulting atmospheric properties. Finally, the interpolation routine has been employed to estimate atmospheric evolutionary tracks for the close-in, high-density planets CoRoT-7 b (Fig. 35) and HD 219134 b,c. Assuming that the planets ever accreted primary, hydrogen-dominated atmospheres, the three planets must have lost them within a few Myr.

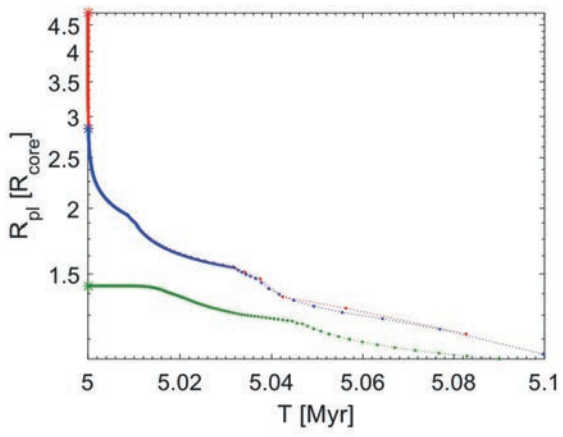

Fig. 35: Evolution of the planetary radius of CoRoT-7 b as a function of time. The colors indicate different initial radii, marked by the asterisks, which correspond to the values obtained by setting the restricted Jeans escape parameter Λ equal to 3 (red), 5 (blue), and 10 (green). The small dots placed along each line indicate the time steps.

YOUNG EXOPLANETS UNDER EXTREME UV IRRADIATION

The K2-33 planetary system hosts one transiting 5 Earth radii planet orbiting its young M-type host star. The planet's mass is still unknown, with an estimated upper limit of 5.4 Jupiter masses. The extreme youth of the system (< 20 Myr) gives the unprecedented opportunity to study the earliest phases of planetary evolution, at a stage when the planet is exposed to an extremely high level of high-energy radiation emitted by the host star. A series of 1D hydrodynamic simulations of the planet's upper atmosphere have been performed, considering a range of possible planetary masses, from 2 to 40 Earth masses, and equilibrium temperatures, from 850 to 1300 K, to account for internal heating as a result of contraction.

The main result is that the temperature profiles are mostly controlled by planetary mass, while the equilibrium temperature has a secondary effect. For planetary masses below 7-10 Earth masses, the atmosphere is subject to extremely high escape rates, driven by the planet's weak gravity and high thermal energy, which increase with decreasing mass and/or increasing temperature. For higher masses, the escape is, instead, driven by the absorption of the high-energy stellar radiation. A rough comparison of the timescales for complete atmospheric escape and age of the system indicates that the planet is more massive than 10 Earth masses (Fig. 36).

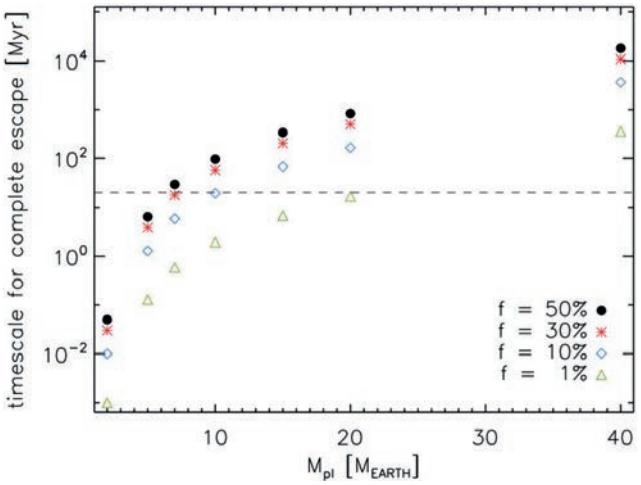

Fig. 36: Timescale, in Myr, estimated for the complete escape of a hydrogen-dominated atmosphere as a function of planetary mass, assuming four different values of the atmospheric mass fraction f of 50% (black dot), 30% (red asterisk), 10% (blue diamond), and 1% (green triangle). The horizontal dashed line indicates the maximum age (i.e. 20 Myr) derived for the K2-33 system.

ENERGY-LIMITED APPROXIMATION FOR PLANET ATMOSPHERIC ESCAPE

Studies of planetary atmospheric composition, variability, and evolution require appropriate theoretical and numerical tools to estimate key atmospheric parameters, among which the mass-loss rate is often the most important. In evolutionary studies, it is common to use the energy-limited formula, which is attractive for its simplicity, but ignores important physical effects and can be inaccurate in many cases. To overcome this problem, a recently developed grid of about 7000 one-dimensional upper-atmosphere hydrodynamic models has been considered to extract the mass-loss rates. An analytical expression for the atmospheric mass-loss rates based on a fit to the values obtained from the grid has been then derived. The expression provides the mass-loss rates as a function of planetary mass, planetary radius, orbital separation, and incident stellar high-energy flux. It has been shown that this expression is a significant improvement to the energy-limited approximation for a wide range of planets (Fig. 37). The analytical expression enables significantly more accurate planetary evolution computations without increasing computing time.

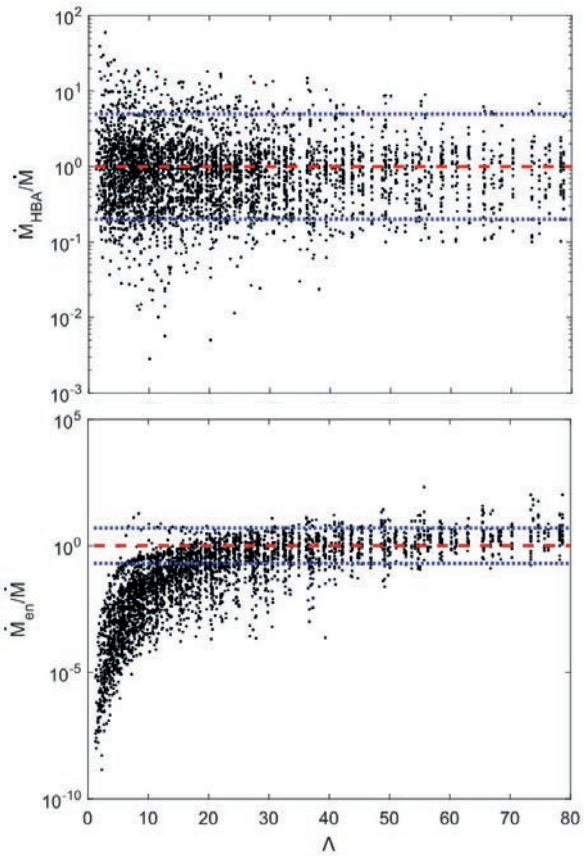

Fig. 37: Top: Ratio between the mass-loss rates obtained from the approximation based on hydrodynamic models and from the hydrodynamic grid as a function of the restricted Jeans escape parameter Λ. Bottom: Same as top, but for the mass-loss rates derived from the energy-limited formula. In both panels, the red line is at one, while the blue lines are at values of 5 and 0.2. Note the difference in the scale of the y-axis between the two plots.

RADIO PROPAGATION: SUPERMASSIVE HOT JUPITER

It was investigated if supermassive hot Jupiters such as Tau Bootis b provide better conditions for radio emission than less massive hot Jupiters. Planets like Tau Bootis b at different orbital locations (between its actual orbit of 0.046 and 0.2 AU) were studied. Due to the strong gravity of such planets and efficient radiative cooling, the upper atmosphere is (almost) hydrostatic and the exobase remains very close to the planet. Fig. 38 shows that hot supermassive planets are expected to have conditions that are more favorable for the generation of radio emission via the cyclotron maser instability than ordinary hot Jupiters such as HD 209458b and HD 189733b.

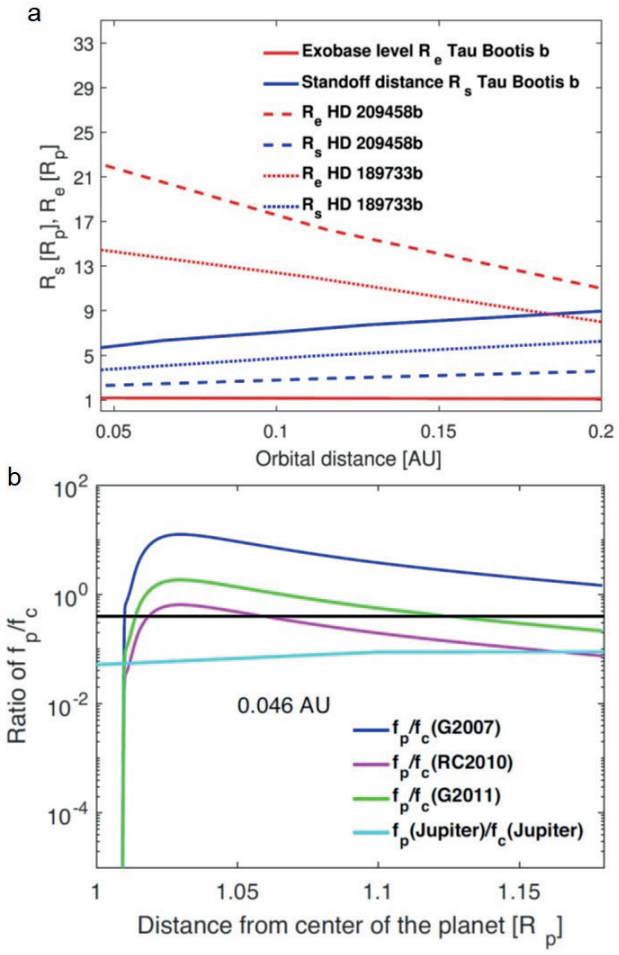

Fig. 38: Panel a: Exobase levels R_e compared to magnetopause standoff distances R_s as a function of magnetic moments predicted for Tau Bootis b and the ordinary hot Jupiters HD 209458b and HD 189733b. Panel b: Ratio of plasma to cyclotron frequency for Tau Bootis b with different estimated magnetic moments compared to Jupiter at 5 AU.

SATELLITE LASER RANGING

In addition to routinely tracking more than 150 targets, which are equipped with laser retro-reflectors, the Graz Satellite Laser Ranging (SLR) station is working on various projects. Highlights include the Expert Coordination Center, the build-up of a new SLR station on Tenerife and attitude measurements to *Galileo* satellites within the Alcantara Initiative.

NEW SLR STATION ON TENERIFE

In cooperation with an international consortium from Austria, Germany, Latvia, and Switzerland the Graz SLR station is involved in the design and build-up of the first ESA SLR station located in Teide on Tenerife. The station consists of an 80 cm Ritchey–Chrétien telescope on an altitude-azimuth mount with two Nasmyth and two folded-Cassegrain foci.

IWF is responsible for the design of the laser system, including laser, beam expansion optics and electronics for start pulse detection. The laser will be mounted directly on the telescope, avoiding any Coudé-path (multiple mirrors directing the laser beam from a laboratory to the telescope). This new setup reduces the necessary alignment steps and is very cost effective and easy to handle. All optical components consist of commercial off the shelf parts. Furthermore, IWF develops the detection package (Fig. 39), which consists of two single photon avalanche diode detectors (for green and infrared wavelength), an optical camera (for monitoring reflected sunlight from satellites) and an optional light curve detection system. Additionally the Astronomical Institute of Bern will install a highly sensitive optical space debris camera. The whole SLR system is built in a highly modular way, future extension of the system includes e.g. a space debris laser module (laser and dedicated single photon detector).

EXPERT COORDINATION CENTER

The second phase of the Expert Coordination Center started in 2018 consisting of experts for optical observations (Astronomical Institute of Bern, Czech Technical University in Prague, SpaceDys) and space debris laser ranging (Graz SLR Station). The main task of the Expert Center is to coordinate external stations, in terms of observation scheduling/tasking and data delivery.

The Graz SLR station is currently developing a validation routine for "passive-only" SLR stations. Within bi- or multi-static measurements, it is firing its new space debris laser (directly mounted on the telescope, less alignment, easier handling) to a target with well-known orbit (e.g. *Envisat*). Passive stations receive diffusely reflected photons by opening their detector exactly correlated to the starting and travel time of the photon in Graz. For passive stations there is no need to act as a fully operating SLR station, they only monitor incoming photons from other stations. The offsets with respect to the *Envisat* reference orbit (calculated by using highly accurate standard SLR measurements) are determined and RMS and standard deviation calculated. The developed validation tools run on a virtual machine at IWF and can be easily accessed by Expert Center operators.

Further software developed by IWF includes a conversion tool from Two Line Element to Consolidated Prediction Format data sets, which are commonly used by SLR stations. Additionally an ftp download tool for the retrieval of SLR data is provided.

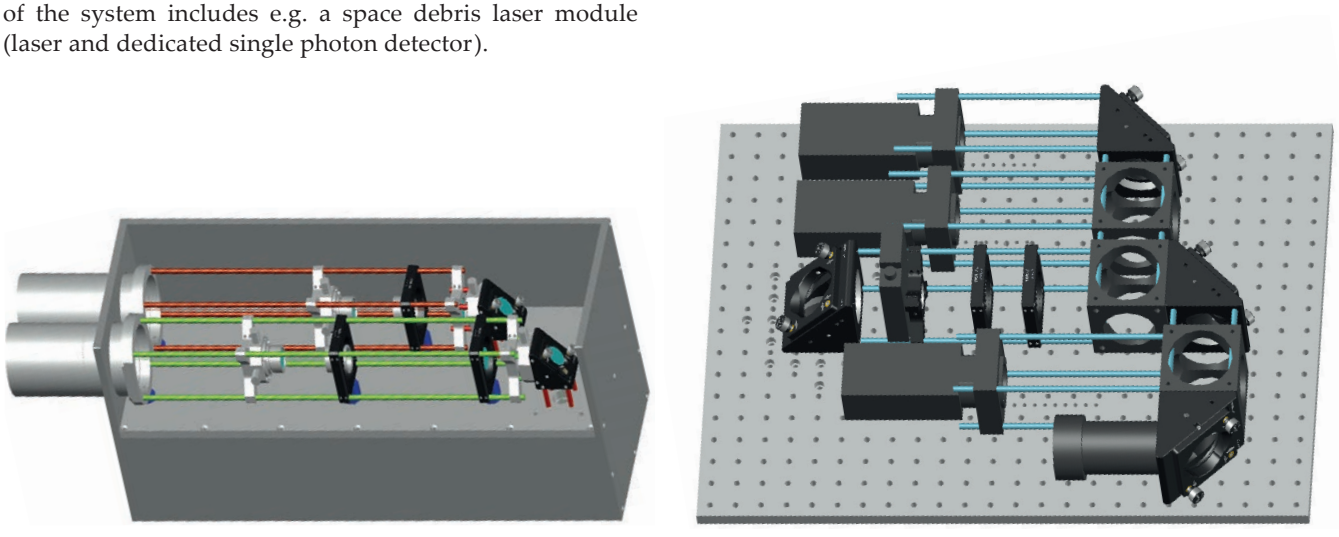

Fig. 39: Final design of the detection package and the laser package with expansion optics (left image) to be installed in Teide on Tenerife.

TECHNOSAT AND S-NET DESIGN

The interest in small spacecraft has been rising rapidly over last years. The application of miniaturization techniques, compact designs, and low-cost COTS (commercial off-the-shelf) components brings more affordable opportunities in space activities for small institutions and companies. Laser ranging is used not only for traditional precise orbit determination, but also for attitude and attitude motion analysis during or even after the spacecraft's lifetime. Satellites are equipped with an exclusive distribution of Corner Cube Retroreflectors (CCRs) on different sides.

TechnoSat (Fig. 40) and the *S-Net series* (four satellites) are developed and built by the Technical University of Berlin and were launched into a lower Earth orbit in 2017 and 2018, respectively. The Graz SLR station designed and simulated the ideal distribution of CCRs, which was tested before launch at a remote location outside of Graz. In orbit, the attitude of *TechnoSat* varies from freely spinning, nadir-pointing or off-nadir-pointing alternately according to the demands of different tasks. The attitude results based on Graz kHz SLR data are analyzed and compared to the records from its on-board gyroscope.

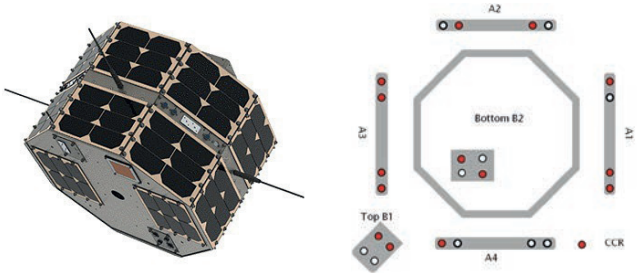

Fig. 40: *TechnoSat:* 14 small CCR (fused silica, COTS) are distributed on six different surfaces of its octagonal prism structure giving the satellite a unique kHz SLR signature.

For *S-Net series* (Fig. 41), in addition to precise orbit and attitude determination, Graz kHz SLR is used to identify single satellites shortly after their separation from the launcher even when the individual satellites are close together.

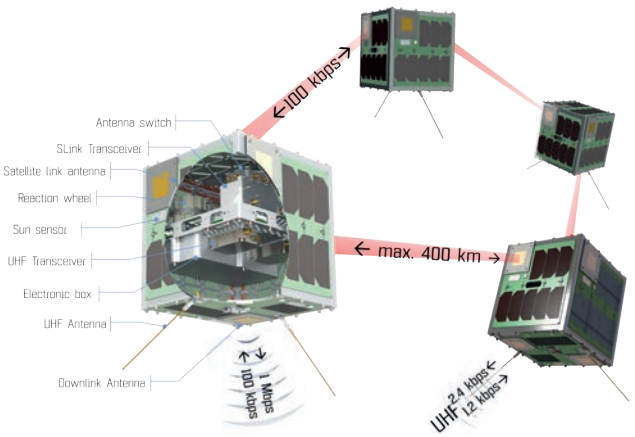

Fig. 41: *S-Net:* Five sides of each of the four satellites are identical and equipped with one CCR. The sixth side of each satellite has a different and unique pattern to distinguish the satellites from each other.

GALILEO ATTITUDE DETERMINATION

Within the ESA Alcantara Initiative the Graz SLR station at Lustbühel had the chance to perform ground-based measurements to a spare *Galileo* retroreflector panel. The panel was mounted on an astronomical tripod and could be rotated between 0 and 18° with steps of 0.1°. It was placed on a hill 32 km outside of Graz (Absetzwirt), and ground-based range measurements were performed. The histogram of the measurement (with a tilt angle of 12.4° around the panel z-axis) is presented in Fig. 42. It shows the number of detected photons within range bins of 500 µm. Due to the tilt of the panel 11 distinguishable peaks appear at distances of up to 6 cm with respect to the panel center. The distances between each of these peaks is determined and from that the panel tilt can be calculated with high accuracy.

Galileo satellites pass in various different tilt angle conditions over Graz. Navigation satellites are continuously rotated around their nadir pointing axis to ensure alignment to the sun (Yaw-steering). A specific orientation (elevation 11.38°, azimuth 90°, station seen from the satellite reference frame) was chosen exactly corresponding to the incident angle conditions measured with the spare panel. The peak positions of the measurements to *Galileo* match very well compared to the ground-based tests. From the peak distances the panel tilt was verified to be 11.37° which is accurate within 0.1° to the calculations. The variation in peak height at the *Galileo* measurement results from reflections from differently clocked (rotated) retroreflectors. The proposed method gives unique way for validating attitude accuracy of *Galileo* satellites.

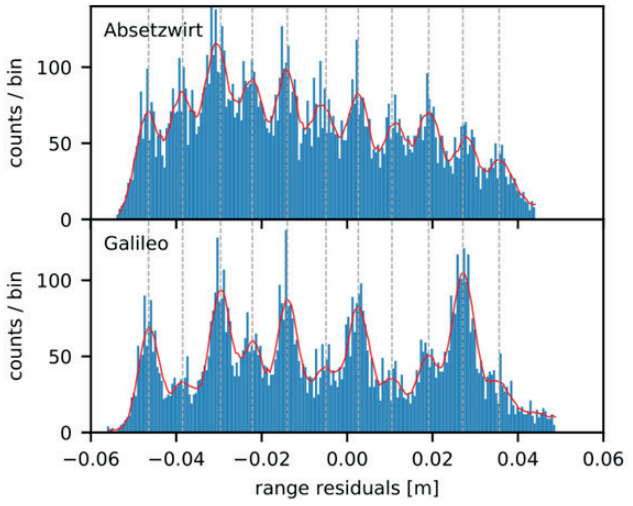

Fig. 42: Comparison of the ground-based range measurements to the *Galileo* spare panel (Absetzwirt) to *Galileo* 103 with similar incident angle conditions.

INFRASTRUCTURE

Instruments aboard spacecraft are exposed to harsh environments, e.g., vacuum, large temperature ranges, radiation, and high mechanical loads during launch. Furthermore, these instruments are expected to be highly reliable, providing full functionality over the entire mission time, which could last for more than a decade.

IWF owns several test facilities and special infrastructure for the production of flight hardware. A high-performance computer helps the scientists to cope with the enormous data, which have to be analyzed for space missions.

VACUUM CHAMBERS

The *Small Vacuum Chamber* is a manually controlled, cylindrical vacuum chamber (160 mm diameter, 300 mm length) for small electronic components or printed circuit boards. It features a turbo molecular pump and a rotary dry scroll forepump. A pressure level of 10^{-10} mbar can be achieved.

The *Medium Vacuum Chamber* has a cylindrical stainless steel body with the overall length of 850 mm and a diameter of 700 mm. A dry scroll forepump and a turbo molecular pump provide a pressure level of about 10^{-7} mbar. A target manipulator with two axes and an ion beam source are installed. This chamber mainly serves for functional tests of the *PICAM* Flight Spare Model.

The *Large Vacuum Chamber* has a horizontal cylindrical stainless steel body and door, a vision panel, two turbo molecular pumps and a dry scroll forepump. A pressure of 10^{-7} mbar can be achieved. The cylinder has a diameter of 650 mm and a length of 1650 mm. During shutdown the chamber is vented with nitrogen. A target manipulator inside the chamber allows for computer-controlled rotation of the target around three mutually independent perpendicular axes. The vacuum chamber is enclosed by a permalloy layer for magnetic shielding. To enable the baking of structures and components (to outgas volatile products and unwanted contaminations), the chamber is equipped with a heater around the circumference.

The *Thermal Vacuum Chamber* is fitted with two turbo molecular pumps, a dry scroll forepump, and an ion getter pump, which together achieve a pressure level of 10^{-6} mbar and allow quick change of components or devices to be tested. A thermal plate installed in the chamber and liquid nitrogen are used for thermal cycling in a temperature range between -90 °C and +140 °C. The vertically oriented cylindrical chamber allows a maximum experiment diameter of 410 mm and a maximum height of 320 mm.

The *Surface Laboratory Chamber* is dedicated to surface science research. It has a diameter of 400 mm and a height of 400 mm, extendable up to 1200 mm. One rotary vane pump and one turbo-molecular pump achieve a minimum pressure of 10^{-5} mbar. With an external thermostat the chamber temperature can optionally be controlled between -90 °C and +50 °C.

The *Sample Chamber* contains an 8µ particle filter and allows measurements of grain sample electrical permittivity. The *Small Sample Chamber* (Fig. 43) has been refitted for measurement of the differential pressure between the upper and the lower volume. It can be used to derive the gas diffusion coefficient in porous samples. One rotary vane pump achieves a minimum pressure of 10^{-3} mbar.

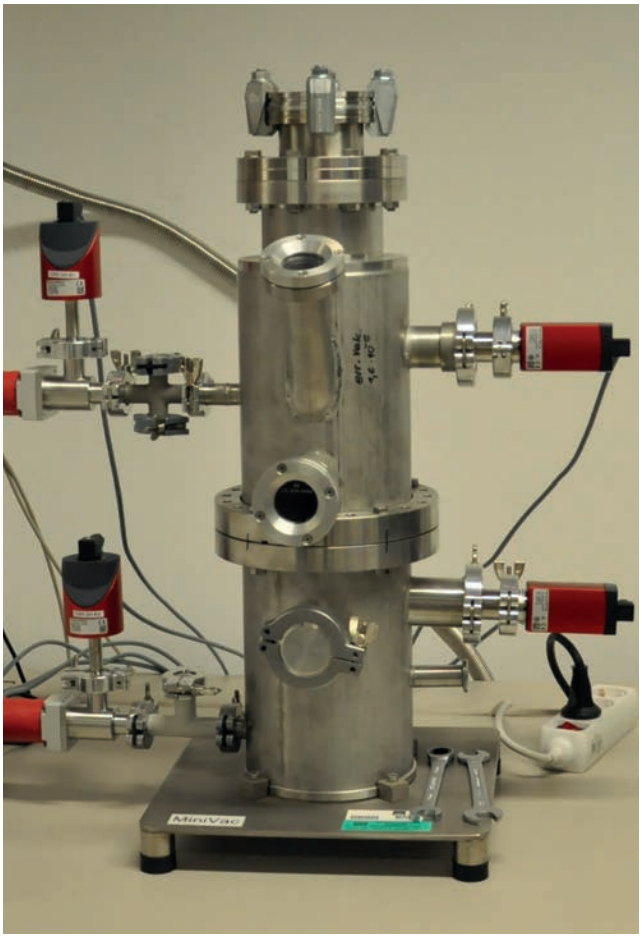

Fig. 43: IWF Small Sample Chamber.

HIGH-PERFORMANCE COMPUTER

With the LEO computing cluster, IWF hosts a small high-performance computer for diverse kinds of simulations, ranging from fundamental plasma physics, electron dynamics, magneto-hydrodynamical models, and magnetic reconnection in the Earth's magnetosphere to the atmospheric evolution on diverse planets. The system also downloads and processes data from the *MMS* mission in an automatic way. Some long-time data storage is provided for the archive of all data from the *Helios-1* and *-2* missions that date back to the year 1974.

The LEO system has now 54 active user accounts of which nine are non-personal project accounts. The storage capacity reaches 300 TB on regular hard disks and 64 TB on especially durable and fast solid state devices. The working memory totals to 8 TB of RAM. Since its inauguration, LEO has now completed 12600 parallel computing jobs. For structural mechanics and heat conduction models, the ANSYS software package is now available.

OTHER TEST FACILITIES

The *Temperature Test Chamber* allows verifying the resistance of electronic components and circuits to most temperatures that occur under natural conditions, i.e., -40 °C to +180 °C. The chamber has a test space of 190 l and is equipped with a 32-bit control and communication system.

The second *Temperature Test Chamber* is used for fast cycling electronic components and circuit. The temperature range is -70 °C to +180 °C. The chamber has a test space of 37 l and is equipped with similar interfaces for communication.

The *Penetrometry Test Stand* is designed to measure mechanical soil properties, like bearing strength. The UV exposure facility is capable to produce radiation between 200-400 nm (UV-A, UV-B, UV-C). The *Test Stand* has been put into deep storage and will be replaced with a smaller device, which can operate in vacuum inside the *Surface Laboratory Chamber*.

Fig. 44: Three-dimensional Merritt coil system at the ZAMG Conrad Observatory.

MAGNETOMETER CALIBRATION

A *three-layer magnetic shielding* made from mu-metal is used for all basic magnetometer performance and calibration tests. The remaining DC field in the shielded volume is <10 nT with a field noise of <2 pT/√Hz at 1 Hz. A special *Helmholtz coil system* allows generating field vectors of up to ±30000 nT around the sensor under test.

The *Magnetometer Temperature Test Facility* is used to test magnetic field sensors between -170 °C and +220 °C in a low field and low noise environment. Liquid nitrogen is the base substance for temperature regulation, which is accurate to ±0.1 °C. A magnetic field of up to ±100000 nT can be applied to the sensor during test cycles.

A *three-dimensional Merritt coil system* (Fig. 44) was installed in cooperation with the Conrad Observatory of the Zentralanstalt für Meteorologie und Geodynamik (ZAMG). It is located within a nature reserve at the outskirts of the Eastern Alps about 50 km SW of Vienna. The remoteness of the location guarantee an undisturbed surrounding for the absolute calibration of magnetic field sensors.

The coil system has a side length of approximately three meters. Two pairs of coils along each axis enable a field homogeneity of better than 10^{-5} in a test volume of 20x20x20 cm^3 in the center of the coil. The coil system features separate coils for Earth's field compensation and the dynamic range of the main coils is ±100000 nT.

FLIGHT HARDWARE PRODUCTION

Flight hardware is assembled and tested in the institute's *Clean Room*, which is a class 10000 (according to U.S. Federal Standard 209e) certified laboratory with a total area of 30 m^2. It accommodates up to six engineers.

The laminar flow *Clean Bench* has its own filtered air supply. It provides product protection by ensuring that the work piece in the bench is exposed only to HEPA-filtered air (HEPA = High Efficiency Particulate Air). The internal dimensions are 118 x 60 x 56 cm^3.

The *Vapor Phase Soldering Machine* is suitable for mid size volume production. The maximum board size is 340 x 300 x 80 mm^3. Vapor phase soldering is currently the most flexible, simplest and most reliable soldering method. It is ideally suited for all types of surface mounted device (SMD) components and base materials. It allows processing of all components without the need of any complicated calculations or having to maintain temperature profiles. For placing of fine pitch parts and rework of electronic boards an *Infrared Soldering Machine* with a precision placing system is used.

The *Fluid Dispensing System* DispenseMate 585 is a solder paste printer in a compact benchtop format. This machine allows a precise dosing of solder pastes on PCBs. As an option, a dispenser for precise glue application can be used. The range of motion is 525 x 525 mm.

OUTREACH

PUBLIC OUTREACH

IWF is actively engaged in science education and public outreach. In 2018, many different groups and school classes visited the institute and were guided through the labs and the planetary garden.

IWF was partner in the "FFG-Talente-Regional" project "Freiflug - Die Geheimnisse des Fliegens". From January through March, the traveling exhibition on aerospace for children and young adults was displayed at the institute. Several schools and individual visitors spent time investigating the history of (space)flight (Fig. 45).

On 9 February, Günter Kargl talked about "Rosetta: The first landing on a comet" in the frame of the public series of talks "Nachts auf der Sternwarte" at the Department of Astrophysics of the University of Vienna.

In February and March, Bruno Besser, Herbert Lichtenegger, and Harald Ottacher participated in a series of lectures about current space topics in "Bildungshaus Sodalitas" in Tainach, Carinthia.

On 12 April, Luca Fossati was invited to the 10th Yuri's Night at Urania Wien, where he presented the Austrian contribution to NASA's *CUTE* mission.

The Austrian "Lange Nacht der Forschung" on 13 April broke all records. With more than 3000 people, IWF doubled the number of its visitors with respect to 2014 (Fig. 46).

Fig. 45: Man at work during the "Freiflug" exhibition at IWF.

Different stations offered a taste of research for each age category: The youngest could build rockets and design their own planets whereas for the older visitors space physics was experimentally explained. Non-stop lectures and laboratory tours completed the program. The Austrian broadcasting service ORF sent its "Radio Steiermark Kinderreporter", who made a report on "adventures in the solar system". IWF would like to say "DANKESCHÖN" to Petra Huber and her team from Kinderbüro and Johannes Kügerl and his students from BG/BRG Kirchengasse, who helped coping with the enormous stream of visitors.

Fig. 46: The crowded IWF headquarters during the "long night of research".

Starting in May, IWF were invited to write monthly science blogs for the Austrian newspaper "Der Standard", which had a great response from online readers. Topics discussed so far were *InSight*, magnetometer testing for *JUICE*, cometary tails, extraterrestrial life, and *MMS*.

On the first Wednesday of every month (during the lecture term), BioTechMed-Graz organizes a Science Breakfast alternately at the University of Graz, Medical University of Graz and Graz University of Technology. On 6 June, Wolfgang Baumjohann gave a lecture on the topic "From Graz into Space".

With more than 200 participants from 20 countries the Austrian Space Cooperation Days 2018 successfully took place at FH Wiener Neustadt from 7 to 8 June. IWF participated with an exhibition on exoplanets and two expert lectures: Georg Kirchner gave an overview of "Satellite Laser Ranging in Graz: Achievements and Advanced Applications" and Werner Magnes presented IWF's "Current and Future Challenges".

During summer time, seven high-school students performed an internship at IWF under the "Talente-Praktika" program of FFG. They worked on space weather, comet Halley, *PICAM* calibration, solar type III radio bursts, *Rosetta/MIDAS* data archiving, and VLF data analysis. In the framework of the "FEMtech" program of FFG, six female students from KFU Graz and University of Vienna worked at IWF on space debris, *MMS* data analysis, dust, and preparations for the exoplanet missions *CHEOPS* and *CUTE*.

On the occasion of DLR's special exhibition "Comets – the Rosetta mission: Journey to the origins of the Solar System", hosted at the Natural History Museum (NHM) in Vienna, Günter Kargl and Thurid Mannel gave presentations during a dedicated symposium, organized by ÖAW and NHM on 12 July.

On 28 August, Magda Delva, Herbert Lichtenegger, and Martin Volwerk talked about our solar system, Mercury, and comets to the ten-year old participants of the space camp during the summer school of WIKU BRG Graz.

On 12 September, Luca Fossati participated in the GLOBART Talk 2018 at NHM, where researchers and artists exchanged their ideas about "Our Place in Space".

On 28 September, IWF presented ESA's *BepiColombo* mission during the European Researchers' Night, a mega event that takes place every year simultaneously in several hundred cities all over Europe and beyond.

On 20 October *BepiColombo* was started, which was celebrated with a (pre-)launch event at IWF. On the eve of the launch, around 100 people listened to several talks about IWF's contribution to this mission. Andreas Geisler, head of FFG's Aeronautics and Space Agency, conveyed supporting greetings from Federal Minister Norbert Hofer. About 50 "night owls" followed the institute's invitation to watch live *BepiColombo's* take-off at 03.45 CEST.

During November, ESA Director General Jan Wörner invited the European space family to promote with a new outreach experience called "Space Talk". IWF sent out Irmgard Jernej, Günter Kargl, Werner Magnes, Harald Ottacher, and Martin Volwerk to present their work in three Austrian states.

In the frame of the winter seminars of the Department of Astrophysics of the University of Vienna, on 5 November, Martin Volwerk talked about "The Io Plasma Torus - Old stuff and new insights".

AWARDS & RECOGNITION

In January, Rumi Nakamura was elected as a regular member of the European Academy of Sciences and Arts and in December she was elected as Fellow of the American Geophysical Union (AGU).

In May, the Styrian government awarded IWF director Baumjohann the Decoration of the province of Styria for science, research and art and in October the International Academy of Astronautics (IAA) awarded him the "Basic Science Award".

IWF reached the top five nominations for the Styrian WKO (Austrian Economic Chambers) PR Panther in the category "science" with the PR project "Mit Bepi zum Merkur" (Fig. 47).

Fig. 47: Part of the IWF *BepiColombo* team during the PR Panther ceremony (Photo: Jorj Konstantinov).

LECTURING AND MENTORING

In summer 2018 and in winter term 2018/2019 IWF members gave lectures at the University of Graz, Graz University of Technology, University of Vienna, TU Braunschweig, FH Joanneum, and FH Wiener Neustadt.

In the framework of the ÖAW mentoring system, organized by the Working Group on Non-Discrimination of ÖAW, Martin Volwerk served as mentor.

MEETINGS

From 6-7 September, the Summer University "Graz in Space" was organized by IWF, the Commission for Astronomy, and the Institute of Physics of the University of Graz. The program concentrated on extrasolar planets, the Sun and space weather, and on *Rosetta*.

Wolfgang Baumjohann served as Vice Director and chair of the Program Committee of the Summer School Alpbach, which took place from 17 to 26 July and was dedicated to "Sample return from small solar system bodies". Every year, 60 students and about 25 lecturers and tutors from among ESA's member states are invited to this meeting.

From 23 to 25 October, IWF organized the *MMS* Fall Science Working Team (SWT) Meeting at Schloss Seggau (Fig. 48).

In addition, B.P. Besser, M.Y. Boudjada, N.K. Dwivedi, H.-U. Eichelberger, K.J. Genestreti, G. Kirchner, G. Kargl, M.L. Khodachenko, H. Lammer, M. Lendl, R. Nakamura, T.K.M. Nakamura, F. Plaschke, and M. Steindorfer were members of scientific program and/or organizing committees at nine international conferences and/or workshops.

THESES

Besides lecturing, members of the institute are supervising Bachelor, Diploma, Master and Doctoral Theses. In 2018, the following supervised theses have been completed:

Fischer, D.: Optimized Merging of Search-Coil and Fluxgate Data for the Magnetospheric Multiscale Mission, Doctoral Thesis, Technische Universität Graz, 151, 2018.

Hofer, B.: Electromotive force deduced from Helios observations during Coronal Mass Ejections, Master Thesis, Universität Graz, 68, 2018.

Juvan, I.: Multicolor Photometry of Transiting Extrasolar Planets, Doctoral Thesis, Universität Graz, 114, 2018.

Mannel, Th.: Cometary dust at the Micrometre Scale - Results of MIDAS, the Atomic Force Microscope aboard the Comet Orbiter Rosetta, Doctoral Thesis, Universität Graz, 125, 2018.

Xiao, S.D.: Solar Wind Interaction with Induced Magnetosphere of Venus, Doctoral Thesis, University of Science and Technology of China, 96, 2018.

Fig. 48: Participants of the *MMS* SWT Meeting (Photo: James F. Spann, NASA).

IN MEMORIAM

WILLIBALD RIEDLER (1932-2018)

Willibald Riedler at the ceremony on the occasion of his 75th birthday at TU Graz (© alumniTUGraz 1887).

On 24 January 2018, Willibald Riedler passed away at the age of 85. He was a pioneer and driving force of Austria's involvement in space research activities, a committed university member and teacher of communication technology and manager of challenging research projects, for more than thirty years.

He studied electrical/communication engineering at Technische Hochschule Wien and graduated in 1956 as "Diplomingenieur". He was university assistant at the Institute for High-Frequency Engineering until 1962 working on electrodynamics and microwave technology and finished his technical doctorate with a thesis on "The Splitting of the Electrokinetic Power Theorem".

Fascinated by the new research opportunities after the launch of the first Earth satellite 1957, Riedler started to work in ionospheric and magnetospheric physics at the Geophysical Observatory of the Royal Swedish Academy in Kiruna 1962. He got involved, first as consultant, after 1966 as "Scientific Director", in the organization and realization of balloon and sounding rocket campaigns, the latter organized by ESRO (European Space Research Organisation). His second doctoral thesis on "Measurements of Energy Spectra and Angular Distributions of Electrons in Polar Light" got approved in 1966 at the Institute of Meteorology and Geophysics of the University of Vienna.

In 1968, Riedler was appointed professor of communications at Technische Hochschule Graz (now TU Graz). He took office in 1969 and acted as head of the Institute of Communications and Wave Propagation up to the end of 2000, when he retired as professor emeritus. From 1973 to 1975 he served as dean of the Faculty of Electrical Engineering and from 1975 to 1977 as rector of TU Graz.

On 26 November 1969, the first space flight of an Austrian instrument, measuring high-energy particles, was launched on a sounding rocket from the Norwegian site Andøya. For the next thirty years many more instruments were flown during either internationally organized balloon campaigns and/or sounding rocket launches.

In 1970, Riedler initiated, together with Otto Burkard, Karl Rinner, and others, the foundation of IWF, where he headed the Department of Experimental Space Research. From 1984 to 2000 he was executive director of the institute.

His department developed and built space hardware for several missions, beginning with a magnetometer for *SPACELAB*, followed by the Soviet *Venera 13 & 14*, *Vega 1 & 2*, *Phobos 1 & 2*, and *Interball*. After Austria joined ESA as full member, the institute got involved in many successful missions, such as *Cassini/Huygens*, the German *Equator-S*, *Cluster*, and *Rosetta*. Riedler also initiated Austria's participation in the Chinese *Double Star* project, with two magnetometers and a spacecraft potential control instrument on two magnetospheric satellites. From 1988 to 1992 he acted as scientific leader of the Austrian cosmonaut project *AustroMir*, organized by the Institute of Applied Systems Technology of Joanneum Research, which Riedler headed from 1978 to 2002.

Riedler was instrumental for the establishment of the Graz Lustbühel Observatory in 1976. In the beginning of the 1990s, IWF expanded rapidly, with many more employees making it necessary to obtain more space in order to facilitate the institute's activities. On his request, the City of Graz donated a plot on which the ÖAW could build the, now called, Victor Franz Hess Research Center, which was opened in 2000.

IWF is mourning its long-term director, who was responsible for Austria's place in space history and turned Graz into an international center of space physics. The institute's members will always remember him gratefully.

PUBLICATIONS

REFEREED ARTICLES

Akhavan-Tafti, M., J.A. Slavin, G. Le, J.P. Eastwood, R.J. Strangeway, C.T. Russell, R. Nakamura, W. Baumjohann, R.B. Torbert, B.L. Giles, D.J. Gershman, J.L. Burch: MMS examination of FTEs at the Earth's subsolar magnetopause, *J. Geophys. Res.*, **123**, 1224-1241, 2018.

Alexeev, I., D. Parunakian, S. Dyadechkin, E. Belenkaya, M.L. Khodachenko, E. Kallio, M. Alho: Calculation of the initial magnetic field for Mercury's magnetosphere hybrid model, *Cosmic Res.*, **56**, 108-114, 2018.

Amerstorfer, T., C. Möstl, P. Hess, M. Temmer, M.L. Mays, M.A. Reiss, P. Lowrance, P.-A. Bourdin: Ensemble prediction of a halo Coronal Mass Ejection using heliospheric imagers, *Space Weather*, **16**, 784-801, 2018.

Andriopoulou, M., R. Nakamura, S. Wellenzohn, K. Torkar, W. Baumjohann, R.B. Torbert, P.-A. Lindqvist, Yu.V. Khotyaintsev, J. Dorelli, J.L. Burch: Plasma density estimates from spacecraft potential using MMS observations in the dayside magnetosphere, *J. Geophys. Res.*, **123**, 2620-2629, 2018.

Argall, M.R., K. Paulson, L. Alm, A. Rager, J. Dorelli, J. Shuster, S. Wang, R.B. Torbert, H. Vaith, I. Dors, M. Chutter, C. Farrugia, J. Burch, C. Pollock, B. Giles, D. Gershman, B. Lavraud, C.T. Russell, R. Strangeway, W. Magnes, P.-A. Lindqvist, Yu.V. Khotyaintsev, R.E. Ergun, N. Ahmadi: Electron dynamics within the electron diffusion region of asymmetric reconnection, *J. Geophys. Res.*, **123**, 146-162, 2018.

Arkhypov, O.V., M.L. Khodachenko, H. Lammer, M. Güdel, T. Lüftinger, C.P. Johnstone: Starspot variability as an X-ray radiation proxy, *MNRAS*, **476**, 1224-1233, 2018.

Arkhypov, O.V., M.L. Khodachenko, H. Lammer, M. Güdel, T. Lüftinger, C.P. Johnstone: Time-scales of stellar rotational variability and starspot diagnostics, *MNRAS*, **473**, L84-L88, 2018.

Arkhypov, O.V., M.L. Khodachenko, M. Güdel, C. Johnstone, T. Lüftinger, H. Lammer: Timescales of starspot variability in slow rotators, *Astron. Astrophys.*, **613**, A31, 2018.

Artemyev, A.V., P.L. Pritchett, V. Angelopoulos, X.-J. Zhang, R. Nakamura, S. Lu, A. Runov, S.A. Fuselier, S. Wellenzohn, F. Plaschke, C.T. Russell, R.J. Strangeway, P.-A. Lindqvist, R.E. Ergun: Field-aligned currents originating from the magnetic reconnection region: Conjugate MMS-ARTEMIS observations, *Geophys. Res. Lett.*, **45**, 5836-5844, 2018.

Bagashvili, S.R., B.M. Shergelashvili, D.R. Japaridze, V. Kukhianidze, S. Poedts, T.V. Zaqarashvili, M.L. Khodachenko, P. De Causmaecker: Evidence for precursors of the coronal hole jets in Solar bright points, *Astrophys. J. Lett.*, **855**, L21, 2018.

Ballester, J.L., I. Alexeev, M. Collados, T. Downes, R.F. Pfaff, H. Gilbert, M.L. Khodachenko, E. Khomenko, I.F. Shaikhislamov, R. Soler, E. Vázquez-Semadeni, T. Zaqarashvili: Partially ionized plasmas in astrophysics, *Space Sci. Rev.*, **214**, 58, 2018.

Barragán, O., D. Gandolfi, A.M.S. Smith, H.J. Deeg, M.C.V. Fridlund, C.M. Persson, P. Donati, M. Endl, Sz. Csizmadia, S. Grziwa, D. Nespral, A.P. Hatzes, W.D. Cochran, L. Fossati, S.S. Brems, J. Cabrera, F. Cusano, Ph. Eigmüller, C. Eiroa, A. Erikson, E. Guenther, J. Korth, D. Lorenzo-Oliveira, L. Mancini, M. Pätzold, J. Prieto-Arranz, H. Rauer, I. Rebollido, J. Saario, O.V. Zakhozhay: K2-139 b: A low-mass warm Jupiter on a 29-d orbit transiting an active K0 V star, *MNRAS*, **475**, 1765-1776, 2018.

Bean, J.L., K.B. Stevenson, N.M. Batalha, Z. Berta-Thompson, L. Kreidberg, N. Crouzet, B. Benneke, M.R. Line, D.K. Sing, H.R. Wakeford, H.A. Knutson, E.M.-R. Kempton, J.-M. Désert, I. Crossfield, N.E. Batalha, J. de Wit, V. Parmentier, J. Harrington, J.I. Moses, M. Lopez-Morales, M.K. Alam, J. Blecic, G. Bruno, A.L. Carter, J.W. Chapman, L. Decin, D. Dragomir, T.M. Evans, J.J. Fortney, J.D. Fraine, P. Gao, A. García Muñoz, N.P. Gibson, J.M. Goyal, K. Heng, R. Hu, S. Kendrew, B.M. Kilpatrick, J. Krick, P.-O. Lagage, M. Lendl, T. Louden, N. Madhusudhan, A.M. Mandell, M. Mansfield, E. M. May, G. Morello, C.V. Morley, N. Nikolov, S. Redfield, J.E. Roberts, E. Schlawin, J.J. Spake, K.O. Todorov, A. Tsiaras, O. Venot, W.C. Waalkes, P.J. Wheatley, R.T. Zellem, D. Angerhausen, D. Barrado, L. Carone, S.L. Casewell, P.E. Cubillos, M. Damiano, M. de Val-Borro, B. Drummond, B. Edwards, M. Endl, N. Espinoza, K. France, J.E. Gizis, T.P. Greene, T.K. Henning, Y. Hong, J.G. Ingalls, N. Iro, P.G.J. Irwin, T. Kataria, F. Lahuis, J. Leconte, J. Lillo-Box, S. Lines, J.D. Lothringer, L. Mancini, F. Marchis, N. Mayne, E. Palle, E. Rauscher, G. Roudier, E.L. Shkolnik, J. Southworth, M.R. Swain, J. Taylor, J. Teske, G. Tinetti, P. Tremblin, G.S. Tucker, R. van Boekel, I.P. Waldmann, I.C. Weaver, T. Zingales: The transiting exoplanet community early release science program for JWST, *Publ. Astron. Soc. Pac.*, **130**, 114402, 2018.

Bisikalo, D.V., A.A. Cherenkov, V.I. Shematovich, L. Fossati, C. Möstl: The influence of stellar flare on dynamical state of the atmosphere of exoplanet HD 209458b, *Astron. Rep.*, **62**, 648–653, 2018.

Bisikalo, D.V., V.I. Shematovich, A.A. Cherenkov, L. Fossati, C. Möstl: Atmospheric mass loss from Hot Jupiters irradiated by stellar superflares, *Astrophys. J.*, **869**, 108, 2018.

Blumenthal, S.D., A.M. Mandell, E. Hebrard, N.E. Batalha, P.E. Cubillos, S. Rugheimer, H.R. Wakeford: A comparison of simulated JWST observations derived from equilibrium and non-equilibrium chemistry models of giant exoplanets, *Astrophys. J.*, **853**, 138, 2018.

Bourdin, P.-A., B. Hofer, Y. Narita: Inner structure of CME shock fronts revealed by the electromotive force and turbulent transport coefficients in Helios-2 observations, *Astrophys. J.*, **855**, 111, 2018.

Bourdin, Ph., A. Brandenburg: Magnetic helicity from multipolar regions on the solar surface, *Astrophys. J.*, **869**, 3, 018.

Bourdin, Ph., N.K. Singh, A. Brandenburg: Magnetic helicity reversal in the corona at small plasma beta, *Astrophys. J.*, **869**, 2, 2018.

Breuillard, H., L. Matteini, M.R. Argall, F. Sahraoui, M. Andriopoulou, O. Le Contel, A. Retinò, L. Mirioni, S.Y. Huang, D.J. Gershman, R.E. Ergun, F.D. Wilder, K.A. Goodrich, N. Ahmadi, E. Yordanova, A. Vaivads, D.L. Turner, Yu.V. Khotyaintsev, D.B. Graham, P.-A. Lindqvist, A. Chasapis, J.L. Burch, R.B. Torbert, C.T. Russell, W. Magnes, R.J. Strangeway, F. Plaschke, T.E. Moore, B.L. Giles, W.R. Paterson, C.J. Pollock, B. Lavraud, S.A. Fuselier, I.J. Cohen: New insights into the nature of turbulence in the Earth's magnetosheath using Magnetospheric MultiScale mission data, *Astrophys. J.*, **859**, 127, 2018.

Breuillard, H., O. Le Contel, T. Chust, M. Berthomier, A. Retino, D.L. Turner, R. Nakamura, W. Baumjohann, G. Cozzani, F. Catapano, A. Alexandrova, L. Mirioni, D.B. Graham, M.R. Argall, D. Fischer, F.D. Wilder, D.J. Gershman, A. Varsani, P.-A. Lindqvist, Yu.V. Khotyaintsev, G. Marklund, R.E. Ergun, K.A. Goodrich, N. Ahmadi, J.L. Burch, R.B. Torbert, G. Needell, M. Chutter, D. Rau, I. Dors, C.T. Russell, W. Magnes, R.J. Strangeway, K.R. Bromund, H. Wei, F. Plaschke, B.J. Anderson, G. Le, T.E. Moore, B.L. Giles, W.R. Paterson, C.J. Pollock, J.C. Dorelli, L.A. Avanov, Y. Saito, B. Lavraud, S.A. Fuselier, B.H. Mauk, I.J. Cohen, J.F. Fennel: The properties of Lion Roars and electron dynamics in mirror mode waves observed by the Magnetospheric MultiScale mission, *J. Geophys. Res.*, **123**, 93-103, 2018.

Britavskiy, N., E. Pancino, V. Tsymbal, D. Romano, L. Fossati: A new method of measuring centre-of-mass velocities of radially pulsating stars from high-resolution spectroscopy, *MNRAS*, **474**, 3344-3360, 2018.

Burch, J.L., J.M. Webster, K.J. Genestreti, R.B. Torbert, B.L. Giles, S.A. Fuselier, J.C. Dorelli, A.C. Rager, T.D. Phan, R.C. Allen, L.-J. Chen, S. Wang, O. Le Contel, C.T. Russell, R.J. Strangeway, R.E. Ergun, A.N. Jaynes, P.-A. Lindqvist, D.B. Graham, F.D. Wilder, K.-J. Hwang, J. Goldstein: Wave phenomena and beam-plasma interactions at the magnetopause reconnection region, *J. Geophys. Res.*, **123**, 1118-1133, 2018.

Burch, J.L., R.E. Ergun, P.A. Cassak, J.M. Webster, R.B. Torbert, B.L. Giles, J.C. Dorelli, A.C. Rager, K.-J. Hwang, T.D. Phan, K.J. Genestreti, R.C. Allen, L.-J. Chen, S. Wang, D. Gershman, O. Le Contel, C.T. Russell, R.J. Strangeway, F.D. Wilder, D.B. Graham, M. Hesse, J.F. Drake, M. Swisdak, L.M. Price, M.A. Shay, P.-A. Lindqvist, C.J. Pollock, R.E. Denton, D.L. Newman: Localized oscillatory energy conversion in magnetopause reconnection, *Geophys. Res. Lett.*, **45**, 1237-1245, 2018.

Castro, N., M.S. Oey, L. Fossati, N. Langer: The spectroscopic Hertzsprung-Russell diagram of hot massive stars in the Small Magellanic Cloud, *Astrophys. J.*, **868**, 57, 2018.

Chang, Q., X. Xu, T. Zhang, L. Chai, Y. Wei, Q. Xu: Magnetic field near Venus: Comparison between solar cycle 24 and previous cycles, *Astrophys. J.*, **867**, 129, 2018.

Cheng, B.J., B. Zhou, W. Magnes, R. Lammegger, A. Pollinger: High precision magnetometer for geomagnetic exploration onboard of the China Seismo-Electromagnetic Satellite, *Sci. China E*, **61**, 659-668, 2018.

Cheng, Z.W., J.K. Shi, J.C. Zhang, K. Torkar, L.M. Kistler, M. Dunlop, C. Carr, H. Rème, I. Dandouras, A. Fazakerley: Influence of the IMF cone angle on invariant latitudes of polar region footprints of FACs in the magnetotail: Cluster observation, *J. Geophys. Res.*, **123**, 2588-2597, 2018.

Chhiber, R., A. Chasapis, R. Bandyopadhyay, T.N. Parashar, W.H. Matthaeus, B.A. Maruca, T.E. Moore, J.L. Burch, R.B. Torbert, C.T. Russell, O. Le Contel, M.R. Argall, D. Fischer, L. Mirioni, R.J. Strangeway, C.J. Pollock, B.L. Giles, D.J. Gershman: Higher-order turbulence statistics in the Earth's magnetosheath and the solar wind using Magnetospheric Multiscale observations, *J. Geophys. Res.*, **123**, 9941-9954, 2018.

Chong, G.S., S.A. Pope, S.N. Walker, R.A. Frahm, T. Zhang, Y. Futaana: A statistical study of ionospheric boundary wave formation at Venus, *J. Geophys. Res.*, **123**, 7668-7685, 2018.

Collinson, G., L.B. Wilson III, N. Omidi, D. Sibeck, J. Espley, C.M. Fowler, D. Mitchell, J. Grebowsky, C. Mazelle, S. Ruhunusiri, J. Halekas, R. Frahm, T. Zhang, Y. Futaana, B. Jakosky: Solar wind induced waves in the skies of Mars: Ionospheric compression, energization, and escape resulting from the impact of ultralow frequency magnetosonic waves generated upstream of the Martian bow shock, *J. Geophys. Res.*, **123**, 7241-7256, 2018.

Comisel, H., Y. Nariyuki, Y. Narita, U. Motschmann: On heating of solar wind protons by the parametric decay of large-amplitude Alfvén waves, *Ann. Geophys.*, **36**, 1647-1655, 2018.

Debrecht, A., J. Carroll-Nellenback, A. Frank, L. Fossati, E.G. Blackman, I. Dobbs-Dixon: Generation of a circumstellar gas disc by Hot Jupiter WASP-12b, *MNRAS*, **478**, 2592–2598, 2018.

Deleuil, M., S. Aigrain, C. Moutou, J. Cabrera, F. Bouchy, H.J. Deeg, J.-M. Almenara, G. Hébrard, A. Santerne, R. Alonso, A.S. Bonomo, P. Bordé, Sz. Csizmadia, R.F. Dìaz, A. Erikson, M. Fridlund, D. Gandolfi, E. Guenther, T. Guillot, P. Guterman, S. Grziwa, A. Hatzes, A. Léger, T. Mazeh, A. Ofir, M. Ollivier, M. Pätzold, H. Parviainen, H. Rauer, D. Rouan, J. Schneider, R. Titz-Weider, B. Tingley, J. Weingrill: Planets, candidates, and binaries from the CoRoT/Exoplanet programme. The CoRoT transit catalogue, *Astron. Astrophys.*, **619**, A97, 2018.

Delrez, L., N. Madhusudhan, M. Lendl, M. Gillon, D.R. Anderson, M. Neveu-VanMalle, F. Bouchy, A. Burdanov, A. Collier-Cameron, B.-O. Demory, C. Hellier, E. Jehin, P. Magain, P.F.L. Maxted, D. Queloz, B. Smalley, A.H.M.J. Triaud: High-precision multiwavelength eclipse photometry of the ultra-hot gas giant exoplanet WASP-103 b, *MNRAS*, **474**, 2334-2351, 2018.

Demangeon, O.D.S., F. Faedi, G. Hébrard, D.J.A. Brown, S.C.C. Barros, A.P. Doyle, P.F.L. Maxted, A. Collier Cameron, K.L. Hay, J. Alikakos, D.R. Anderson, D.J. Armstrong, P. Boumis, A.S. Bonomo, F. Bouchy, L. Delrez, M. Gillon, C.A. Haswell, C. Hellier, E. Jehin, F. Kiefer, K.W.F. Lam, M. Lendl, L. Mancini, J. McCormac, A.J. Norton, H.P. Osborn, E. Palle, F. Pepe, D.L. Pollacco, J. Prieto-Arranz, D. Queloz, D. Ségransan, B. Smalley, A.H.M.J. Triaud, S. Udry, R. West, P.J. Wheatley: The discovery of WASP-151b, WASP-153b, WASP-156b: Insights on giant planet migration and the upper boundary of the Neptunian desert, *Astron. Astrophys.*, **610**, A63, 2018.

Denisenko, V.V., M.Y. Boudjada, H. Lammer: Propagation of seismogenic electric currents through the Earth's atmosphere, *J. Geophys. Res.*, **123**, 4290-4297, 2018.

Denisenko, V.V., S.A. Nesterov, M.Y. Boudjada, H.Lammer: A mathematical model of quasistationary electric field penetration from ground to the ionosphere with inclined magnetic field, *J. Atmos. Sol.-Terr. Phys.*, **178**, 527-537, 2018.

Dimmock, A.P., M. Alho, E. Kallio, S.A. Pope, T.L. Zhang, E. Kilpua, T.I. Pulkkinen, Y. Futaana, A.J. Coates: The response of the Venusian plasma environment to the passage of an ICME: Hybrid simulation results and Venus Express observations, *J. Geophys. Res.*, **123**, 3580-3601, 2018.

Ellmeier, M., C. Hagen, J. Piris, R. Lammegger, I. Jernej, M. Woschank, W. Magnes, E. Murphy, A. Pollinger, C. Erd, W. Baumjohann, L. Windholz: Accelerated endurance test of single-mode vertical-cavity surface emitting lasers under vacuum used for a scalar space magnetometer, *Appl. Phys. B*, **124**, 18, 2018.

Erard, S., B. Cecconi, P. Le Sidaner, A.P. Rossi, M.T. Capria,B. Schmitt, V. Genot, N. Andre, A.C. Vandaele, M. Scherf, R. Hueso, A. Määttänen, W. Thuillot, B. Carry, N. Achilleos, C. Marmo, O. Santolik, K. Benson, P. Fernique, L. Beigbeder, E. Millour, B. Rousseau, F. Andrieu, C. Chauvin, M. Minin, S. Ivanoski, A. Longobardo, P. Bollard, D. Albert, M. Gangloff, N. Jourdane, M. Bouchemit, J.-M. Glorian, L. Trompet, T. Al-Ubaidi, J. Juaristi, J. Desmars, P. Guio, O. Delaa, A. Lagain, J. Soucek, D. Pisa: VESPA: A community-driven Virtual Observatory in Planetary Science, *Planet. Space Sci.*, **150**, 65-85, 2018.

Ergun, R.E., K.A. Goodrich, F.D. Wilder, N. Ahmadi, J.C. Holmes, S. Eriksson, J.E. Stawarz, R. Nakamura, K.J. Genestreti, M. Hesse, J.L. Burch, R.B. Torbert, T.D. Phan, S.J. Schwartz, J.P. Eastwood, R.J. Strangeway, O. Le Contel, C.T. Russell, M.R. Argall, P.-A. Lindqvist, L.J. Chen, P.A. Cassak, B.L. Giles, J.C. Dorelli, D. Gershman, T.W. Leonard, B. Lavraud, A. Retino, W. Matthaeus, A. Vaivads: Magnetic reconnection, turbulence, and particle acceleration: Observations in the Earth's magnetotail, *Geophys. Res. Lett.*, **45**, 3338-3347, 2018.

Farihi, J., L. Fossati, P.J. Wheatley, B.D. Metzger, J. Mauerhan, S. Bachman, B.T. Gänsicke, S. Redfield, P.W. Cauley, O. Kochukhov, N. Achilleos, N. Stone: Magnetism, x-rays, and accretion rates in WD 1145+017 and other polluted white dwarf systems, *MNRAS*, **474**, 947-960, 2018.

Farrugia, C.J., I.J. Cohen, B.J. Vasquez, N. Lugaz, L. Alm, R.B. Torbert, M.R. Argall, K. Paulson, B. Lavraud, D.J. Gershman, F.T. Gratton, H. Matsui, A. Rogers, T.G. Forbes, D. Payne, R.E. Ergun, B. Mauk, J.L. Burch, C.T. Russell, R.J. Strangeway, J. Shuster, R. Nakamura, S.A. Fuselier, B.L. Giles, Y.V. Khotyaintsev, P.A. Lindqvist, G.T. Marklund, S.M. Petrinec, C.J. Pollock: Effects in the near-magnetopause magnetosheath elicited by large-amplitude Alfvénic fluctuations terminating in a field and flow discontinuity, *J. Geophys. Res.*, **123**, 8983-9004, 2018.

Fichtner, H., K. Scherer, M. Lazar, H.J. Fahr, Z. Vörös: Entropy of plasmas described with regularized κ distributions, *Phys. Rev. E*, **98**, 053205, 2018.

Fleming, B.T., K.C. France, N. Nell, R.A. Kohnert, K. Pool, A. Egan, L. Fossati, T.T. Koskinen, A.A. Vidotto, K. Hoadley, J.-M. Desert, M. Beasley, P.M. Petit: Colorado Ultraviolet Transit Experiment: A dedicated CubeSat mission to study exoplanetary mass loss and magnetic fields, *JATIS*, **4**, 014004, 2018.

Folsom, C.P., L. Fossati, B.E. Wood, A.G. Sreejith, P.E. Cubillos, A.A. Vidotto, E. Alecian, V. Girish, H. Lichtenegger, J. Murthy, P. Petit, G. Valyavin: Characterization of the HD 219134 multiplanet system I. Observations of stellar magnetism, wind, and high-energy flux, *MNRAS*, **481**, 5286-5295, 2018.

Fossati, L., T. Koskinen, J.D. Lothringer, K. France, M.E. Young, A.G. Sreejith: Extreme-ultraviolet radiation from A-stars: Implications for ultra-hot Jupiters, *Astrophys. J. Lett.*, **868**, L30, 2018.

Fossati, L., T. Koskinen, K. France, P.E. Cubillos, C.A. Haswell, A.F. Lanza, I. Pillitteri: Suppressed far-UV stellar activity and low planetary mass loss in the WASP-18 system, *Astron. J.*, **155**, 113, 2018.

France, K., N. Arulanantham, L. Fossati, A.F. Lanza, R.O. Parke Loyd, S. Redfield, P.C. Schneider: Far-ultraviolet activity levels of F, G, K, and M dwarf exoplanet host stars, *Astrophys. J. Suppl. Ser.*, **239**, 16, 2018.

Friedrich, M., C. Pock, K. Torkar: FIRI-2018, an updated empirical model of the lower ionosphere, *J. Geophys. Res.*, **123**, 6737-6751, 2018.

Gandolfi, D., O. Barragán, J.H. Livingston, M. Fridlund, A.B. Justesen, S. Redfield, L. Fossati, S. Mathur, S. Grziwa, J. Cabrera, R.A. García, C.M. Persson, V. Van Eylen, A.P. Hatzes, D. Hidalgo, S. Albrecht, L. Bugnet, W.D. Cochran, Sz. Csizmadia, H. Deeg, Ph. Eigmüller, M. Endl, A. Erikson, M. Esposito, E. Guenther, J. Korth, R. Luque, P. Montañes Rodríguez, D. Nespra, G. Nowak, M. Pätzold, J. Prieto-Arranz: TESS's first planet. A super-Earth transiting the naked-eye star π Mensae, *Astron. Astrophys.*, **619**, L10, 2018.

Genestreti, K.J., A. Varsani, J.L. Burch, P.A. Cassak, R.B. Torbert, R. Nakamura, R.E. Ergun, T.-D. Phan, S. Toledo-Redondo, M. Hesse, S. Wang, B.L. Giles, C.T. Russell, Z. Vörös, K.-J. Hwang, J.P. Eastwood, B. Lavraud, C.P. Escoubet, R.C. Fear, Y. Khotyaintsev, T.K.M. Nakamura, J.M. Webster, W. Baumjohann: MMS observation of asymmetric reconnection supported by 3-D electron pressure divergence, *J. Geophys. Res.*, **123**, 1806-1821, 2018.

Genestreti, K.J., P.A. Cassak, A. Varsani, J.L. Burch, R. Nakamura, S. Wang: Assessing the time dependence of reconnection with Poynting's theorem: MMS observations, *Geophys. Res. Lett.*, **45**, 2886-2892, 2018.

Genestreti, K.J., T.K.M. Nakamura, R. Nakamura, R.E. Denton, R.B. Torbert, J.L. Burch, F. Plaschke, S.A. Fuselier, R.E. Ergun, B.L. Giles, C.T. Russell: How accurately can we measure the reconnection rate E_M for the MMS diffusion region event of 11 July 2017?, *J. Geophys. Res.*, **123**, 9130-9149, 2018.

Genot, V., L. Beigbeder, D. Popescu, N. Dufourg, M. Gangloff, M. Bouchemit, S. Caussarieu, J.-P. Toniutti, J. Durand, R. Modolo, N. Andre, B. Cecconi, C. Jacquey, F. Pitout, A. Rouillard, R. Pinto, S. Erard, N. Jourdane, L. Leclercq, S. Hess, M. Khodachenko, T. Al-Ubaidi, M. Scherf, E. Budnik: Science data visualization in planetary and heliospheric contexts with 3DView, *Planet. Space Sci.*, **150**, 111-130, 2018.

Golombek, M., M. Grott, G. Kargl, J. Andrade, J. Marshall, N. Warner, N.A. Teanby, V. Ansan, E. Hauber, J. Voigt, R. Lichtenheldt, B. Knapmeyer-Endrun, I.J. Daubar, D. Kipp, N. Muller, P. Lognonné, C. Schmelzbach, D. Banfield, A. Trebi-Ollennu, J. Maki, S. Kedar, D. Mimoun, N. Murdoch, S. Piqueux, P. Delage, W.T. Pike, C. Charalambous, R. Lorenz, L. Fayon, A. Lucas, S. Rodriguez, P. Morgan, A. Spiga, M. Panning, T. Spohn, S. Smrekar, T. Gudkova, R. Garcia, D. Giardini, U. Christensen, T. Nicollier, D. Sollberger, J. Robertsson, K. Ali, B. Kenda, W.B. Banerdt: Geology and physical properties investigations by the InSight lander, *Space Sci. Rev.*, **214**, 84, 2018.

Good, S.W., R.J. Forsyth, J.P. Eastwood, C. Möstl: Correlation of ICME magnetic fields at radially aligned spacecraft, *Solar Phys.*, **293**, 52, 2018.

Graham, D.B., A. Vaivads, Yu.V. Khotyaintsev, A.I. Eriksson, M. André, D.M. Malaspina, P.-A. Lindqvist, D.J. Gershman, F. Plaschke: Enhanced escape of spacecraft photoelectrons caused by Langmuir and upper hybrid waves, *J. Geophys. Res.*, **123**, 7534-7553, 2018.

Graham, D.B., A. Vaivads, Yu.V. Khotyaintsev, M. André, O. Le Contel, D.M. Malaspina, P.-A. Lindqvist, F.D. Wilder, R.E. Ergun, D.J. Gershman, B.L. Giles, W. Magnes, C. T. Russell, J.L. Burch, R.B. Torbert: Large-amplitude high-frequency waves at Earth's magnetopause, *J. Geophys. Res.*, **123**, 2630-2657, 2018.

Grant, S.D.T., D.B. Jess, T.V. Zaqarashvili, C. Beck, H. Socas-Navarro, M.J. Aschwanden, P.H. Keys, D.J. Christian, S.J. Houston, R.L. Hewitt: Alfvén wave dissipation in the solar chromosphere, *Nat. Phys.*, **14**, 480-483, 2018.

Harrison, R.A., J.A. Davies, D. Barnes, J.P. Byrne, C.H. Perry, V. Bothmer, J.P. Eastwood, P.T. Gallagher, E.K.J. Kilpua, C. Möstl, L. Rodriguez, A.P. Rouillard, D. Odstrcil: CMEs in the heliosphere: I. A statistical analysis of the observational properties of CMEs detected in the heliosphere from 2007 to 2017 by STEREO/HI-1, *Solar Phys.*, **293**, 77, 2018.

Hesse, M., C. Norgren, P. Tenfjord, J.L. Burch, Y.-H. Liu, L.-J. Chen, N. Bessho, S. Wang, R. Nakamura, J.P. Eastwood, M. Hoshino, R.B. Torbert, R.E. Ergun: On the role of separatrix instabilities in heating the reconnection outflow region, *Phys. Plasmas*, **25**, 122902, 2018.

Hesse, M., Y.-H. Liu, L.-J. Chen, N. Bessho, S. Wang, J.L. Burch, T. Moretto, C. Norgren, K.J. Genestreti, T.D. Phan, P. Tenfjord: The physical foundation of the reconnection electric field, *Phys. Plasmas*, **25**, 032901, 2018.

Hietala, H., T.D. Phan, V. Angelopoulos, M. Oieroset, M.O. Archer, T. Karlsson, F. Plaschke: In situ observations of a magnetosheath high-speed jet triggering magnetopause reconnection, *Geophys. Res. Lett.*, **145**, 1732-1740, 2018.

Hodzic, V., A.H.M.J. Triaud, D.R. Anderson, F. Bouchy, A. Collier Cameron, L. Delrez, M. Gillon, C. Hellier, E. Jehin, M. Lendl, P.F.L. Maxted, F. Pepe, D. Pollacco, D. Queloz, D. Ségransan, B. Smalley, S. Udry, R. West: WASP-128b: A transiting brown dwarf in the dynamical-tide regime, *MNRAS*, **481**, 5091-5097, 2018.

Holmes, J.C., R.E. Ergun, D.L. Newman, N. Ahmadi, L. Andersson, O. Le Contel, R.B. Torbert, B.L. Giles, R.J. Strangeway, J.L. Burch: Electron phase-space holes in three dimensions: Multispacecraft observations by Magnetospheric Multiscale, *J. Geophys. Res.*, **123**, 9963-9978, 2018.

Imai, M., A. Lecacheux, T.E. Clarke, C.A. Higgins, M. Panchenko, J. Dowell, K. Imai, A.I. Brazhenko, A.V. Frantsuzenko, A.A. Konovalenko: Erratum: "The beaming structures of Jupiter's decametric common S-bursts observed from the LWA1, NDA, and URAN2 radio telescopes" (2016, ApJ, 826, 176), *Astrophys. J.*, **862**, 175, 2018.

Ismayilli, R.F., N.S. Dzhalilov, B.M. Shergelashvili, S. Poedts, M.Sh. Pirguliyev: MHD Kelvin-Helmholtz instability in the anisotropic solar wind plasma, *Phys. Plasmas*, **25**, 062903, 2018.

Johnstone, C.P., M. Güdel, H. Lammer, K.G. Kislyakova: Upper atmospheres of terrestrial planets: Carbon dioxide cooling and the Earth's thermospheric evolution, *Astron. Astrophys.*, **617**, A107, 2018.

Juvan, I.G., M. Lendl, P.E. Cubillos, L. Fossati, J. Tregloan-Reed, H. Lammer, E.W. Guenther, A. Hanslmeier: PyTranSpot: A tool for multiband light curve modeling of planetary transits and stellar spots, *Astron. Astrophys.*, **610**, A15, 2018.

Karlsson, T., F. Plaschke, H. Hietala, M. Archer, X. Blanco-Cano, P. Kajdic, P.-A. Lindqvist, G. Marklund, D.J. Gershman: Investigating the anatomy of magnetosheath jets - MMS observations, *Ann. Geophys.*, **36**, 655-677, 2018.

Khalafinejad, S., M. Salz, P.E. Cubillos, G. Zhou, C. von Essen, T.-O. Husser, D.D.R. Bayliss, M. López-Morales, S. Dreizler, J.H.M.M. Schmitt, T. Lüftinger: The atmosphere of WASP-17b: Optical high-resolution transmission spectroscopy, *Astron. Astrophys.*, **618**, A98, 2018.

Kiehas, S.A., A. Runov, V. Angelopolos, H. Hietala, D. Korovinksiy: Magnetotail fast flow occurrence rate and dawn-dusk asymmetry at X_{GSM} ~−60 R_E, *J. Geophys. Res.*, **123**, 1767-1778, 2018.

Kilpatrick, B.M., P.E. Cubillos, K.B. Stevenson, N.K. Lewis, H.R. Wakeford, R.J. MacDonald, N. Madhusudhan, J. Blecic, G. Bruno, A. Burrows, D. Deming, K. Heng, M.R. Line, C.V. Morley, V. Parmentier, G.S. Tucker, J.A. Valenti, I.P. Waldmann, J.L. Bean, C. Beichman, J. Fraine, J.E. Krick, J.D. Lothringer, A.M. Mandell: Community targets of JWST's early release science program: Evaluation of WASP-63b, *Astron. J.*, **156**, 103, 2018.

Kislyakova, K.G., L. Fossati, C.P. Johnstone, L. Noack, T. Lüftinger, V.V. Zaitsev, H. Lammer: Effective induction heating around strongly magnetized stars, *Astrophys. J.*, **858**, 105, 2018.

Kitzmann, D., K. Heng, P.B. Rimmer, H.J. Hoeijmakers, S.-M. Tsai, M. Malik, M. Lendl, R. Deitrick, B.-O. Demory: The peculiar atmospheric chemistry of KELT-9b, *Astrophys. J.*, **863**, 183, 2018.

Kömle, N.I., P. Tiefenbacher, A. Kahr: Melting probe experiments under Mars surface conditions - the influence of dust layers, CO2-ice and porosity, *Icarus*, **315**, 7-19, 2018.

Kömle, N.I., P. Tiefenbacher, P. Weiss, A. Bendiukova: Melting probes revisited - ice penetration experiments under Mars surface pressure conditions, *Icarus*, **308**, 117-127, 2018.

Korovinskiy, D.B., D.I. Kubyshkina, V.S. Semenov, M.V. Kubyshkina, N.V. Erkaev, S.A. Kiehas: On application of asymmetric Kan-like exact equilibria to the Earth magnetotail modeling, *Ann. Geophys.*, **36**, 641-653, 2018.

Korovinskiy, D.B., N.V. Erkaev, V.S. Semenov, I.B. Ivanov, S.A. Kiehas, I.I. Ryzhkov: On the influence of the local maxima of total pressure on the current sheet stability to the kink-like (flapping) mode, *Phys. Plasmas*, **25**, 022904, 2018.

Korovinskiy, D.B., V.S. Semenov, N.V. Erkaev, I.B. Ivanov, S.A. Kiehas: Current sheet bending as destabilizing factor in magnetotail dynamics, *Phys. Plasmas*, **25**, 092901, 2018.

Krauss, S., M. Temmer, S. Vennerstrom: Multiple satellite analysis of the Earth's thermosphere and interplanetary magnetic field variations due to ICME/CIR events during 2003-2015, *J. Geophys. Res.*, **123**, 8884-8894, 2018.

Kubyshkina, D., L. Fossati, N.V. Erkaev, C.P. Johnstone, P.E. Cubillos, K.G. Kislyakova, H. Lammer, M. Lendl, P. Odert: Grid of upper atmosphere models for 1-40 $M_\oplus$ planets: Application to CoRoT-7 b and HD219134 b,c, *Astron. Astrophys.*, **619**, A151, 2018.

Kubyshkina, D., L. Fossati, N.V. Erkaev, P.E. Cubillos, C.P. Johnstone, K.G. Kislyakova, H. Lammer, M. Lendl, P. Odert: Overcoming the limitations of the energy-limited approximation for planet atmospheric escape, *Astrophys. J. Lett.*, **866**, L18, 2018.

Kubyshkina, D., M. Lendl, L. Fossati, P.E. Cubillos, H. Lammer, N.V. Erkaev, C.P. Johnstone: Young planets under extreme UV irradiation. I. Upper atmosphere modelling of the young exoplanet K2-33b, *Astron. Astrophys.*, **612**, A25, 2018.

Kumar, S., N.K. Dwivedi, R.P. Sharma, Y.-J. Moon: A two-fluid modeling of kinetic Alfvén wave turbulence, *Astrophys. Space Sci.*, **363**, 204, 2018.

Lakhina, G.S., B.T. Tsurutani, G.J. Morales, A. Pouquet, M. Hoshino, J.A. Valdivia, Y. Narita, R. Grimshaw: Preface: Nonlinear waves and chaos, *Nonlin. Proc. Geophys.*, **25**, 477-479, 2018.

Lammer, H., A.L. Zerkle, S. Gebauer, N. Tosi, L. Noack, M. Scherf, E. Pilat-Lohinger, M. Güdel, J.L. Grenfell, M. Godolt, A. Nikolaou: Origin and evolution of the atmospheres of early Venus, Earth and Mars, *Astron. Astrophys. Rev.*, **26**, 2, 2018.

Lammer, H., M. Blanc: From disks to planets: The making of planets and their early atmospheres. An introduction, *Space Sci. Rev.*, **214**, 60, 2018.

Levasseur-Regourd, A.C., J. Agarwal, H. Cottin, C. Engrand, G. Flynn, M. Fulle, T. Gombosi, Y. Langevin, J. Lasue, T. Mannel, S. Merouane, O. Poch, N. Thomas, A. Westphal: Cometary dust, *Space Sci. Rev.*, **214**, 64, 2018.

Liao, S.-K., W.-Q. Cai, J. Handsteiner, B. Liu, J. Yin, L. Zhang, D. Rauch, M. Fink, J.-G. Ren, W.-Y. Liu, Y. Li, Q. Shen, Y. Cao, F.-Z. Li, J.-F. Wang, Y.-M. Huang, L. Deng, T. Xi, L. Ma, T. Hu, L. Li, N.-L. Liu, F. Koidl, P. Wang, Y.-A. Chen, X.-B. Wang, M. Steindorfer, G. Kirchner, C.-Y. Lu, R. Shu, R. Ursin, T. Scheidl, C.-Z. Peng, J.-Y. Wang, A. Zeilinger, J.-W. Pan: Satellite-relayed intercontinental quantum network, *Phys. Rev. Lett.*, **120**, 030501, 2018.

Libano, F., P. Rech, L. Tambara, J. Tonfat, F. Kastensmidt: On the reliability of linear regression and pattern recognition feedforward artificial neural networks in FPGAs, *IEEE Trans. Nucl. Sci.*, **65**, 288-295, 2018.

Lillo-Box, J., A. Leleu, H. Parviainen, P. Figueira, M. Mallonn, A.C.M. Correia, N.C. Santos, P. Robute, M. Lendl, H.M.J. Boffin, J.P. Faria, D. Barrado, J. Neal: The TROY project. II. Multi-technique constraints on exotrojans in nine planetary systems, *Astron. Astrophys.*, **618**, A42, 2018.

Liu,Y.-H., M. Hesse, F. Guo, H. Li, T.K.M. Nakamura: Strongly localized magnetic reconnection by the super-Alfvénic shear flow, *Phys. Plasmas*, **25**, 080701, 2018.

Mallonn, M., E. Herrero, I.G. Juvan, C. von Essen, A. Rosich, I. Ribas, T. Granzer, X. Alexoudi, K.G. Strassmeier: GJ 1214: Rotation period, starspots, and uncertainty on the optical slope of the transmission spectrum, *Astron. Astrophys.*, **614**, A35, 2018.

Martin, A.J., C. Neiner, M.E. Oksala, G.A. Wade, Z. Keszthelyi, L. Fossati, W. Marcolino, S. Mathis, C. Georgy: First results from the LIFE project: Discovery of two magnetic hot evolved stars, *MNRAS*, **475**, 1521-1536, 2018.

Mathew, J., S. Ambily, A. Prakash, M. Sarpotdar, K. Nirmal, A.G. Sreejith, M. Safonova, J. Murthy, N. Brosch: Wide-field ultraviolet imager for astronomical transient studies, *Exp. Astron.*, **45**, 201-218, 2018.

Melnik, V.N., A.I. Brazhenko, A.A. Konovalenko, V.V. Dorovskyy, H.O. Rucker, M. Panchenko, A.V. Frantsuzenko, M.V. Shevchuk: Decameter type IV burst associated with a behind-the-limb CME observed on 7 November 2013, *Solar Phys.*, **293**, 53, 2018.

Meng, L.F., Z.H. Pan, Z. Yi, G.Q. Wang, T.L. Zhang: Error properties of the fluxgate magnetometer offset based on Davis-Smith method, *Chin. J. Geophys.*, **61**, 3545-3551, 2018.

Mghebrishvili, I., T.V. Zaqarashvili, V. Kukhianidze, D. Kuridze, D. Tsiklauri, B.M. Shergelashvili, S. Poedts: Association between tornadoes and instability of hosting prominences, *Astrophys. J.*, **861**, 112, 2018.

Modolo, R., S. Hess, V. Genot, L. Leclercq, F. Leblanc, J.-Y. Chaufray, P. Weill, M. Gangloff, A. Fedorov, E. Budnik, M. Bouchemit, M. Steckiewicz, N. Andre, L. Beigbeder, D. Popescu, J.-P. Toniutti, T. Al-Ubaidi, M. Khodachenko, D. Brain, S. Curry, B. Jakosky, M. Holmström: The LatHyS database for planetary plasma environment investigations: Overview and a case study of data/model comparisons, *Planet. Space Sci.*, **150**, 13-21, 2018.

Morbidelli, A., S.-I. Karato, M. Ikoma, Y. Alibert, M. Blanc, L. Elkins-Tanton, P. Estrada, K. Hamano, H. Lammer, S. Raymond, M. Schönbächler: Editorial: Topical collection on the delivery of water to proto-planets, planets and satellites, *Space Sci. Rev.*, **214**, 110, 2018.

Möstl, C., T. Amerstorfer, E. Palmerio, A. Isavnin, C.J. Farrugia, C. Lowder, R.M. Winslow, J.M. Donnerer, E.K.J. Kilpua, P.D. Boakes: Forward modeling of coronal mass ejection flux ropes in the inner heliosphere with 3DCORE, *Space Weather*, **16**, 216-229, 2018.

Murphy, K.R., A.R. Inglis, D.G. Sibeck, I.J. Rae, C.E.J. Watt, M. Silveira, F. Plaschke, S.G. Claudepierre, R. Nakamura: Determining the mode, frequency, and azimuthal wave number of ULF waves during a HSS and moderate geomagnetic storm, *J. Geophys. Res.*, **123**, 6457-6477, 2018.

Nakamura, R., A. Varsani, K.J. Genestreti, O. Le Contel, T.K.M. Nakamura, W. Baumjohann, T. Nagai, A. Artemyev, J. Birn, V.A. Sergeev, S. Apatenkov, R.E. Ergun, S.A. Fuselier, D.J. Gershman, B.J. Giles, Y.V. Khotyaintsev, P.-A. Lindqvist, W. Magnes, B. Mauk, A. Petrukovich, C.T. Russell, J. Stawarz, R.J. Strangeway, B. Anderson, J.L. Burch, K.R. Bromund, I. Cohen, D. Fischer, A. Jaynes, L. Kepko, G. Le, F. Plaschke, G. Reeves, H.J. Singer, J.A. Slavin, R.B. Torbert, D.L. Turner: Multiscale currents observed by MMS in the flow braking region, *J. Geophys. Res.*, **123**, 1260-1278, 2018.

Nakamura, T.K.M., K.J. Genestreti, Y.-H. Liu, R. Nakamura, W.-L. Teh, H. Hasegawa, W. Daughton, M. Hesse, R.B. Torbert, J.L. Burch, B.L. Giles: Measurement of the magnetic reconnection rate in the Earth's magnetotail, *J. Geophys. Res.*, **123**, 9150-9168, 2018.

Nakamura, T.K.M., R. Nakamura, A. Varsani, K.J. Genestreti, W. Baumjohann, Y.-H. Liu: Remote sensing of the reconnection electric field from in situ multipoint observations of the separatrix boundary, *Geophys. Res. Lett.*, **45**, 3829-3837, 2018.

Narita, Y.: Space-time structure and wavevector anisotropy in space plasma turbulence, *Living Rev. Sol. Phys.*, **15**, 2, 2018.

Narita, Y., T. Hada: Density response to magnetic field fluctuation in the foreshock plasma, *Earth Planets Space*, **70**, 171, 2018.

Narita, Y., U. Motschmann: Can an interplanetary magnetic field reach the surface of Venus?, *Ann. Geophys.*, **36**, 1537-1543, 2018.

Narita, Y., Z. Vörös: Evaluation of electromotive force in interplanetary space, *Ann. Geophys.*, **36**, 101-106, 2018.

Nirmal, K., S. Rengaswamy, S. Sriram, J. Murthy, S. Jayant, S. Ambily, M. Safonova, A.G. Sreejith, J. Mathew, M. Sarpotdar: Design and modeling of a tunable spatial heterodyne spectrometer for emission line studies, *J. Astron. Telesc. Instrum. Syst.*, **4**, 025001, 2018.

Norgren, C., D.B. Graham, Yu.V. Khotyaintsev, M. André, A. Vaivads, M. Hesse, E. Eriksson, P.-A. Lindqvist, B. Lavraud, J. Burch, S. Fuselier, W. Magnes, D.J. Gershman, C.T. Russell: Electron reconnection in the magnetopause current layer, *J. Geophys. Res.*, **123**, 9222-9238, 2018.

Odert, P., H. Lammer, N.V. Erkaev, A. Nikolaou, H.I.M. Lichtenegger, C.P. Johnstone, K.G. Kislyakova, M. Leitzinger, N. Toside: Escape and fractionation of volatiles and noble gases from Mars-sized planetary embryos and growing protoplanets, *Icarus*, **307**, 327-346, 2018.

Oghrapishvili, N.B., S.R. Bagashvilida, D.A. Maghradze, T.Z. Gachechiladze, D.R. Japaridze, B.M. Shergelashvili, T.G. Mdzinarishvili, B.B. Chargeishvili: Study of the solar coronal hole rotation, *Adv. Space Res.*, **61**, 3039-3050, 2018.

Palmerio, E., E.K.J. Kilpua, C. Möstl, V. Bothmer, A.W. James, L.M. Green, A. Isavnin, J.A. Davies, R.A. Harrison: Coronal magnetic structure of earthbound CMEs and in situ comparison, *Space Weather*, **16**, 442-460, 2018.

Palmroth, M., H. Hietala, F. Plaschke, M. Archer, T. Karlsson, X. Blanco-Cano, D. Sibeck, P. Kajdic, U. Ganse, Y. Pfau-Kempf, M. Battarbee, L. Turc: Magnetosheath jet properties and evolution as determined by a global hybrid-Vlasov simulation, *Ann. Geophys.*, **36**, 1171-1182, 2018.

Panchenko, M., S. Rošker, H.O. Rucker, A. Brazhenko, P. Zarka, G. Litvinenko, V.E. Shaposhnikov, A.A. Konovalenko, V. Melnik, A.V. Franzuzenko, J. Schiemel: Zebra pattern in decametric radio emission of Jupiter, *Astron. Astrophys.*, **610**, A69, 2018.

Panov, E.V., P.L. Pritchett: Dawnward drifting interchange heads in the Earth's magnetotail, *Geophys. Res. Lett.*, **45**, 8834-8843, 2018.

Panov, E.V., P.L. Pritchett: Ion cyclotron waves rippling ballooning/interchange instability heads, *J. Geophys. Res.*, **123**, 8261-8274, 2018.

Paschmann, G., S.E. Haaland, T.D. Phan, B.U.Ö. Sonnerup, J.L. Burch, R.B. Torbert, D.J. Gershman, J.C. Dorelli, B.L. Giles, C. Pollock, Y. Saito, B. Lavraud, C.T. Russell, R.J. Strangeway, W. Baumjohann, S.A. Fuselier: Large-scale survey of the structure of the dayside magnetopause by MMS, *J. Geophys. Res.*, **123**, 2018-2033, 2018.

Persson, C.M., M. Fridlund, O. Barragán, F. Dai, D. Gandolfi, A.P. Hatzes, T. Hirano, S. Grziwa, J. Korth, J. Prieto-Arranz, L. Fossati, V. Van Eylen, A.B. Justesen, J. Livingston, D. Kubyshkina, H.J. Deeg, E.W. Guenther, G. Nowak, J. Cabrera, Ph. Eigmüller, Sz. Csizmadia, A.M.S. Smith, A. Erikson, S. Albrecht, A. Sobrino, W.D. Cochran, M. Endl, M. Esposito, A. Fukui, P. Heeren, D. Hidalgo, M. Hjorth, M. Kuzuhara, N. Narita, D. Nespra, E. Palle, M. Pätzold, H. Rauer, F. Rodler, J.N. Winn: Super-Earth of 8 $M_{\oplus}$ in a 2.2-day orbit around the K5V star K2-216, *Astron. Astrophys.*, **618**, A33, 2018.

Phan, T.D., J.P. Eastwood, M.A. Shay, J.F. Drake, B.U.Ö. Sonnerup, M. Fujimoto, P.A. Cassak, M. Øieroset, J.L. Burch, R.B. Torbert, A.C. Rager, J.C. Dorelli, D.J. Gershman, C. Pollock, P.S. Pyakurel, C.C. Haggerty, Y. Khotyaintsev, B. Lavraud, Y. Saito, M. Oka, R.E. Ergun, A. Retino, O. Le Contel, M.R. Argall, B.L. Giles, T.E. Moore, F.D. Wilder, R.J. Strangeway, C.T. Russell, P.A. Lindqvist, W. Magnes: Electron magnetic reconnection without ion coupling in Earth's turbulent magnetosheath, *Nature*, **557**, 202-206, 2018.

Pillitteri, I., L. Fossati, L., N.C. Rodriguez, L. Oskinova, S.J. Wolk: Detection of magnetic field in the B2 star rho Ophiuchi A with ESO FORS2, *Astron. Astrophys.*, **610**, L3, 2018.

Plaschke, F., H. Hietala: Plasma flow patterns in and around magnetosheath jets, *Ann. Geophys.*, **36**, 695-703, 2018.

Plaschke, F., H. Hietala, M. Archer, X. Blanco-Cano, P. Kajdic, T. Karlsson, S.H. Lee, N. Omidi, M. Palmroth, V. Roytershteyn, D. Schmid, V. Sergeev, D. Sibeck: Jets downstream of collisionless shocks, *Space Sci. Rev.*, **214**, 81, 2018.

Plaschke, F., T. Karlsson, C. Götz, C. Möstl, I. Richter, M. Volwerk, A. Eriksson, E. Behar, R. Goldstein: First observations of magnetic holes deep within the coma of a comet, *Astron. Astrophys.*, **618**, A114, 2018.

Pollinger, A., R. Lammegger, W. Magnes, C. Hagen, M. Ellmeier, I. Jernej, M. Leichtfried, C. Kürbisch, R. Maierhofer, R. Wallner, G. Fremuth, C. Amtmann, A. Betzler, M. Delva, G. Prattes, W. Baumjohann: Coupled dark state magnetometer for the China Seismo-Electromagnetic Satellite, *Meas. Sci. Technol.*, **29**, 095103, 2018.

Riley, P., M. Leila Mays, J. Andries, T. Amerstorfer, D. Biesecker, V. Delouille, M. Dumbović, X. Feng, E. Henley, J.A. Linker, C. Möstl, M. Nuñez, V. Pizzo, M. Temmer, W.K. Tobiska, C. Verbeke, M.J. West, X. Zhao: Forecasting the arrival time of Coronal Mass Ejections: Analysis of the CCMC CME scoreboard, *Space Weather*, **16**, 1245–1260, 2018.

Roberts, O.W., S. Toledo-Redondo, D. Perrone, J. Zhao, Y. Narita, D. Gershman, R. Nakamura, B. Lavraud, C.P. Escoubet, B. Giles, J. Dorelli, C. Pollock, J. Burch: Ion-scale kinetic Alfvén turbulence: MMS measurements of the Alfvén ratio in the magnetosheath, *Geophys. Res. Lett.*, **45**, 7974-7984, 2018.

Roberts, O.W., Y. Narita, C.-P. Escoubet: Multi-scale analysis of compressible fluctuations in the solar wind, *Ann. Geophys.*, **36**, 47-52, 2018.

Roberts, O.W., Y. Narita, C.-P. Escoubet: Three-dimensional density and compressible magnetic structure in solar wind turbulence, *Ann. Geophys.*, **36**, 527-539, 2018.

Sasunov, Yu.L., M.L. Khodachenko, I.I. Alexeev, E.S. Belenkaya, V.M. Gubchenko, N. Dwivedi, A. Hanslmeier: Self-consistent description of the tangential-discontinuity-type current sheet, using the particle trajectory method and angular variables, *Phys. Plasmas*, **25**, 092110, 2018.

Schneider, F.R.N., H. Sana, C.J. Evans, J.M. Bestenlehner, N. Castro, L. Fossati, G. Gräfener, N. Langer, O.H. Ramírez-Agudelo, C. Sabín-Sanjulián, S. Simón-Díaz, F. Tramper, P.A. Crowther, A. de Koter, S.E. de Mink, P.L. Dufton, M. Garcia, M. Gieles, V. Hénault-Brunet, A. Herrero, R.G. Izzard, V. Kalari, D.J. Lennon, J. Maíz Apellániz, N. Markova, F. Najarro, Ph. Podsiadlowski, J. Puls, W.D. Taylor, J.Th. van Loon, J.S. Vink, C. Norman: An excess of massive stars in the local 30 Doradus starburst, *Science*, **359**, 69-71, 2018.

Schneider, F.R.N., H. Sana, C.J. Evans, J.M. Bestenlehner, N. Castro, L. Fossati, G. Gräfener, N. Langer, O.H. Ramírez-Agudelo, C. Sabín-Sanjulián, S. Simón-Díaz, F. Tramper, P.A. Crowther, A. de Koter, S.E. de Mink, P.L. Dufton, M. Garcia, M. Gieles, V. Hénault-Brunet, A. Herrero, R.G. Izzard, V. Kalari, D.J. Lennon, J. Maíz Apellániz, N. Markova, F. Najarro, P. Podsiadlowski, J. Puls, W.D. Taylor, J.Th. van Loon, J.S. Vink, C. Norman: Response to Comment on "An excess of massive stars in the local 30 Doradus starburst", *Science*, **361**, eaat7032, 2018.

Schneider, F.R.N., O.H. Ramírez-Agudelo, F. Tramper, J.M. Bestenlehner, N. Castro, H. Sana, C.J. Evans, C. Sabín-Sanjulián, S. Simón-Díaz, N. Langer, L. Fossati, G. Gräfener, P.A. Crowther, S.E. de Mink, A. de Koter, M. Gieles, A. Herrero, R.G. Izzard, V. Kalari, R.S. Klessen, D.J. Lennon, L. Mahy, J. Maíz Apellániz, N. Markova, J.Th. van Loon, J.S. Vink, N.R. Walborn: The VLT-FLAMES Tarantula Survey. XXIX. Massive star formation in the local 30 Doradus starburst, *Astron. Astrophys.*, **618**, A73, 2018.

Schwarz, R., A. Bazso, N. Georgakarakos, B. Loibnegger, T.I. Maindl, D. Bancelin, E. Pilat-Lohinger, K.G. Kislyakova, R. Dvorak, I. Dobbs-Dixon: Exocomets in the Proxima Centauri system and their importance for water transport, *MNRAS*, **480**, 3595-3608, 2018.

Serrano, L.M., S.C.C. Barros, M. Oshagh, N.C. Santos, J.P. Faria, O. Demangeon, S.G. Sousa, M. Lendl: Distinguishing the albedo of exoplanets from stellar activity, *Astron. Astrophys.*, **611**, A8, 2018.

Shaikhislamov, I.F., M.L. Khodachenko, H. Lammer, A.G. Berezutsky, I.B. Miroshnichenko, M.S. Rumenskikh: 3D aeronomy modelling of close-in exoplanets, *MNRAS*, **481**, 5315-5323, 2018.

Shaikhislamov, I.F., M.L. Khodachenko, H. Lammer, L. Fossati, N. Dwivedi, M. Güdel, K.G. Kislyakova, C.P. Johnstone, A.G. Berezutsky, I.B. Miroshnichenko, V.G. Posukh1, N.V. Erkaev, V.A. Ivanov: Modeling of absorption by heavy minor species for the Hot Jupiter HD 209458b, *Astrophys. J.*, **866**, 47, 2018.

Shan, L., C. Mazelle, K. Meziane, N. Romanelli, Y.S. Ge, A. Du, Q. Lu, T.L. Zhang: The quasi-monochromatic ULF wave boundary in the Venusian foreshock: Venus Express observations, *J. Geophys. Res.*, **123**, 374-384, 2018.

Shkuratov, Y.G., A.A. Konovalenko, V.V. Zakharenko, A.A. Stanislaysky, E.Y. Bannikova, V.G. Kaydash, D.G. Stankevich, V.V. Krokhin, D.M. Vavriv, V.G. Galushko, S.N. Yerin, I.N. Bubnov, P.L. Tokarsky, O.M. Ulyanov, S.V. Stepkin, L.N. Lytvynenko, Y.S. Yatskiv, G. Videen, P. Zarka, H.O. Rucker: A twofold mission to the moon: Objectives and payloads, *Acta Astronaut.*, **154**, 214-226, 2018.

Snodgrass, C., G.H. Jones, H. Boehnhardt, A. Gibbings, M. Homeister, N. Andre, P. Beck, M.S. Bentley, I. Bertini, N. Bowles, M.T. Capria, C. Carr, M. Ceriotti, A.J. Coates, V. Della Corte, K.L. Donaldson Hanna, A. Fitzsimmons, P.J. Gutiérrez, O.R. Hainaut, A. Herique, M. Hilchenbach, H.H. Hsieh, E. Jehin, O. Karatekin, W. Kofman, L.M. Lara, K. Laudan, J. Licandro, S.C. Lowry, F. Marzari, A. Masters, K.J. Meech, F. Moreno, A. Morse, R. Orosei, A. Pack, D. Plettemeier, D. Prialnik, A. Rotundi, M. Rubin, J.P. Sánchez, S. Sheridan, M. Trieloff, A. Winterboer: The Castalia mission to Main Belt Comet 133P/Elst-Pizarro, *Adv. Space Res.*, **62**, 1947-1976, 2018.

Souchay, J., C. Lhotka, G. Heron, Y. Hervé, V. Puente, M. Folgueira Lopez: Changes of spin axis and rate of the asteroid (99942) Apophis during the 2029 close encounter with Earth: A constrained model, *Astron. Astrophys.*, **617**, A74, 2018.

Srivastava, A.K., K. Murawski, B. Kuźma, D.P. Wójcik, T.V. Zaqarashvili, M. Stangalini, Z.E. Musielak, J.G. Doyle, P. Kayshap, B.N. Dwivedi: Confined pseudo-shocks as an energy source for the active solar corona, *Nat. Astron.*, **2**, 951-956, 2018.

Stanislavsky, A.A., A.A. Konovalenko, E.P. Abranin, V.V. Dorovskyy, A. Lecacheux, H.O. Rucker, P. Zarka: Revisiting the frequency drift rates of decameter type III solar bursts observed in July -August 2002, *Solar Phys.*, **293**, 152, 2018.

Stanislavsky, A.A., A.A. Konovalenko, S.N. Yerin, I.N. Bubnov, V.V. Zakharenko, Yu.G. Shkuratov, P.L. Tokarsky, Ya.S. Yatskiv, A.I. Brazhenko, A.V. Frantsuzenko, V.V. Dorovskyy, H.O. Rucker, Ph. Zarka: Solar bursts as can be observed from the lunar farside with a single antenna at very low frequencies, *Astron. Nachr.*, **339**, 559-570, 2018.

Stawarz, J.E., J.P. Eastwood, K.J. Genestreti, R. Nakamura, R.E. Ergun, D. Burgess, J.L. Burch, S.A. Fuselier, D.J. Gershman, B.L. Giles, O. Le Contel, P.-A. Lindqvist, C.T. Russell, R.B. Torbert: Intense electric fields and electron-scale substructure within magnetotail flux ropes as revealed by the Magnetospheric Multiscale mission, *Geophys. Res. Lett.*, **45**, 8783-8792, 2018.

Sturner, A.P., S. Eriksson, T.K.M. Nakamura, D.J. Gershman, F. Plaschke, R.E. Ergun, F.D. Wilder, B. Giles, C. Pollock, W.R. Paterson, R.J. Strangeway, W. Baumjohann, J.L. Burch: On multiple Hall-like electron currents and tripolar guide magnetic field perturbations during Kelvin-Helmholtz waves, *J. Geophys. Res.*, **123**, 1305-1324, 2018.

Szabo, P.S., R. Chiba, H. Biber, R. Stadlmayr, B.M.Berger, D. Mayer, A. Mutzke, M. Doppler, M. Sauer, J. Appenroth, J. Fleig, A. Foelske-Schmitz, H. Hutter, K. Mezger, H. Lammer, A. Galli, P. Wurz, F. Aumayr: Solar wind sputtering of wollastonite as a lunar analogue material - Comparisons between experiments and simulations, *Icarus*, **314**, 98-105, 2018.

Takahashi, Y., M. Sato, M. Imai, R. Lorenz, Y. Yair, K. Aplin, G. Fischer, M. Nakamura, N. Ishii, T. Abe, T. Satoh, T. Imamura, C. Hirose, M. Suzuki, G.L. Hashimoto, N. Hirata, A. Yamazaki, T.M. Sato, M. Yamada, S. Murakami, Y. Yamamoto, T. Fukuhara, K. Ogohara, H. Ando, K. Sugiyama, H. Kashimura, S. Ohtsuki: Initiation of a lightning search using the lightning and airglow camera onboard the Venus orbiter Akatsuki, *Earth Planets Space*, **70**, 88, 2018.

Teh, W.-L., T.K.M. Nakamura, R. Nakamura, T. Umeda: Oblique ion-scale magnetotail flux ropes generated by secondary tearing modes, *J. Geophys. Res.*, **123**, 8122-8130, 2018.

Temmer, M., J. Hinterreiter, M.A. Reiss: Coronal hole evolution from multi-viewpoint data as input for a STEREO solar wind speed persistence model, *J Space Weather Space Clim*, **8**, A18, 2018.

Temple, L.Y., C. Hellier, Y. Almleaky, D.R. Anderson, F. Bouchy, D.J.A. Brown, A. Burdanov, A. Collier Cameron, L. Delrez, M. Gillon, R. Hall, E. Jehin, M. Lendl, P.F.L. Maxted, L.D. Nielsen, F. Pepe, D. Pollacco, D. Queloz, D. Ségransan, B. Smalley, S. Sohy, S. Thompson, A.H.M.J. Triaud, O.D. Turner, S. Udry, R.G. West: Discovery of WASP-174b: Doppler tomography of a near-grazing transit, *MNRAS*, **480**, 5307-5313, 2018.

Tian, F., M. Güdel, C.P. Johnstone, H. Lammer, R. Luger, P. Odert: Water loss from young planets, *Space Sci. Rev.*, **214**, 65, 2018.

Torbert, R.B., J.L. Burch, T.D. Phan, M. Hesse, M.R. Argall, J. Shuster, R.E. Ergun, L. Alm, R. Nakamura, K.J. Genestreti, D.J. Gershman, W.R. Paterson, D.L. Turner, I. Cohen, B.L. Giles, C.J. Pollock, S. Wang, L.-J. Chen, J.E. Stawarz, J.P. Eastwood, K.J. Hwang, C. Farrugia, I. Dors, H. Vaith, C. Mouikis, A. Ardakani, B.H. Mauk, S.A. Fuselier, C.T. Russell, R.J. Strangeway, T.E. Moore, J.F. Drake, M.A. Shay, Yu.V. Khotyaintsev, P.-A. Lindqvist, W. Baumjohann, F.D. Wilder, N. Ahmadi, J.C. Dorelli, L.A. Avanov, M. Oka, D.N. Baker, J.F. Fennell, J.B. Blake, A.N. Jaynes, O. Le Contel, S.M. Petrinec, B. Lavraud, Y. Saito: Electron-scale dynamics of the diffusion region during symmetric magnetic reconnection in space, *Science*, **362**, 1391-1395, 2018.

Treumann, R.A., W. Baumjohann: The differential cosmic ray energy flux in the light of an ultrarelativistic generalized Lorentzian thermodynamics, *Astrophys. Space Sci.*, **363**, 37, 2018.

Treumann, R.A., W. Baumjohann: The mirror mode: A "superconducting" space plasma analogue, *Ann. Geophys.*, **36**, 1015-1026, 2018.

Treumann, R.A., W. Baumjohann: Electron mirror branch: Observational evidence from "historical" AMPTE-IRM and Equator-S measurements, *Ann. Geophys.*, **36**, 1563-1576, 2018.

Umeda, T., T.K.M. Nakamura: Electromagnetic linear dispersion relation for plasma with a drift across magnetic field revisited, *Phys. Plasmas*, **25**, 102109, 2018.

Valyavin, G.G., D.R. Gadelshin, A.F. Valeev, T.E. Burlakova, K.A. Antonyuk, G.A. Galazutdinov, N.V. Pit, A.S. Moskvitin, E.N. Sokov, I.A. Sokova, B.C. Lee, I. Han, M. Lendl, L. Fossati, A.O. Grauzhanina, T.A. Fatkhullin: Exoplanet studies. Photometric analysis of the transmission spectra of selected exoplanets, *Astrophys. Bull.*, **73**, 225-234, 2018.

Vidotto, A.A., H. Lichtenegger, L. Fossati, C.P. Folsom, B.E. Wood, J. Murthy, P. Petit, A.G. Sreejith, G. Valyavin: Characterization of the HD 219134 multi-planet system II. Stellar-wind sputtered exospheres in rocky planets b & c, *MNRAS*, **481**, 5296-5306, 2018.

Volwerk, M.: On the location of the Io plasma torus: Voyager 1 observations, *Ann. Geophys.*, **36**, 831-839, 2018.

Volwerk, M., C. Goetz, I. Richter, M. Delva, K. Ostaszewski, K. Schwingenschuh, K.-H. Glassmeier: A tail like no other. The RPC-MAG view of Rosetta's tail excursion at comet 67P/Churyumov-Gerasimenko, *Astron. Astrophys.*, **614**, A10, 2018.

Wang, B., Y. Nishimura, H. Hietala, L. Lyons, V. Angelopoulos, F. Plaschke, Y. Ebihara, A. Weatherwax: Impacts of magnetosheath high-speed jets on the magnetosphere and ionosphere measured by optical imaging and satellite observations, *J. Geophys. Res.*, **123**, 4879-4894, 2018.

Wang, R., Q. Lu, R. Nakamura, W. Baumjohann, C. Huang, C.T. Russell, J.L. Burch, C.J. Pollock, D. Gershman, R.E. Ergun, S. Wang, P.A. Lindqvist, B. Giles: An electron-scale current sheet without bursty reconnection signatures observed in the near-Earth tail, *Geophys. Res. Lett.*, **45**, 4542-4549, 2018.

Wang, Y., C. Shen, R. Liu, J. Liu, J. Guo, X. Li, M. Xu, Q. Hu, T. Zhang: Understanding the twist distribution inside magnetic flux ropes by anatomizing an interplanetary magnetic cloud, *J. Geophys. Res.*, **123**, 3238-3261, 2018.

Weber, C., N.V. Erkaev, V.A. Ivanov, P. Odert, J.-M. Griessmaier, L. Fossati, H. Lammer, H.O. Rucker: Supermassive hot Jupiters provide more favourable conditions for the generation of radio emission via the cyclotron maser instability - A case study based on Tau Bootis b, *MNRAS*, **480**, 3680-3688, 2018.

Webster, J.M., J.L. Burch, P.H. Reiff, A.G. Daou, K.J. Genestreti, D.B. Graham, R.B. Torbert, R.E. Ergun, S.Y. Sazykin, A. Marshall, R.C. Allen, L.-J. Chen, S. Wang, T.D. Phan, B.L. Giles, T.E. Moore, S.A. Fuselier, G. Cozzani, C.T. Russell, S. Eriksson, A.C. Rager, J.M. Broll, K. Goodrich, F. Wilder: Magnetospheric Multiscale dayside reconnection electron diffusion region events, *J. Geophys. Res.*, **123**, 4858-4878, 2018.

Wilder, F.D., R.E. Ergun, J.L. Burch, N. Ahmadi, S. Eriksson, T.D. Phan, K.A. Goodrich, J. Shuster, A.C. Rager, R.B. Torbert, B.L. Giles, R.J. Strangeway, F. Plaschke, W. Magnes, P.A. Lindqvist, Y.V. Khotyaintsev: The role of the parallel electric field in electron-scale dissipation at reconnecting currents in the magnetosheath, *J. Geophys. Res.*, **123**, 6533-6547, 2018.

Wu, M., Q. Lu, M. Volwerk, R. Nakamura, T.-L. Zhang: Electron acceleration behind a wavy dipolarization front, *Astrophys. Space Sci.*, **363**, 22, 2018.

Xiao, S.D., T.L. Zhang: Solar cycle variation of the Venus magnetic barrier, *Planet. Space Sci.*, **158**, 53-62, 2018.

Xiao, S.D., T.L. Zhang, Z. Vörös: Magnetic fluctuations and turbulence in the Venusian magnetosheath downstream of different types of bow shock, *J. Geophys. Res.*, **123**, 8219-8226, 2018.

Ye, S.-Y., G. Fischer, W.S. Kurth, J.D. Menietti, D.A. Gurnett: An SLS5 longitude system based on the rotational modulation of Saturn radio emissions, *Geophys. Res. Lett.*, **45**, 7297-7305, 2018.

Yu, W., C.J. Farrugia, N. Lugaz, A.B. Galvin, C. Möstl, K. Paulson, P. Vemareddy: The magnetic field geometry of small solar wind flux ropes inferred from their twist distribution, *Solar Phys.*, **293**, 165, 2018.

Yushkov, E.V., A.G. Frank, A.V. Artemyev, A.A. Petrukovich, R. Nakamura: Hall effect in laboratory and space current sheets, *Plasma Phys. Rep.*, **44**, 1126-1134, 2018.

Zaqarashvili, T.: Equatorial magnetohydrodynamic shallow water waves in the Solar tachocline, *Astrophys. J.*, **856**, 32, 2018.

Zaqarashvili, T.V., E. Gurgenashvili: Magneto-Rossby waves and seismology of solar interior, *Front. Physics*, **5**, 7, 2018.

Zhelyazkov, I., T.V. Zaqarashvili, L. Ofman, R. Chandra: Kelvin-Helmholtz instability in a twisting solar polar coronal hole jet observed by SDO/AIA, *Adv. Space Res.*, **61**, 628-638, 2018.

PROCEEDINGS & BOOK CHAPTERS

Ambily, S., J. Mathew, M. Sarpotdar, J. Murthy, V.K. Aggarval, S. Nagabhushanam, D.A. Rao, S. Jeeragal, K. Nirmal, A.G. Sreejith, B. Gopalakrishnan, M. Safonova: PIONS: A CubeSat imager to observe variable UV sources, In: *Proc. SPIE 10699, Space Telescopes and Instrumentation 2018: Ultraviolet to Gamma Ray*, Eds. den Herder, J.-W., S. Nikzad, K. Nakazawa, SPIE, Bellingham, 106993E, 2018.

Auer, M., M. Scherzer, A. Valavanoglou, S. Leitner, W. Magnes: Prototype design of a magnetometer frontend-ASIC for spaceborne applications, In: *Proc. 26th Austrochip Workshop on Microelectronics*, Eds. Institute of Electronics, University of Technology, Graz, IEEE, Graz, 10-14, 2018.

Besser, B.P.: Die Steiermark und der Weltraum, In: *Die Steiermark. Eine Landvermessung*, Eds. Hösele, H., M. Prisching, Brandstätter, Wien, 472-473, 2018.

Besser, B.P.: Willibald Riedler - der Weltraumforscher, In: *Die Steiermark. Eine Landvermessung*, Eds. Hösele, H., M. Prisching, Brandstätter, Wien, 477, 2018.

Bouret, J.C., C. Neiner, A.I.G. de Castro, C. Evans, B. Gaensicke, S. Shoref, L. Fossati, C. Gry, S. Charlot, F. Marin, P. Noterdaeme, J.Y. Chaufray: The science case for POLLUX, a high-resolution UV spectropolarimeter onboard LUVOIR, In: *Proc. SPIE 10699, Space Telescopes and Instrumentation 2018: Ultraviolet to Gamma Ray*, Eds. den Herder, J.-W., S. Nikzad, K. Nakazawa, SPIE, Bellingham, 106993B, 2018.

Egan, A., B.T. Fleming, K. France, N. Nell, S. Ulrich, N. DeCicco, R. Kohnert, A.G. Sreejith, L. Fossati, N. Kruczek: The Colorado Ultraviolet Transit Experiment (CUTE): Final design and projected performance, In: *Proc. SPIE 10699, Space Telescopes and Instrumentation 2018: Ultraviolet to Gamma Ray*, Eds. den Herder, J.-W., S. Nikzad, K. Nakazawa, SPIE, Bellingham, 106990C, 2018.

Fischer, G., W.S. Kurth, D.A. Gurnett, G.B. Hospodarsky, P. Zarka, U.A. Dyudina, M. Delcroix: Saturn lightning after Cassini, In: *Proc. of XVI International Conference on Atmospheric Electricity (ICAE)*, Eds. ICAE Committee, ICAE, Nara, O-07-06, 2018.

Focardi, M., S.Pezzuto, R. Cosentino, G. Giusi, A.M. Di Giorgio, D. Biondi, C.D.V. Blanco, L. Serafini, D. Vangelista, M. Steller, H. Jeszenszky, H. Ottacher, G. Laky, R. Ottensamer, F. Kerschbaum, M. Guedel, V. Noce, E. Pace, M. Pancrazzi, K. Westerdorff, G. Peter, B. Ulmer, R. Berlin, P. Plasson, I. Pagano, E. Tommasi, S. Natalucci: The design of the Instrument Control Unit and its role within the Data Processing System of the ESA PLATO Mission, In: *Proc. SPIE 10698, Space Telescopes and Instrumentation 2018: Optical, Infrared, and Millimeter Wave*, Eds. Lystrup, M., H.A. MacEwen, G.G. Fazio, N. Batalha, N. Siegler, E.C. Tong, SPIE, Bellingham, Washington, USA, 106984G, 2018.

Mathew, J., B.G. Nair, S. Sriram, P.U. Kamath, A. Prakash, M. Sarpotdar, S. Ambily, K. Nirmal, A.G. Sreejith, M. Safonova, J. Murthy, N. Broschn: Opto-mechanical assembly and ground calibration of LUCI, In: *Proc. SPIE 10699, Space Telescopes and Instrumentation 2018: Ultraviolet to Gamma Ray*, Eds. den Herder, J.-W., S. Nikzad, K. Nakazawa, SPIE, Bellingham, 106992V, 2018.

Sreejith, A.G., L. Fossati, M. Steller, B.T. Fleming, K. France: CUTE data simulator and reduction pipeline, In: *Proc. SPIE 10699, Space Telescopes and Instrumentation 2018: Ultraviolet to Gamma Ray*, Eds. den Herder, J.-W., S. Nikzad, K. Nakazawa, SPIE, Bellingham, 1069932, 2018.

Volwerk, M.: Currents in cometary comae, In: *Electric Currents in Geospace and Beyond*, Eds. Keiling, A., O. Marghitu, M. Wheatland, John Wiley & Sons, Hoboken, NJ, USA, 513-533, 2018.

Wang, P., G. Kirchner, F. Koidl, M.A. Steindorfer, E. Döberl, M. Ploner, P. Keller, M. Taubenberger, E. Leitgeb: Upgrade of an astronomical telescope for satellite laser ranging up to geostationary targets, In: *Proceedings 2018 International Conference on Broadband Communications for Next Generation Networks and Multimedia Applications (CoBCom)*, Eds. Plank, T., Inst. of Microwave and Photonic Engineering, Graz University of Technology, Graz, 4 pp., 2018.

Wellenreiter, V., R. Monier, L. Fossati: Elemental abundances of HD 87240, member of the young open cluster NGC 3114, In: *Proceedings of the Annual meeting of the French Society of Astronomy and Astrophysics, SF2A-2018*, Eds. Di Matteo, P., F. Billebaud, F. Herpin, N. Lagarde, J.-B. Marquette, A. Robin, O. Venot, French Society of Astronomy and Astrophysics, Paris, 181-182, 2018.

For oral presentations and posters please refer to the "Publications" menu on www.iwf.oeaw.ac.at.

PERSONNEL

Agú, Martin A., Dipl.-Ing.
Aickara Gopinathan, Sreejith, Dr.
Al-Ubaidi, Tarek, Dipl.-Ing.
Almer, Hannes
Amerstorfer, Tanja, Dr.
Amerstorfer, Ute, Dr.
Arkhypov, Oleksiy, Dr.
Aydogar, Özer, Dipl.-Ing.
Baumjohann, Wolfgang, Prof.
Berghofer, Gerhard, Ing.
Besser, Bruno P., Dr.
Boakes, Peter D., Dr.
Boudjada, Mohammed Y., Dr.
Bourdin, Philippe, Dr.
Cubillos, Patricio, Dr.
Delva, Magda, Dr.
Dwivedi, Navin K., Dr.
Ederle, Vincent
Eichelberger, Hans U., Dr.
Ellmeier, Michaela, Mag.
Fischer, David, Dipl.-Ing.
Fischer, Georg, Dr.
Flock, Barbara, Mag.
Fossati, Luca, Dr.
Fremuth, Gerhard, Dipl.-Ing.
Genestreti, Kevin J., Dr.
Giner, Franz, Dipl.-Ing.
Graf, Christian, Ing.
Gratzer, Alexander J.
Grill, Claudia
Hasiba, Johann, Dipl.-Ing.
Hofmann, Karl, Dipl.-Ing.
Hofwimmer, Thomas, Ing.
Höck, Eduard, Dipl.-Ing.
Hradecky, Doris
Hummel, Fabian N.J.
Jernej, Irmgard, Ing.
Jeszenszky, Harald, Dipl.-Ing.
Juvan, Ines, Mag.
Kargl, Günter, Dr.
Khodachenko, Maxim L., Dr.
Kirchner, Georg, Dr.
Koidl, Franz, Ing.
Kömle, Norbert I., Doz.
Korovinskiy, Daniil, Dr.
Krauss, Sandro, Dr.
Kubyshkina, Daria, Dr.
Kürbisch, Christoph, Ing.
Laky, Gunter, Dipl.-Ing.
Lammer, Helmut, Dr.
Leichtfried, Mario, Ing.
Lendl, Monika, Dr.
Lhotka, Christoph, Dr.
Lichtenegger, Herbert I.M., Dr.
Macher, Wolfgang, Dr.
Magnes, Werner, Dr.
Mannel, Thurid, MSc
Močnik, Karl, Dr.
Möstl, Christian, Dr.
Muck, Cosima
Nakamura, Rumi, Doz.
Nakamura, Takuma, Dr.
Narita, Yasuhito, Doz.
Neukirchner, Sonja, Ing.
Nischelwitzer-Fennes, Ute, Ing.
Ottacher, Harald, Dipl.-Ing.
Panov, Evgeny, Dr.
Pitterle, Martin
Prattes, Gustav, Dipl.-Ing.
Reimond, Stefan, Dipl.-Ing.
Rojas-Castillo, Diana, Dr.
Scherf, Manuel, Mag.
Scherr, Alexandra, Mag.
Seibezeder, Julia
Stachel, Manfred, Dipl.-Ing.
Steinberger, Michael, Dipl.-Ing.
Steindorfer, Michael, Dr.
Steller, Manfred B., Dr.
Stieninger, Reinhard, Ing.
Sulis, Sophia, Dr.
Tiefenbacher, Patrick, Mag.
Tonfat Seclen, Jorge L., Dr.
Valavanoglou, Aris, Dipl.-Ing.
Voller, Wolfgang G., Mag.
Volwerk, Martin, Dr.
Wallner, Robert, Ing.
Wang, Peiyuan, Mag.
Wellenzohn, Simon
Wilfinger, Josef, BSc
Wirnsberger, Harald, Dipl.-Ing.
Wolf, Carina
Young, Mitchell E., Dr.
Zaqarashvili, Teimuraz, Dr.
Zhang, Tie-Long, Prof.

As of 31 December 2018

IMPRESSUM

PUBLISHER

Wolfgang Baumjohann, Director
Institut für Weltraumforschung (IWF)
Österreichische Akademie der Wissenschaften (ÖAW)
Schmiedlstraße 6, 8042 Graz, Austria
www.iwf.oeaw.ac.at

EDITORS

Bruno Besser, Alexandra Scherr, Martin Volwerk

DESIGN

Alexandra Scherr
pr.iwf@oeaw.ac.at
Twitter: @IWF_Graz

PRINT

Servicebetrieb ÖH-Uni Graz GmbH


ÖAW IWF